PHILOSOPHICAL TRANSACTIONS OF THE ROYAL SOCIETY A MATHEMATICAL, PHYSICAL & ENGINEERING SCIENCES

Turbulence and Mixing in a Scottish Loch

S. A. Thorpe

Phil. Trans. R. Soc. Lond. A 1977 **286**, 125-181
doi: 10.1098/rsta.1977.0112

TURBULENCE AND MIXING IN A SCOTTISH LOCH

By S. A. THORPE
Institute of Oceanographic Sciences, Wormley, Godalming, Surrey
(*Communicated by Sir George Deacon, F.R.S. – Received 5 July* 1976)

[Plate 1]

CONTENTS

It is nearly three-quarters of a century since E. R. Watson (1904) and E. M. Wedderburn (1907) made the observations in Loch Ness which showed conclusively, and for the first time, that large bodies of water contain beneath their surface the wave motions which have now come to be known as internal waves. The observations and theory of these waves have developed much since those days, but the Loch is still very useful as a site in which to observe and examine phenomena which are also found in other bodies of water, particularly the ocean. In particular the Loch provides a large-scale natural 'laboratory' in which a variety of small-scale phenomena associated with turbulence in a stratified fluid may be studied. Observations have been made with a novel profiling instrument which measures the horizontal velocity of the water and its temperature, from which the density may be inferred. These observations serve to illustrate a variety of local conditions which occur in calm weather, as the Loch responds to the wind and during the passage of an internal surge.

Vol. 286. A 1334. 17 [Published 4 July 1977

Analysis of the records is conducted in terms of an intermittency index (the fraction of fluid in which the density decreases with depth), the Richardson number and a length scale which characterizes the vertical scale of the regions which are found to be unstably stratified. Semi-empirical formulae for the eddy diffusion coefficient and the rate of dissipation of kinetic energy in the turbulent motion are examined to see whether they are consistent with observations. No universal value of the Richardson number is found, but this may be a consequence of the rather low values of Reynolds number found in the Loch thermocline.

1. Introduction

Many observations of mixing and turbulence have been made in the atmosphere, especially in the atmospheric boundary layer over land but, mainly because of instrumental problems, comparable measurements in naturally occurring bodies of water are very few. Our work began with a view of investigating some of the small and medium scale† effects of buoyancy as they occur naturally in a liquid which is generally stably stratified, a progression from earlier laboratory work (Thorpe 1973) to phenomena on a geophysical scale and in a wider parameter range than was accessible in the laboratory. We were particularly concerned with obtaining measurements in conditions in which the cause or source of mixing was thought to be understood, both for descriptive purposes and so as to provide examples against which other observations, made in circumstances in which the cause was uncertain, might be compared. The most important parameter controlling stability of a gravitationally stable stratified fluid is the Richardson number (see, for example, Turner 1973), and one product of the study is a description of the variation of this parameter and related quantities.

For several reasons Loch Ness was chosen as a site for the experiments. Historically it was the first water mass in which internal waves were measured and recognized as such (Watson 1904; Wedderburn 1907) and through the later studies of Wedderburn & Watson (1909), Mortimer (1955), Thorpe (1971), and Thorpe, Hall & Crofts (1972) the basic circulation and the internal seiche have become fairly well, although not fully, understood. Some further 'background' observations are described in § 3. The Loch provides a variety of phenomena, wind-mixed upper layers, internal surges and internal waves which can be studied in an environment which exhibits much of the complexity of the ocean but which is much more accessible. Investigation of the small-scale vertical temperature structure of the Loch begun by Wedderburn (1907) and continued by Simpson & Woods (1970), Thorpe *et al.* (1972) showed that the basic structure in autumn was very similar to that often found in the upper layers of the ocean with a partially mixed layer overlying a thermocline at about 30–50 m which exhibits structure with horizontal coherence over scales of 1 km or more. With the virtual absence of dissolved salts, the density of the Loch is primarily determined by temperature, a quantity which can be measured to high resolution with rapid response thermistors. Moreover double-diffusive convection (Turner 1973, ch. 8), depending on the presence of two components (salt and heat in the ocean) with different coefficients of molecular diffusion, cannot occur in the Loch, and our observations neither provide examples of phenomena associated with this convection nor are caused, or 'contaminated', by it. The Loch (figure 1) has no islands other than a small man-made island of antiquity near the

† The distinction is arbitrary, but we shall take small to mean scales on which the motion is nearly isotropic and medium to mean those in which buoyancy forces impose some anisotropy but which are yet very small in comparison with the distance between the boundaries of the fluid.

shore at Fort Augustus, and has a fairly uniform cross section. It is deep and steepsided,† providing water deeper than most of the water on the continental shelf only some 300 m offshore, and this has proved a great asset in the design of instruments (see appendix 1). The Loch is approximately aligned in the direction of the dominant prevailing (southwesterly) winds and has high hills on either side which further restrict the wind direction at low levels, and cause a main circulation of water along the length of the Loch. Several minor rivers enter the Loch and, after heavy precipitation, may significantly affect the Loch in the neighbourhoods of their outfalls (Wedderburn 1907), but the wind appears to be the dominant factor controlling circulation. The fetch at our site (marked A in figure 1) is over 11 km for winds which blow along the axis of the Loch, and white-caps are usually observed for winds exceeding $5\,\mathrm{m\,s^{-1}}$.

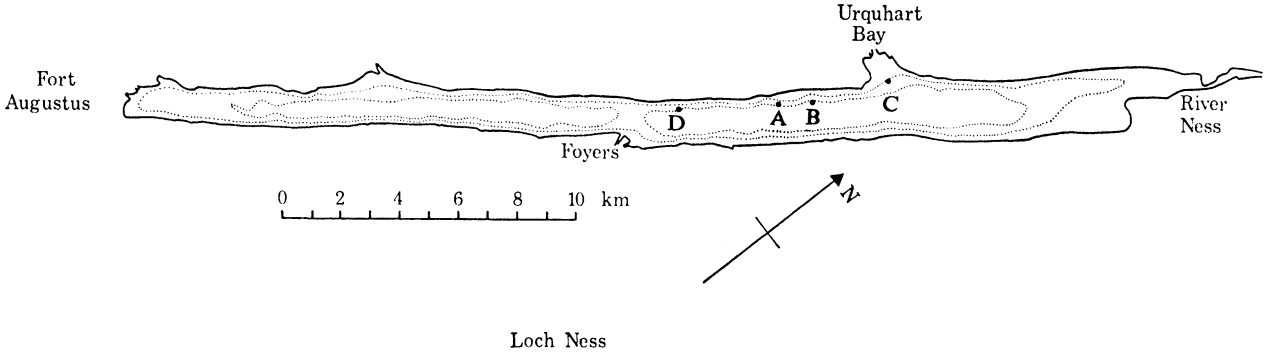

FIGURE 1. Loch Ness. The dotted contours are at 91.4 m and 182.9 m. The site of the present observations is at A. B and D are the positions of the moorings referred to in the captions of figures 2 and 5 respectively, and C is the position of the thermistor chain (caption of figure 3).

We have made measurements with a profiling current meter (P.C.M.) which, together with the spar buoy for the measurement of wind, air and water temperatures, is described in detail in appendix 1. Section 2 is devoted to some measurements with more conventional instruments which illustrate the general variability of temperature and currents in the Loch and provide a background to the more detailed measurements or 'case studies', obtained by using the P.C.M. described in § 3. Vertical profiles and contours of density and current are presented which serve to portray a variety of interesting physical phenomena and which are analysed using a number of different techniques described in § 3.1. In particular we investigate the depth variation of the Richardson number,

$$R_i = N^2/U'^2, \tag{1}$$

where N is the Brunt-Väisälä frequency and U' is the vertical derivative of the horizontal current. In § 4 the results of all these observations are discussed and analysed collectively, and compared with existing observations. Particular attention is given to estimates of the rate of dissipation of turbulent kinetic energy and the vertical diffusion coefficient for heat. The frequency of occurrence of small density inversions in the Loch appears to be related to the local Richardson number, and so too are the statistics of vertical temperature gradient.

† See for example Gardener (1745) and Johnston (1904).

2. Scales of variability in loch ness and instrumental limitations

Although in the sections which follow we wish to concentrate attention on local mixing processes rather than the overall diffusion and circulation of the loch which depends upon its particular geometry, it is essential in properly interpreting the measurements to know something of the background environment in which these were made.

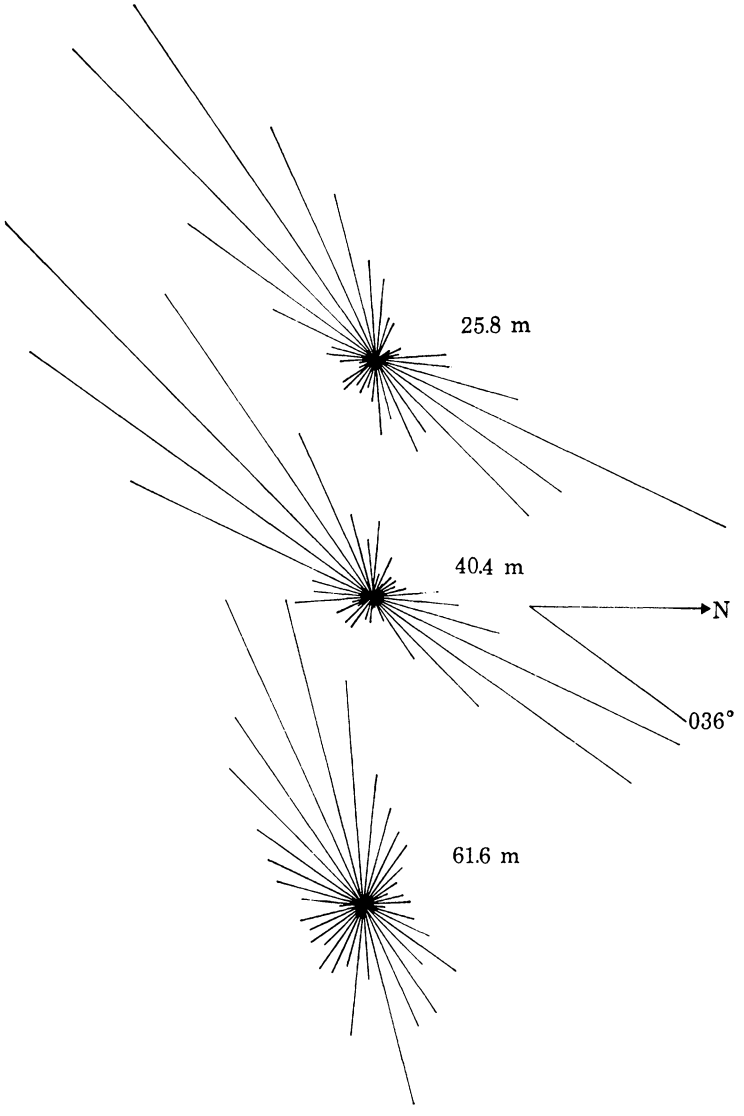

Figure 2. Star diagrams showing the frequency of currents in different directions at position B, figure 1, 4–19 August 1971. The length of each line represents the proportion of currents within ±5° of the direction in which the line is pointing. The depths of observation are shown.

Loch Ness (figure 1) is about 35 km in length, 1.4 km wide and has a mean depth of about 140 m. It is divided into two main basins each about 220 m deep by a low sill at Foyers, the result of siltation from the Foyers river, where the depth is about 150 m, still much deeper than the typical September thermocline depths of 30–50 m.

PHILOSOPHICAL TRANSACTIONS OF THE ROYAL SOCIETY A MATHEMATICAL, PHYSICAL & ENGINEERING SCIENCES

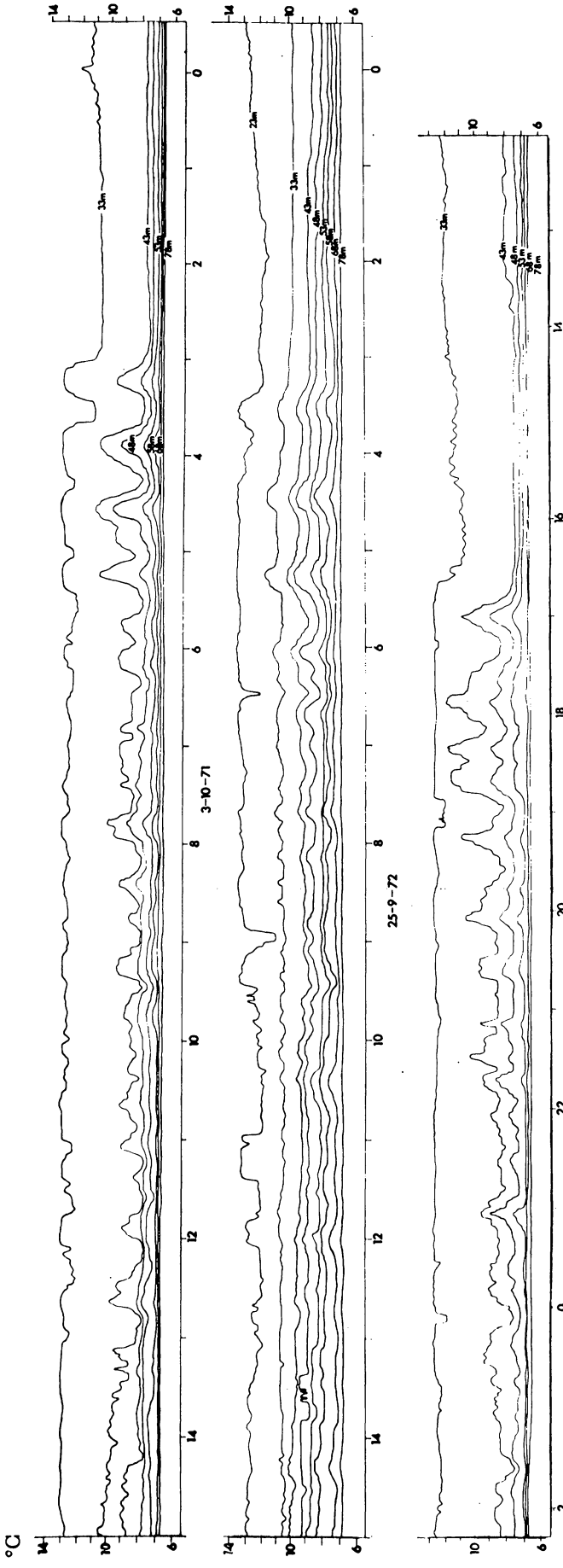

FIGURE 3. The variation of temperature at a vertical array of thermistors at position C, figure 1. The horizontal scale is the time in hours increasing towards the left and the vertical scale is the temperature in °C. The depths of the thermistors are written against each trace.

PHILOSOPHICAL TRANSACTIONS OF THE ROYAL SOCIETY A MATHEMATICAL, PHYSICAL & ENGINEERING SCIENCES

Wedderburn & Watson (1909) and Mortimer (1955) measured typical current speeds of 10 cm s^{-1}, frequently directed across, rather than directly along, the axis of the Loch. Our observations from moored Aanderaa current meters with subsurface buoyancy show a consistent tendency for currents below the surface wind mixing layer to be directed towards the southwest with a mean direction a few degrees to the right of the Loch axis (figure 2). This tendency presumably reflects the dominance of the southwesterly winds which, driving a northeasterly flow near the surface, cause mixing and a reverse flow at depth, affected by the Earth's rotation. The tracks of drogues at 40 m depth in light winds frequently showed marked transverse motions.

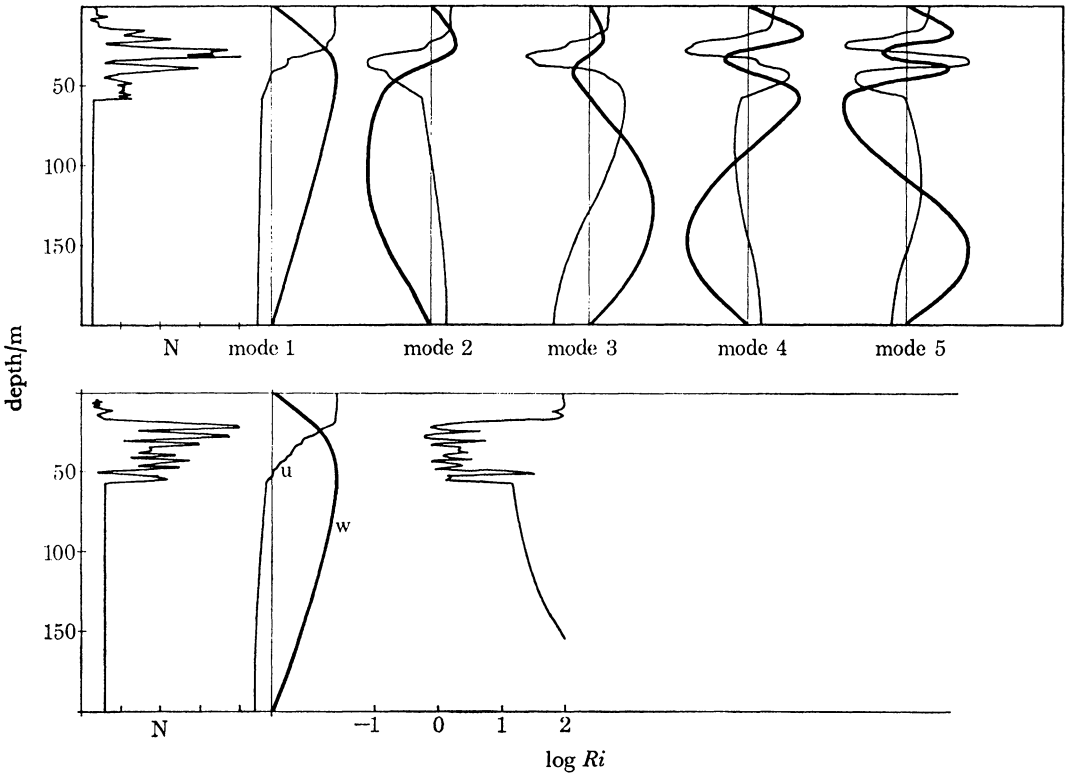

FIGURE 4. *Top*: the structure of internal wave modes for the Brunt–Väisälä frequency, N, calculated by using the density measured in profile 5 on 31 August (§3.2.1). Below 60 m, N was not measured, but has been supposed constant and determined by assuming a temperature of 5.78 °C at the bottom of the Loch (observed in experiments in 1971). The broad line shows the variation of the vertical displacements, and the narrow lines the horizontal currents, for the first five modes corresponding to a wavenumber 2.36×10^{-3} m^{-1}. *Bottom*: the same for profile 10 on 24 September (§3.2.3) for the first mode and zero wavenumber. The profile of log Richardson number, Ri, shown has been calculated from the horizontal current, u, with the smallest value arbitrarily set equal to 0.25.

The periods of the first three (longitudinal) surface seiches are 31.5, 15.3 and 8.8 min (Crystal 1910) and the first usually dominates, having an amplitude of about 5 cm in exceptional conditions. The period of the first longitudinal internal wave mode (the wave with a single subsurface displacement maximum which has a wavelength twice the length of the Loch) depends on the density structure of the Loch, but is typically about 52 h in September. The first internal seiche is observed to be highly nonlinear, having the form of an undular bore, propagating at about 35 cm s^{-1}, and the thermocline is lowered after its passage. Thorpe (1974) has described the way in which the surge may be generated by wind. The waves which follow the front of the

bore, or surge, have a period of about 40 min and a wavelength of 1 km. Examples of the temperatures recorded by a thermistor chain at position B, figure 1, during the passage of the surge during observations in 1972 are shown in figure 3. The isotherms are tilted across the Loch during the passage of the surge as the result of the Coriolis force of the Earth's rotation (Mortimer 1955; Thorpe *et al.* 1972). More detailed observations of the fine structure of the surge will be shown later (§ 3.2.6). The waves following the surge appear to dissipate on the irregular and gently shelving northeast end of the Loch and are not observed in the reflected wave.

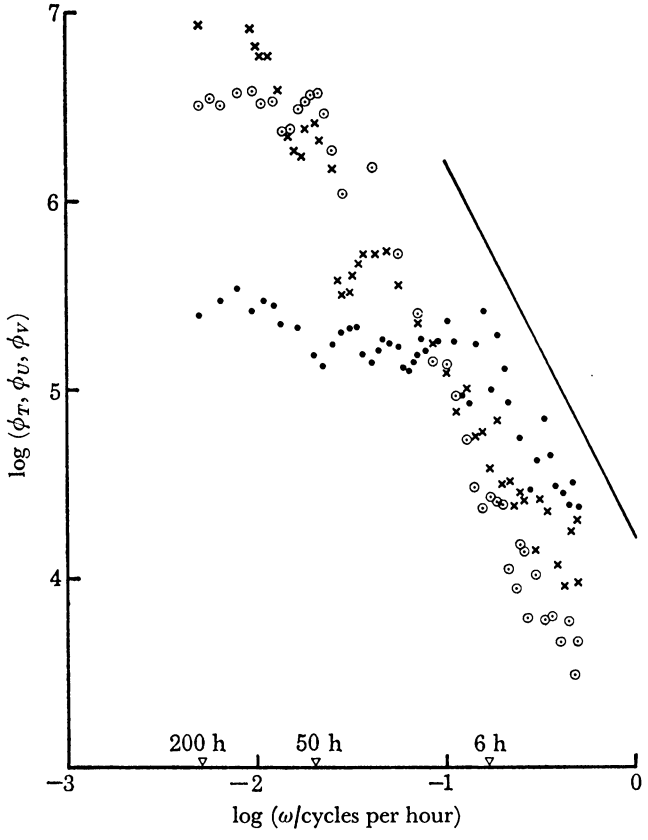

FIGURE 5. The frequency spectrum of the temperature (circles), current along the Loch (crosses) and current across the Loch (dots) measured by a current meter at 49.5 m depth at D (figure 1), 19 August–20 October 1971. The line shows a −2 slope.

An example of the calculated form of the first five internal modes is given in figure 4. The wavelength chosen corresponds to twice the width of the Loch, although this is so long in comparison with the depth that the model structure is scarcely affected if longer waves are considered. The frequency of each wave is given in the caption. Figure 4 also illustrates how irregular is the distribution of Richardson number, which Phillips (1966) has shown is proportional to N^{-2} for very long waves. The distribution of Richardson number in internal waves is considered in appendix 3.

Figure 5 shows the power spectra of longitudinal and transverse currents, and of the temperature. The temperature spectrum is flat for periods higher than about 100 h, shows a peak near 50 h and a first subharmonic, and decays at higher frequencies with a power law near −2. The longitudinal current shows a similar behaviour, but rises somewhat higher at frequencies

below 50 h. The transverse current is almost flat for periods which exceed 6 h (approximately the period of the second transverse internal mode) and then decays at higher frequencies although containing slightly more power than the longitudinal current. We conclude that longitudinal internal waves with periods exceeding 50 h (those of higher vertical wave number than the first) are not strongly excited and that the high frequency oscillations are almost isotropic in horizontal wave number. Dr J. Simpson (private communication) has found that the inverse square law for temperature continues to frequencies of 10 cycles h^{-1}, comparable to the local Brunt–Väisälä frequency.

The period of the longest wind generated waves observed was about 3 s corresponding to a wavelength of 14 m. In strong winds groups of 4 or 5 waves are commonly observed with one or two of the highest in the group breaking and producing whitecaps. The highest waves have amplitudes of about 50 cm, and near-surface particle speeds of about 1 m s^{-1}. These near-surface motions will not properly be followed by the P.C.M. (see appendix 1).

The surface wavelengths are however so much less than the mixing layer thickness that little of the layer is influenced by wave-induced motions, and the estimates of shear by the P.C.M. will not suffer from sampling problems arising from resulting non-stationarity of the flow in the wave field. The particle speeds are approximately $a\sigma \exp(-kz)$ where a is the wave amplitude, σ the frequency, k the wavenumber and z the depth. For example at a depth of half a wavelength the surface speeds are reduced by a factor 0.043. Near-surface values are comparable with the probe ascent speeds used to make estimates of the horizontal currents, which are therefore subject to error. Measurements of the wave-produced horizontal velocity at the sampling intervals of 0.5 s as the probe rises lead to apparent vertical shear and even though the vane cannot respond sufficiently rapidly to follow the motions, near-surface values of apparent shear may exceed the shear in the mean flow and lead to spurious results. In the analysis these have been removed by temporal averages, but they can be seen in some of the profiles of velocity which are presented below. Similar apparent shear may be produced by the external seiche motions, but the currents associated with them are small (of order 1 cm s^{-1}) and the net shear is below the noise threshold. However, the internal waves which follow the internal surge have periods which are not sufficiently large in comparison with the time taken to make a profile, and some spurious shears may result.

If we take an estimate for ϵ, the rate at which energy is dissipated per unit volume in the near-surface layers, as 10^{-3} $cm^2 s^{-3}$ (consistent with estimates by Stewart & Grant 1962; Grant, Moilliet & Voget 1968; and the estimates in § 4 below), we find a Kolmogoroff dissipation scale, $(\nu^3/\epsilon)^{\frac{1}{4}}$, for the turbulence of 0.18 cm, where ν is the kinematic viscosity, about 0.01 $cm^2 s^{-1}$, and a Batchelor scale $(\nu^2 K/\epsilon)^{\frac{1}{4}}$ for diffusive cut-off as 0.11 cm, where K is the molecular thermal diffusivity, about 1.4×10^{-3} $cm^2 s^{-1}$. Both these scales are well below the sampling interval and thus the turbulent dissipation spectrum and the fine turbulent structure cannot be resolved. In particular the failure to resolve the temperature to the Batchelor scale means that estimates of the eddy thermal diffusivity based on KD, where D is the Cox number, the ratio of temperature gradient variance to square of the mean gradient (Osborne & Cox 1972; Gregg, Cox & Hacker 1973; Gregg 1975) will lead to serious underestimates. (A similar limitation would apply to estimates of ϵ based on the formula $\epsilon = \frac{15}{2}\nu(\overline{\partial u/\partial z})^2$, where $\partial u/\partial z$ is the velocity gradient, and the bar implies a temporal and spatial average, used, for example, by Osborne (1974).) The Brunt–Väisälä frequency, N, has mean values of typically 1.7×10^{-3} s^{-1} or less corresponding to periods of 1 h or more in the near-surface mixing layer and 0.02 s^{-1} or less in the thermocline.

The Ozmidov length scale, $l_c \equiv \alpha \epsilon^{\frac{1}{2}} N^{-\frac{3}{2}}$, is postulated to be that vertical scale below which isotropy of the turbulent motion may be expected (Ozmidov 1965). The universal constant α is found to be approximately unity (Ozmidov 1965; Thorpe 1973). The scale l_c is calculated to be about 4.5 m in the mixing layer and less in the thermocline. Larger scales of motion are limited in their vertical extent by the effects of buoyancy and are expected to be non-isotropic. The sampling interval of the P.C.M. is sufficiently small to resolve scales below the Ozmidov length scale. (In § 4 we shall describe how an estimate of l_c may be made and thence estimates of ϵ and of K_B, the turbulent diffusion coefficient of heat.)

The vertical velocities below the region of influence of surface waves are probably small and no direct measurements have been made. About 1 cm s^{-1} may be typical of convective conditions, although rather higher values may occur beneath the surface convergences of wind rows in association with the Langmuir vortex circulation. Vertical velocities in billows resulting from Kelvin–Helmholtz billows have been estimated as 0.2 cm s^{-1} (Thorpe & Hall 1974) and might reach 1 cm s^{-1} in extreme conditions.

The largest vertical particle speeds induced by internal waves occur in the wave train following the surge and has been estimated in particular cases by following isotherms and may be derived from theoretical models of the waves. Maximum values of 1.3 cm s^{-1} are typical. These various vertical motions produce corrections to the estimates of horizontal current of less than about 10 %, and may be expected to occur in easily recognizable conditions.

3. Measurements of small- and medium-scale structure

3.1. *Introduction*

The observations which are discussed below are a selection of the more interesting events in August, September or October 1973 measured at position A in figure 1. We shall describe them in chronological order. In some cases the events observed on one day have repercussions on another; the surge observed on 30 September was the result of the storms of the preceding days. For each day we shall present a description of the weather and a variety of diagrams which illustrate the nature of the most significant events or portray the mixing processes.

The profiles of density frequently show a layered structure similar to that found in the Mediterranean thermocline (Woods 1969) with large temperature gradients (the 'sheets') alternating with relatively uniform layers. To obtain a measure of the intervals between the 'sheets' we have constructed 'structure histograms' of the vertical distances between successive density gradient maxima which exceed a certain given value (see figure 6). Examples are given in figures 10 and 22.

On 31 August and 6 and 28 September strong winds blew, causing near-surface mixing and frequent inversions (or regions of gravitational instability in which the density increases upwards) in the upper layers. These are analysed in terms of the frequency of the occurrence of inversions, a parameter analogous to an intermittency factor in the study of turbulence in a homogeneous fluid (see, for example, Townsend 1956). Intermittency has proved a very valuable diagnostic tool for analysing turbulent boundary layers in homogeneous laboratory flows. The concept is valid because of the sharp distinction which exists between turbulent and laminar homogeneous flows, the former being rotational and the latter irrotational. Such a formal distinction is not possible in stratified fluids, for laminar flows, internal waves for example, may be rotational. In practice however such a distinction is seldom exploited for vorticity is very difficult to measure,

and a semi-subjective criterion for turbulence, for example, the magnitude of the r.m.s. speed derivative, is used (see Hedley & Keffer 1974, for a discussion). From a practical point of view, the stratified flow affords an advantage. The magnitude of the noise level, $\Delta\sigma_T$, of the sigma T estimate from the P.C.M., implies that, when the density is increasing as the probe ascends, so that the water is gravitationally unstable, the smallest Rayleigh number,

$$Ra = \frac{gd^3(0.001\Delta\sigma_T)}{\nu k}, \tag{2}$$

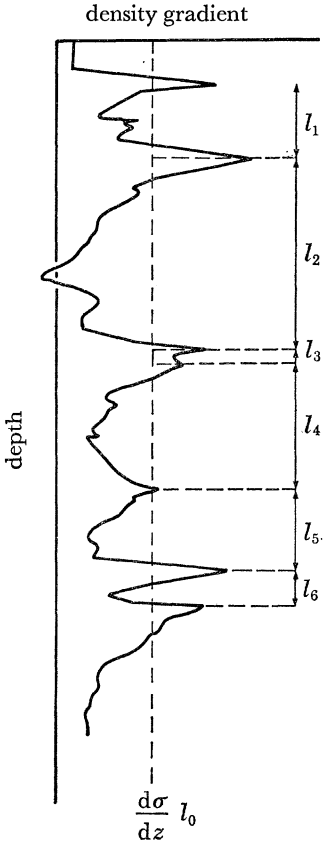

FIGURE 6. The set $\{l_i\}$ of intervals between density gradient maxima which exceed a threshold value $d\sigma_T/dz|_0$. Histograms over several profiles are used to construct the 'structure histograms', figures 11 and 23.

which can be resolved above noise level, is 2.3×10^4. (Here ν is the kinematic viscosity of water, about 0.01 $cm^2 s^{-1}$ and g is the acceleration due to gravity.) This far exceeds the critical Rayleigh number (657.5 for free-free boundaries (Chandrasekhar 1961)) at which natural convection may be expected to set in, and hence any significant inversion in density (that is an increase of density above noise level as the probe ascends) necessarily implies that instability and mixing is either present or immediately imminent. In the absence of any other test, we use this as a criterion for the presence of turbulence. This criterion is not of course absolute. Turbulence may occur at large Reynolds number in a homogeneous fluid in which the Rayleigh number is zero, or in a stably stratified fluid, although in the latter density inversions will usually occur. The inability of the probe to measure smaller density differences implies that 'fossil turbulence', the thermal remains of an active mixing event, is not resolved and therefore does not complicate the interpretation of the observations. We shall use χ, the proportion of fluid which is unstably stratified

in a given vertical interval, as an intermittency index. (2χ would correspond approximately to the classical intermittency index.) In calculating χ, we include only differences in σ_T which exceed the noise level, taken as $10^{-3}\sigma_T$ units.

A second index which is used to indicate the presence of fine structure is the Cox number,

$$D(h, z) = \overline{(\partial\rho/\partial z)^2}/(\overline{\partial\rho/\partial z})^2, \tag{3}$$

where $\partial\rho/\partial z$ is the density gradient and the average is taken over some selected vertical interval, h. This is not a precise measure of diffusion for the reasons given in § 2. Both χ and D may be averaged over several profiles made through the same depth range, or contoured together with values of Richardson number, Ri, estimated for the same vertical intervals.

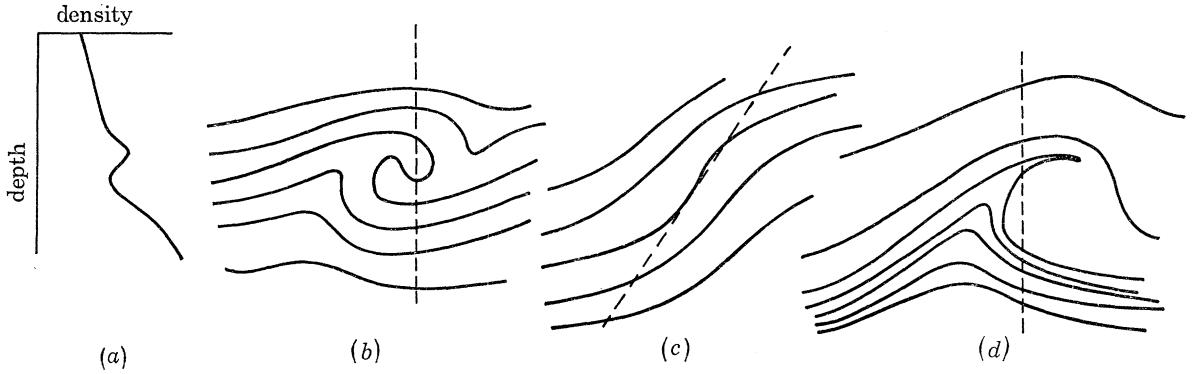

FIGURE 7. (*a*) Sketch of a density profile containing an apparent inversion, produced as a result of the P.C.M. passing through the structure of isotherms shown in (*b*), (*c*) and (*d*). The dotted line shows the hypothetical path of the instrument.

The presence of inversions may be used as a gauge of the vertical displacements which occur in the Loch. Suppose that a profile of density like that shown in figure 7*a* is measured by the P.C.M. This might be the result of an upward vertical motion of a stable stratification at a speed which temporally exceeded the vertical probe speed, but, except in the near-surface wave induced motions this is unlikely (§ 2). Three other possibilities exist which are shown in figure 7*b*, *c* and *d*, where the line indicates the upward path of the probe through hypothetical contours of σ_T. (In practice both probe and contours are moving.) All examples are supposed to be gravitationally stable on the left. Both (*b*) and (*d*) are truly unstable, the former representing Kelvin–Helmholtz instability and the latter Holmboe instability (for examples, see figures 5*a* and 3*d*, Thorpe 1968). However (*c*) is not unstable, and contains no true inversions. It may occur when sloping isotherms are carried, or propagate, past the ascending thermistor. This is possible if the relative horizontal speed of the pattern exceeds the vertical speed of the probe divided by the tangent of the isotherm slope. The maximum relative horizontal speeds† are about one and a half times the vertical probe speed and hence wave slopes exceeding about 34° must be present for this apparent instability to appear. Although such extreme slopes may sometimes occur, they will usually be associated with incipient wave breaking (Orlanski & Bryan 1969) or a shear instability of the kind already mentioned. We shall therefore assume that apparent inversions reflect true instability. It remains to quantify the vertical displacement involved.

† Larger speeds of internal wave propagation are found associated with long internal waves. For example, the surge propagates at about 35 cm s^{-1} but has tangent slope of only about 0.03. Shorter waves may have higher slopes, but move less rapidly.

PHILOSOPHICAL TRANSACTIONS OF THE ROYAL SOCIETY A MATHEMATICAL, PHYSICAL & ENGINEERING SCIENCES

Our first inclination was to compare the observed profile with an average of several profiles but it soon became clear that because of internal waves and gradual temporal changes, perhaps due to horizontal advection or general cooling or heating of the lake, such a process led to estimates which were not statistically independent of the averaging process, and a method was therefore evolved in which the displacements are determined from individual profiles, and afterwards averaged over several. We compare the observed profile of σ_T with one obtained by rearranging this profile, conserving mass (and heat), to form a stable profile. Each half second observation of density is supposed to represent a block of fluid (a 'fluid particle') extending for a distance on either side of the depth of the observation equal to the distance moved by the probe in one quarter of a second. The vertical displacements are then the minimum distances which fluid particles need be moved from the observed profile to produce the synthetic stable profile. (For an example see figure 14.)

We may formally define the 'stable' profile as follows. If $\rho(z)$ is the observed density profile, measured between $z=-H$ and $z=H$, and $\Pi(z)$ is the equivalent stable profile (so that $\mathrm{d}\Pi/\mathrm{d}z \leqslant 0$ everywhere) then $\Pi(z)$ is given by

$$z+H=-\int_{\max\rho}^{\Pi}(\Sigma|(\mathrm{d}\rho/\mathrm{d}z)^{-1}|)\,\mathrm{d}r,$$

where the summation is taken over all values of $|(\mathrm{d}\rho/\mathrm{d}z)^{-1}|$ for which $\rho=r$. For example if

$$\rho(z)=\begin{cases}\rho_0(1-\Delta), & H\geqslant z\geqslant h,\\ \rho_0(1+\Delta\sin(3\pi z/2h)), & |z|<h,\\ \rho_0(1+\Delta), & -H\leqslant z\leqslant -h,\end{cases}$$

giving a continuous profile of density and its first derivative, with an unstable region between $-h$ and h, it may easily be shown that the equivalent stable profile is

$$\Pi(z)=\begin{cases}\rho(z), & H>|z|>h\\ \rho_0(1-\Delta\sin(\pi z/2h)), & |z|<h.\end{cases}$$

Since $\int_{-h}^{h}\rho\,\mathrm{d}z=\int_{-h}^{h}\Pi(z)\,\mathrm{d}z=2h\rho_0$, the total mass is conserved. The 'displacement', d, is the vertical shift of fluid of given density. If at level z the observed density is ρ_1 and in the stable profile the density Π is equal to ρ_1 at level y (and, if $\Pi(y)$ is constant at $\Pi=\rho_1$, $z-y$ is a minimum), then $d(z)=z-y$. The mean displacement $\int_{-H}^{H}\mathrm{d}(z)\,\mathrm{d}z$ is zero. The r.m.s. displacement between $-h$ and h in the given example is $(8h/9)\{1+(3/\pi^2)(\pi^2-8)\}^{\frac{1}{2}}\approx 1.18h$, and gives a measure of the depth of gravitationally unstable fluid. The difference between the potential energies of the observed and the 'stable' profiles is $\int_{-H}^{H}g\rho\,\mathrm{d}(z)\,\mathrm{d}z$, which equals $(88/9\pi^2)\,\Delta\rho_0 h^2 g$ in the example, and depends both on the total density increment as well as on the r.m.s. displacement.

To be consistent with the known noise levels of σ_T of the instruments, we shall only recognize a displacement if the density in the observed profiles differs from that in the synthetic profile by more than the calculated noise level. In a profile which is entirely stably stratified the displacements, as defined, are everywhere zero, and so too is χ, the intermittency index. If unstable regions occur, then both χ and the displacements will be non-zero, and the r.m.s. displacement averaged over several profiles and over a small depth range, is a measure of the vertical displacements caused by the turbulent motions before significant molecular diffusion has occurred.

These displacements will be used to characterize the nature of the disturbance by identifying the level of origin of unstable fluid, to compare the magnitude of these displacements in different levels of the Loch and to provide estimates of the potential energy involved in the mixing process.

3.2. *Observations*

3.2.1. 31 *August; wind mixing and internal motions*

On the preceding days the wind strength had been variable, mainly southwest and reaching 8 m s^{-1} on 30 August. Heavy rain and overcast skies at 09h00 G.M.T. on the 31st gave way to showery weather and occasional sunshine in the late afternoon. The southwesterly wind increased from 8 to 10.5 m s^{-1} at 14h00 G.M.T. and then remained fairly steady, causing frequent white-capping throughout the day. The air temperature rose from 12.1 to 16.1 °C, exceeding the Loch surface temperature at mid-day, while the latter fell steadily from 13.6 to 13.4 °C.

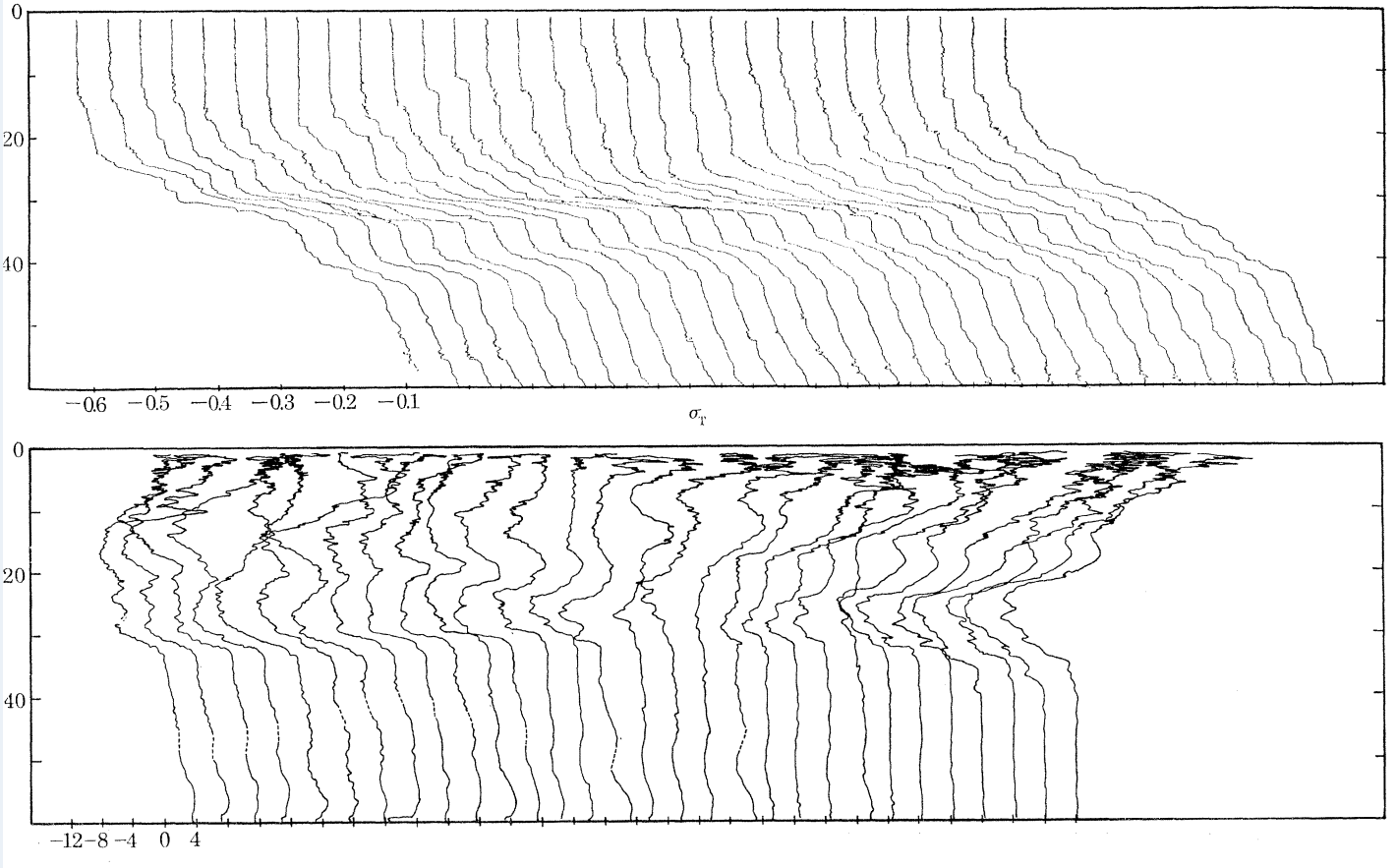

FIGURE 8. Profiles of density (σ_T) and current along the Loch in direction 036° on 31 August. Each successive density profile is displaced by 0.05 σ_T units to the right, and each velocity profile by 4 cm s^{-1}. The times of the profiles are shown in figure 9.

The profiles obtained by the P.C.M. are shown in figure 8 and contoured in figure 9. The near-surface drift is to the northeast but in the thermocline at 25 m a southwest going jet of variable strength is observed, and deeper still the flow is again northeasterly, although of decreasing strength.

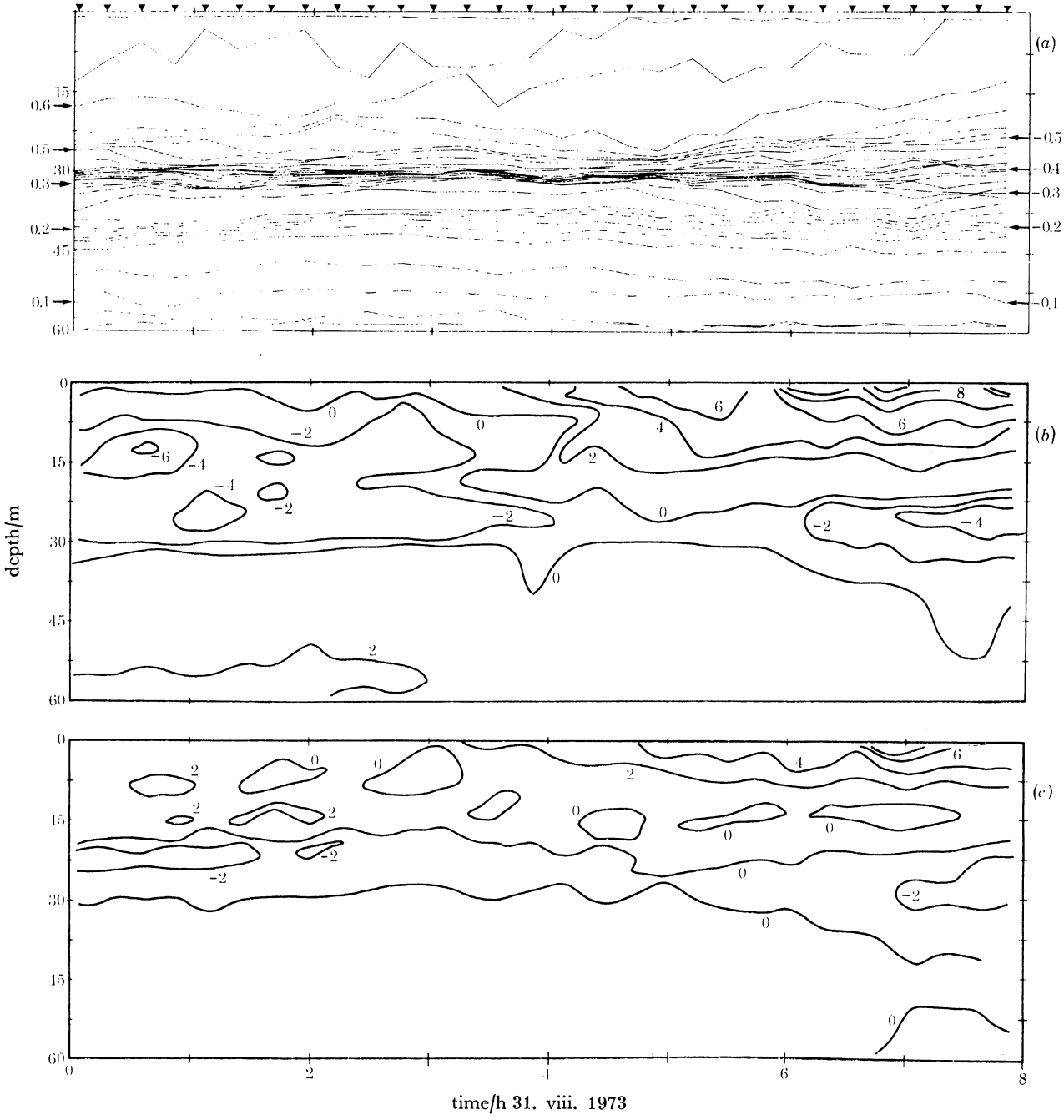

FIGURE 9. (*a*) Contours of density (σ_T), (*b*) current along (longitudinal, in direction 036° *T*) and (*c*) across (lateral, 126° *T*) the Loch on 31 August. The density contours are at $0.02\sigma_T$ units interval and current at 2 cm s^{-1} interval. The time is measured from 09h05 G.M.T. and the times at which profiles were started are marked by triangles on the top axis. The lines at the top and bottom of each contour set mark the limits of the sampled depth. The contours have been drawn as if the profiles were made instantaneously at their starting times.

PHILOSOPHICAL TRANSACTIONS OF THE ROYAL SOCIETY A MATHEMATICAL, PHYSICAL & ENGINEERING SCIENCES

The variable velocity structure in the thermocline may possibly be due to internal waves of the second mode. The structure in the internal modes corresponding to the density distribution of the fifth profile made on 31 August with wavelengths of 3 km is shown in figure 4. The second mode has a horizontal velocity distribution with a thermocline jet-like structure which resembles that observed.

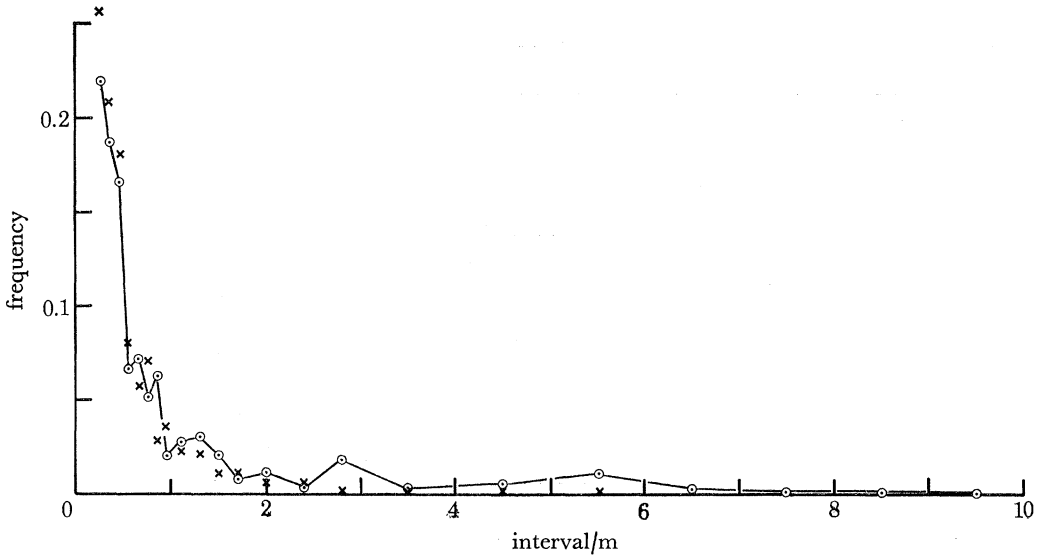

FIGURE 10. The 'structure histogram' (see figure 6) for profiles of density on 31 August. The circles are for the threshold value of gradient $6.0 \times 10^{-4}\sigma_T$ units cm^{-1} and the crosses are for $1.7 \times 10^{-4}\sigma_T$ units cm^{-1}.

Two regions of large density gradient are present near 30 m and 40 m, although the former becomes more diffuse during the day. The layered structure is revealed in the structure histogram (see § 3.1), figure 10. Weak frequency maxima are seen at separations between successive density gradient maxima of 2.8 m and 5.5 m for gradients exceeding $6 \times 10^{-4}\sigma_T$ units cm^{-1}, but none at the lower threshold. The most frequent vertical distances between successive maxima are however less than 30 cm, implying that the layers which are observed are usually not single maxima but have a small-scale structure consisting of several large and small gradients. The relation of the density and current field is shown in figure 11, where the arrows show the direction and strength of the mean current between the dotted positions where the density gradient exceeds $7.5 \times 10^{-4}\sigma_T$ units cm, approximately 1 °C m^{-1}. The density gradient has several peak in each of the regions of large gradient as shown by figure 10. There is little current shear across the lower region of large density gradient, but generally large shear across the upper.

Near the surface the motions are perturbed by the surface waves (figure 8). Their influence is seen to extend to a depth of 4 or 5 m at the end of the observation period. Frequent inversions are seen in the upper 20 m. In the first 8 profiles a fairly well-mixed layer appears to be developing, but this is then lost, possibly a result of horizontal non-uniformity in the near-surface regions and advection, although the increasing stability as the air temperature rose to exceed the Loch surface temperature may have played a part. These changes are not accompanied by any reduction of the intensity of inversions near 20 m depth.

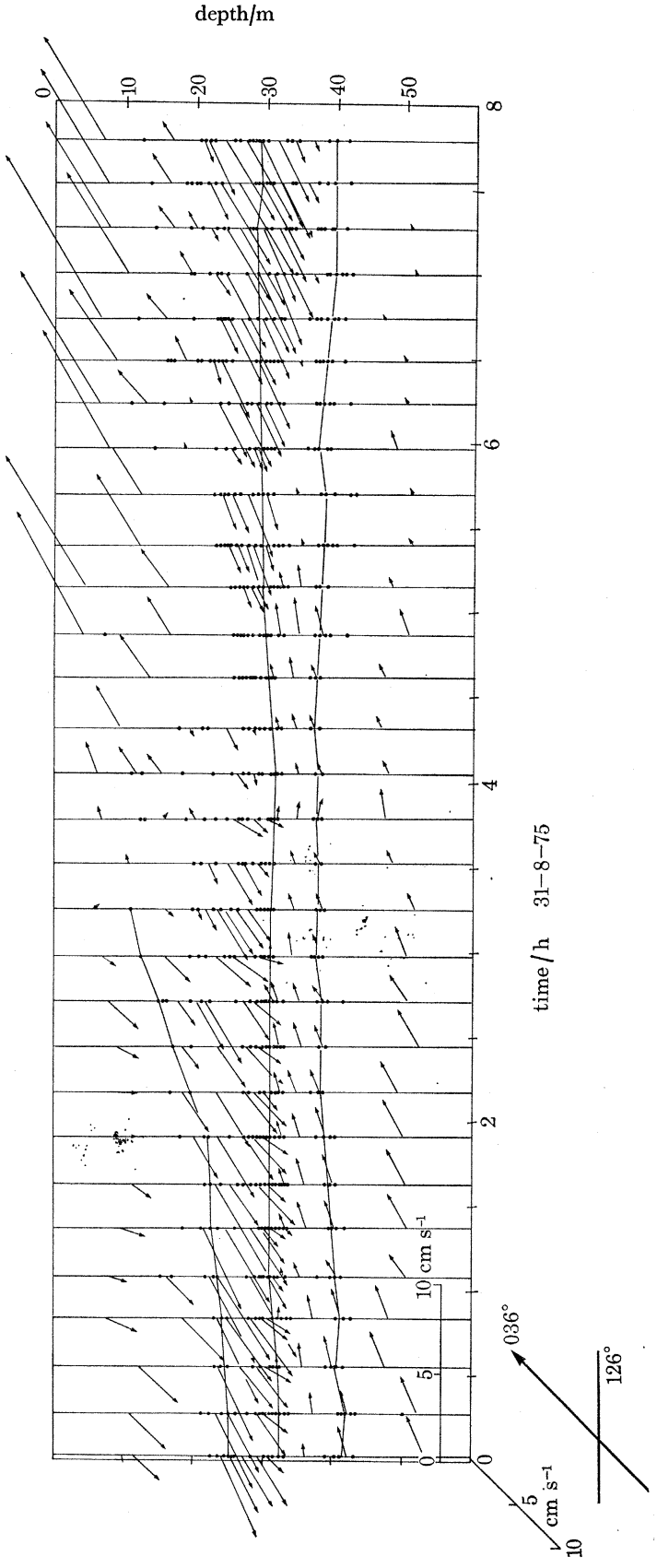

FIGURE 11. Diagram relating the currents in the Loch, indicated by the direction and length of the arrows, to the density structure. The horizontal scale is the time in hours after 09h05 G.M.T. and the vertical scale is depth (m). Each successive vertical line represents a profile, and positions at which the density gradient reaches a maximum exceeding $7.5 \times 10^{-4} \sigma_T$ units are marked by dots. The current, averaged between successive dots, is indicated by the length and direction of the arrows. The lines joining dots on successive profiles show the trend of well-defined regions of large density gradient.

PHILOSOPHICAL TRANSACTIONS OF THE ROYAL SOCIETY A MATHEMATICAL, PHYSICAL & ENGINEERING SCIENCES

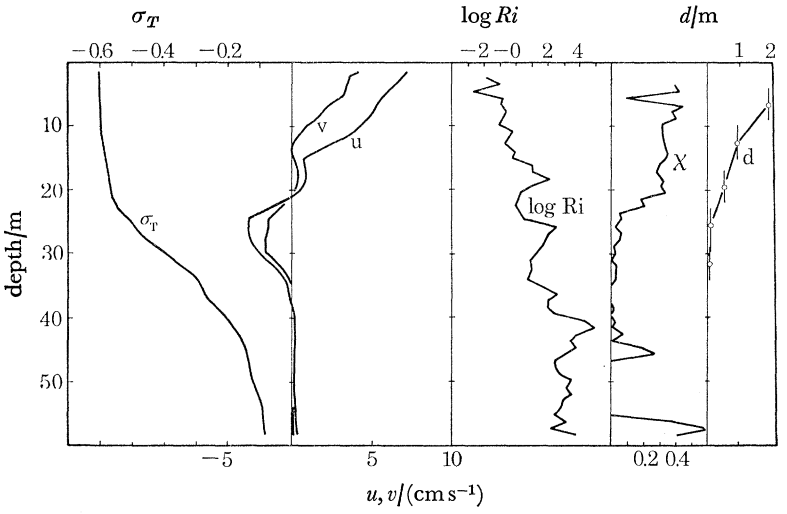

FIGURE 12. Mean values of density (σ_T), velocity components (u in direction 036° T along the Loch and v in direction 126° T across), log Ri (calculated from the mean currents and densities), χ and r.m.s. displacements. The averages (except those of d) are taken over successive 1.06 m depth intervals for the last nine profiles on 31 August. The vertical bars on the d-profile indicate the vertical distances over which the r.m.s. displacements are calculated. The large values of χ below 40 m appear to be due to disturbances caused by the P.C.M. during its descent.

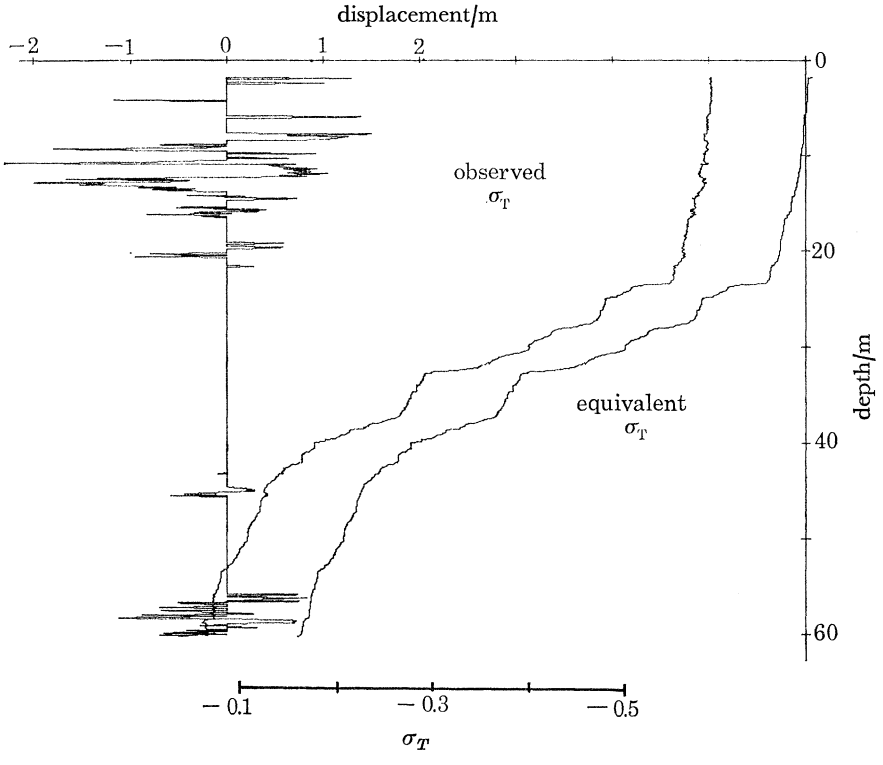

FIGURE 13. The 25th profile of density (σ_T) on 31 August as observed, the 'equivalent' stable profile (moved 0.1σ_T units to the right) and the displacements needed to produce the stable profile from that observed as explained in §3.1. The inversions and corresponding displacements near the bottom of the profile appear to be due to disturbances caused by the P.C.M. during its descent.

A northeasterly drift extending down to 15 m is established in the last 3 h of observation. The flow is then more uniform and the last 9 profiles have been analysed together. (These will be referred to as 31–8 below.) Figure 12 shows the mean values averaged over the 9 profiles and over vertical distances of 1.06 m. The Richardson number has a mean value close to 0.1 in the near-surface shear layer, but rises to values exceeding unity below. The shear layer overlying the southwesterly flow near 25 m has a minimum Richardson number close to unity, but higher values, between 2 and 10^4 are found at greater depths. The intermittency function χ has high values of 0.3 to 0.4 near the surface, but fails suddenly at about 23 m to values near 0.05. The profile of the r.m.s. displacements (see § 3.1) shows the amplitude of the mean vertical motions falls from values exceeding 1 m above 15 m to less than 10 cm at 25 m. The mean potential energy per unit volume associated with these displacements in the upper 15 m is 0.073 ± 0.031 $\mathrm{cm^2\,s^{-2}}$ (± 1 s.d.). An example of the observed profile, the reordered stable profile and the displacements involved, are shown in figure 13.

3.2.2. 6 *September; wind mixing in the upper layers*

The preceding two days were calm with rain, but a southwesterly wind rose during the night of 5 September and by 09h00 G.M.T. on 6 September exceeded 10 $\mathrm{m\,s^{-1}}$ in gusts while averaging 8.5 $\mathrm{m\,s^{-1}}$. The wind speed fell gradually during the day to about 6.5 $\mathrm{m\,s^{-1}}$ at 18h00. Widespread whitecapping was observed with waves of up to 30 cm amplitude and 3 s period. The sky was overcast with fair visibility, improving during the day. The air temperature exceeded the Loch surface temperature by an average of 1.5 °C. There was a steady decrease in the surface temperature of the Loch from 13.5 to 12.9 °C during the day, probably the result of mixing with the deeper cold water in the Loch and advection, rather than to radiative cooling.

Figures 14 and 15 show the profiles and contours of density and current. The times at which profiles were made are marked in figure 15. The σ_T contours (figure 15) show a general rise during the day. This is probably a response to large scale changes (a gradual depression of the thermocline at the northeast end of the Loch) and does not reflect local mixing. The mean shear is most intense in the upper 10 m where it increases during the day, and throughout the upper layer frequent inversions occur but do not persist in any obviously ordered way from one profile to the next. There are two persistent regions of large density gradient, one beginning at about 15 m and the other at 30 m, but rising some 7 m during the day. A third large gradient region beginning at about 20 m disappears after about 3 h. These large gradient regions have been emphasized in figure 16 by plotting the positions of density gradient maxima which exceed $6.0 \times 10^{-4}\sigma_T$ units/cm (approximately 0.80 °C $\mathrm{m^{-1}}$) and averaging the intermediate currents. When this simplified pattern is compared with the profiles (figure 14), it can be seen that frequently (but not always) the regions of strong density gradient form boundaries of different current patterns. (Figure 4 shows that this would be consistent with currents generated by long internal waves. It might also be due to spreading and interleaving of waters of different temperature in a collapse of regions which had been mixed, perhaps by the breaking of internal waves on the sides or ends of the Loch.) Below 30 m the currents are directed towards the south-west, that is against the wind direction. The flow direction was confirmed by the current meter records. The mean shear measured by the P.C.M. agreed well with the current meter values, but the current magnitudes were some 3.5 $\mathrm{cm\,s^{-1}}$ less, presumably because the time to reach equilibrium at the bottom of the profile was not sufficient.

PHILOSOPHICAL TRANSACTIONS OF THE ROYAL SOCIETY A MATHEMATICAL, PHYSICAL & ENGINEERING SCIENCES

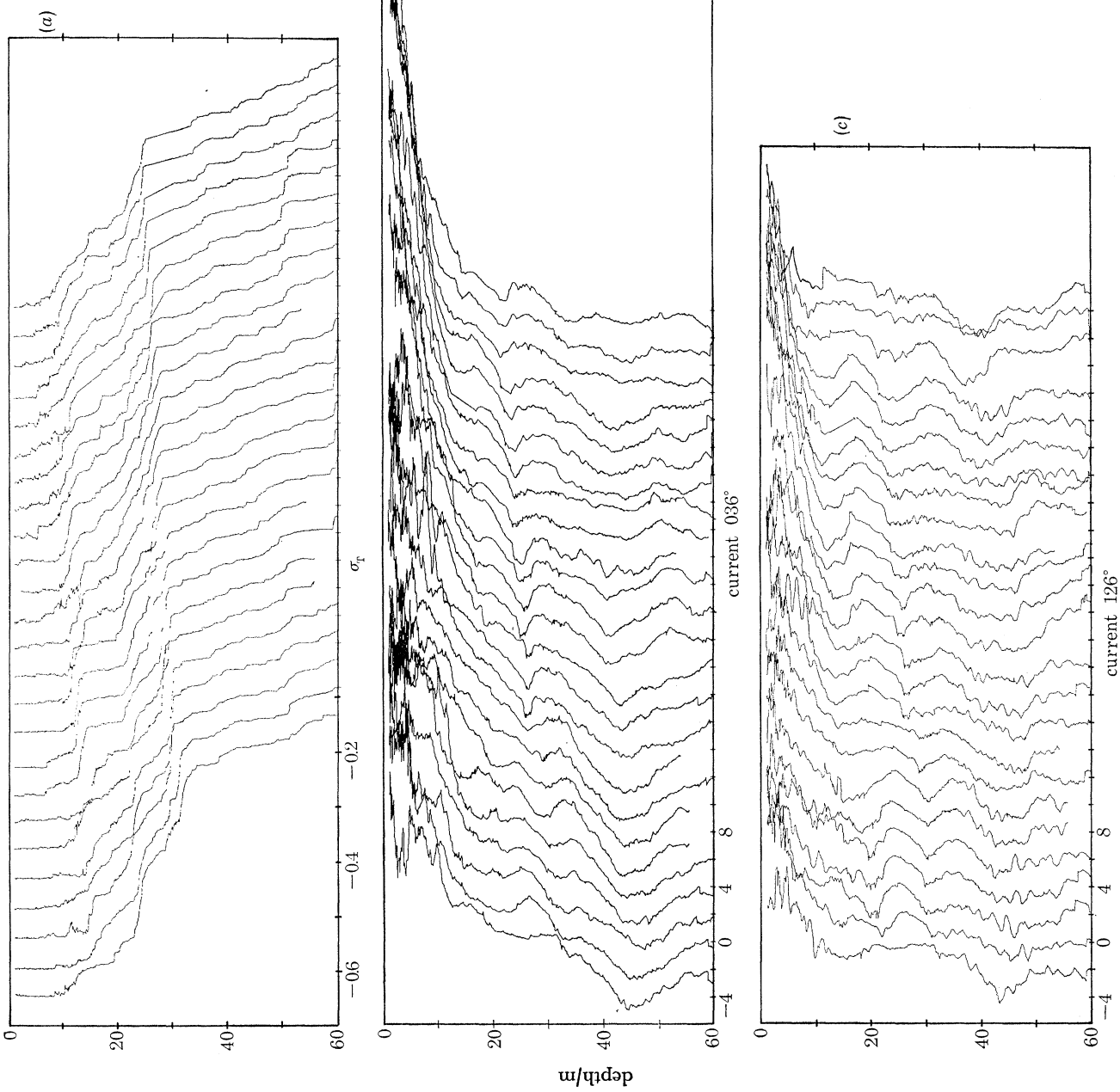

FIGURE 14. Profiles of (*a*) density (σ_T) and current (*b*, longitudinal, *c*, lateral) along the Loch in direction 036° on 6 September. Each successive density profile is displaced by $0.05\sigma_T$ units to the right, and each velocity profile by 4 cm s^{-1}. The times of the profiles are shown in figure 16.

Figure 17*a* shows the profiles for χ and that, although buffered from the surface by a region of large density gradient, the layer below 15 m contains frequent inversions. Below 30 m the inversions are rare and seldom can signs of inversion be traced from one profile to the next. The profiles of D and Ri averaged over 1.5 m intervals are shown in figure 17*b*, *c* and the influence of the layers can be seen generally to reduce D and increase Ri. The Richardson number is lowest near the surface and decreases during the day, but like the other contours, exhibits a high degree

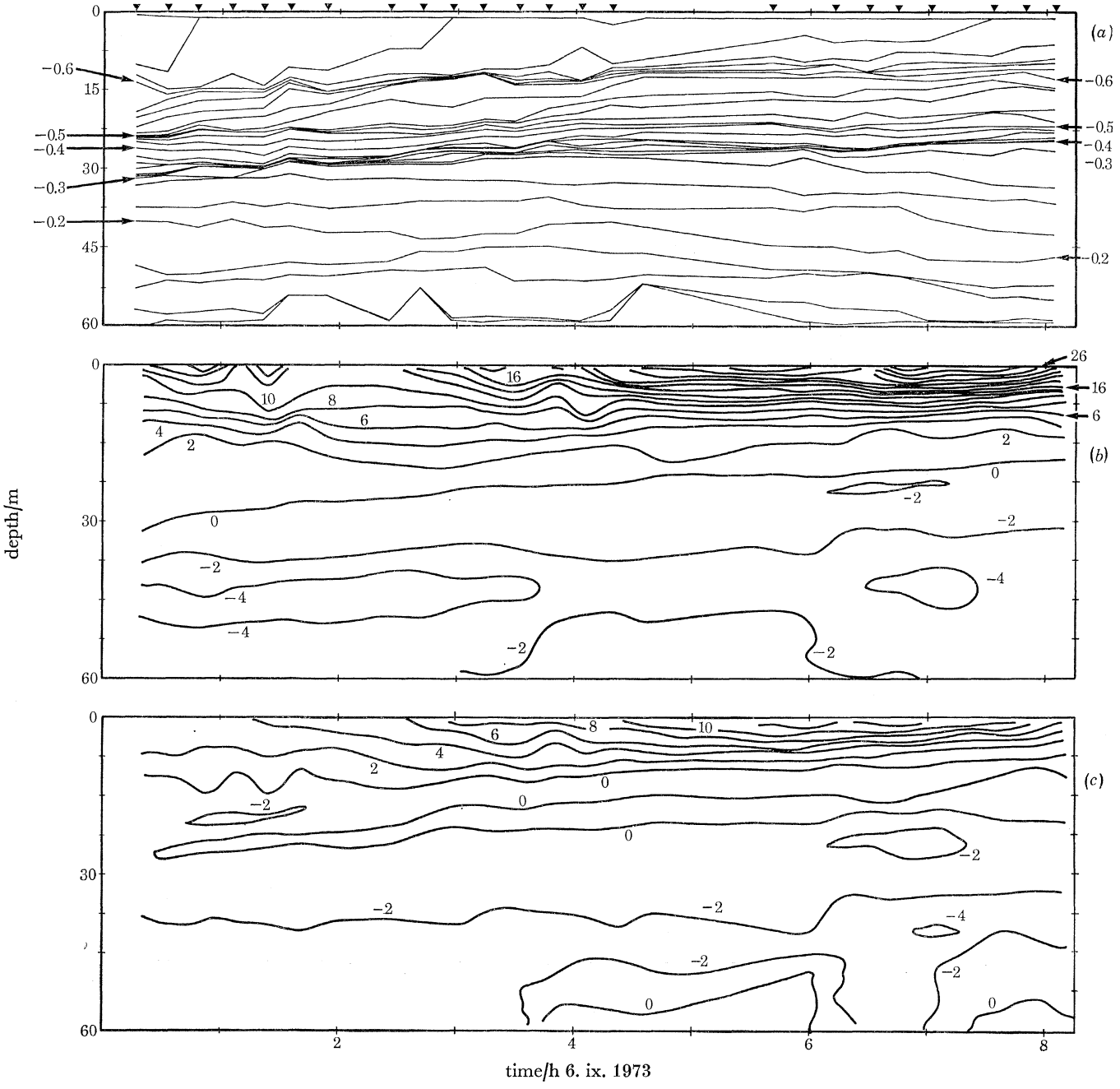

FIGURE 15. Contours of density (σ_T) and current on 6 September. The time is measured from 08h50 G.M.T. Other details are given in the caption to figure 9.

PHILOSOPHICAL TRANSACTIONS OF THE ROYAL SOCIETY A MATHEMATICAL, PHYSICAL & ENGINEERING SCIENCES

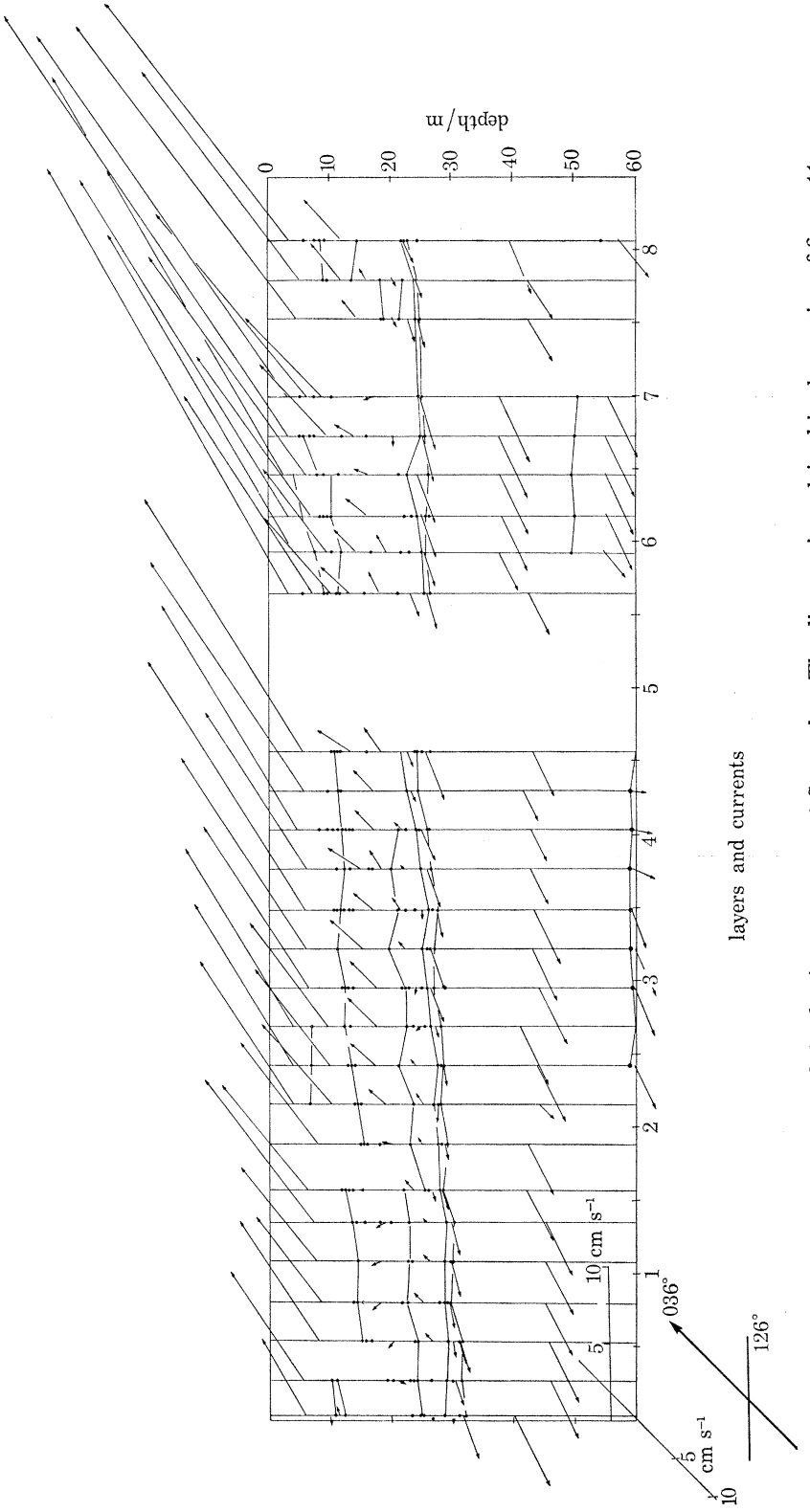

FIGURE 16. The currents and the density structure on 6 September. The diagram is explained in the caption of figure 11.

PHILOSOPHICAL TRANSACTIONS OF THE ROYAL SOCIETY A MATHEMATICAL, PHYSICAL & ENGINEERING SCIENCES

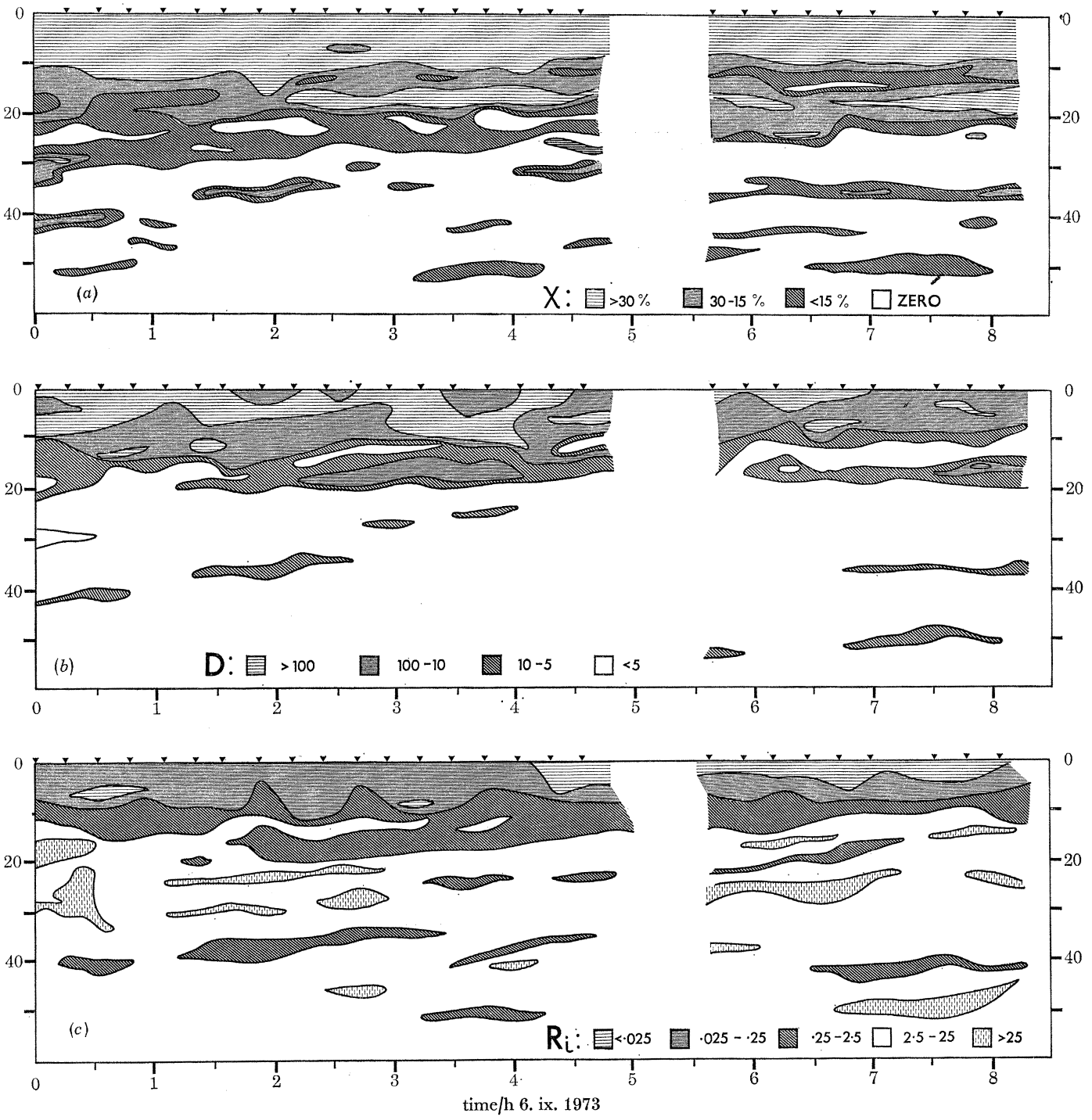

FIGURE 17. Contours of (*a*) frequency of density inversions, χ, (*b*) the parameter D (equation (4)) and (*c*) Richardson number, Ri, based on averages taken over 1.5 m on 6 September. The time is measured from 08h50 G.M.T.

of uniformity from one profile to the next in the upper layers, becoming less firmly structured at depth.

Mean profiles are shown in figure 18. Three profiles of Richardson number derived in different ways are shown. The values of Ri calculated by using the r.m.s. shear are much smaller than those using the mean shear. The mean depth-averaged value of the r.m.s. shear divided by mean shear is 6.95, and there is no notable trend in the ratio with depth. The mean χ profiles have values exceeding 0.4 in the upper 10 m where turbulence is almost continuous, but these fall to 0.1 at about 15 m, where the upper density gradient maximum is found. The profile then exhibits the

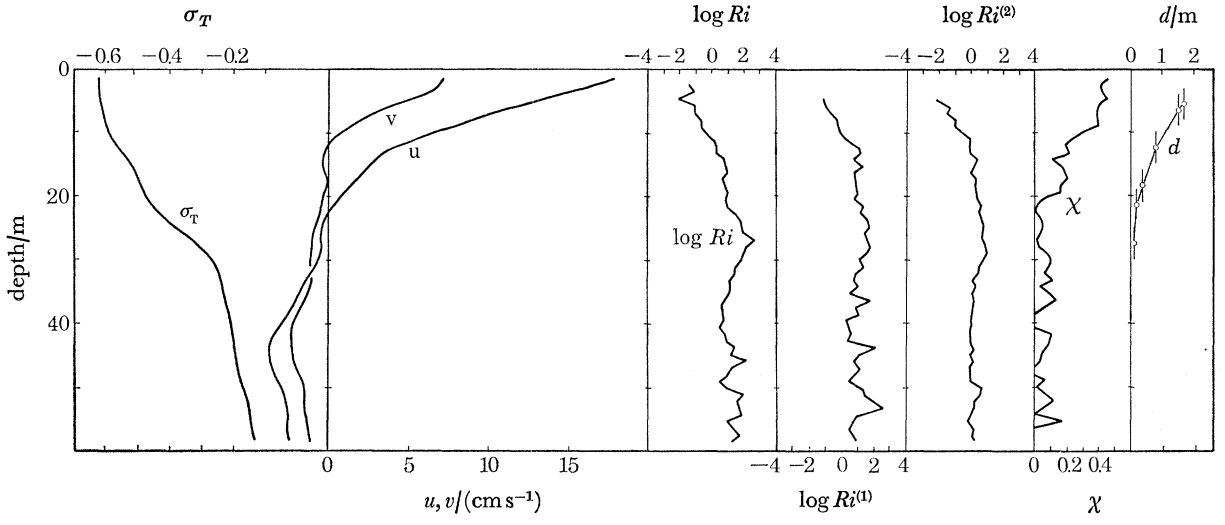

FIGURE 18. Mean values of density (σ_T), velocity components (u in direction 036° T along the Loch and v in direction 126° T across), log Richardson number (log Ri) derived from the mean currents and density, log $Ri^{(1)}$ (where the Richardson number, $Ri^{(1)}$, is the mean Richardson number), log $Ri^{(2)}$ (where the Richardson number, $Ri^{(2)}$, is based on the r.m.s. shear), χ and r.m.s. displacements, d. The averages (except for d) are taken over successive 1.06 m depth intervals for the profiles on 6 September. The vertical bars on the d-profile indicate the vertical distance over which the r.m.s. displacements are calculated.

second maximum at about 18 m on which we remarked in connection with figure 17. Below 25 m χ has an irregular structure with a mean value of 0.04 reflecting a low and intermittent level of turbulence. The r.m.s. displacements increase from about 20 cm at 27 m to 1.7 m at 6 m depth. Above 9 m, 3.5% of the displacements exceed 4 m and 17.5% exceed 2 m. The intermittent character of the displacement below 10 m is reflected in high values of the excess

$$E = m_4/m_2^2 - 3,$$

where m_i is the ith moment of the distribution of the displacement about the mean. The values of E exceed 80 below 20 m, have value of about 5 in 10–20 m, and are less than unity between 10 m and the surface. The increase in potential energy needed to change the stable profile into the observed (with of course no diffusion) is 0.03 erg cm^{-3} averaged over the whole depth, but 0.3 erg cm^{-3} if only the upper 10 m are considered. The mean kinetic energy of the water column increased from 14 erg cm^{-3} to 37 erg cm^{-3} during the 7 h of the experiment, but fluctuations of amplitude 5 erg cm^{-3} occur between successive profiles.

The variation of Richardson number with depth is further demonstrated in figure 19 which shows the histograms of Ri in three depth ranges, the near-surface range where $\chi, > 0.4$, indicates

that turbulence is almost continuous, an intermediate range where turbulence is intermittent but common, and a deep range where turbulence is very infrequent.

Because of the gradual changes during the day, some important trends are masked by these total averages, and in figure 20 average values of the upper 13 m of the final ten profiles are presented. (This set is referred to below as 6–9.) Between 2 m and 5.5 m the speed and density

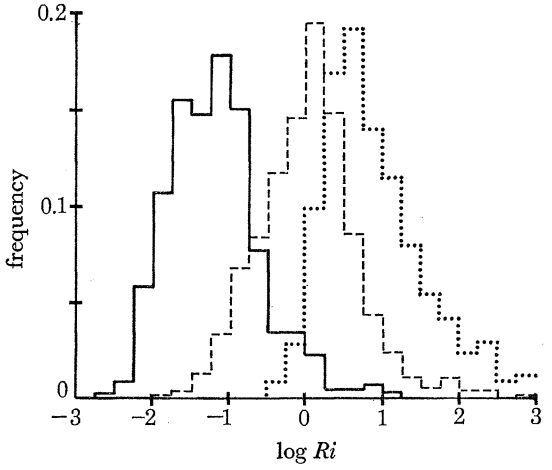

FIGURE 19. Histograms of log Richardson numbers between −3 and 3 measured by taking differences in density and current over 1.06 m intervals for the profiles on 6 September. Three depth ranges are shown. The full line is 1.5–6.5 m where $\chi = 0.43$, the dashed line is 8–13 m where $\chi = 0.25$ and the dotted line is 25–30 m where $\chi = 0.03$.

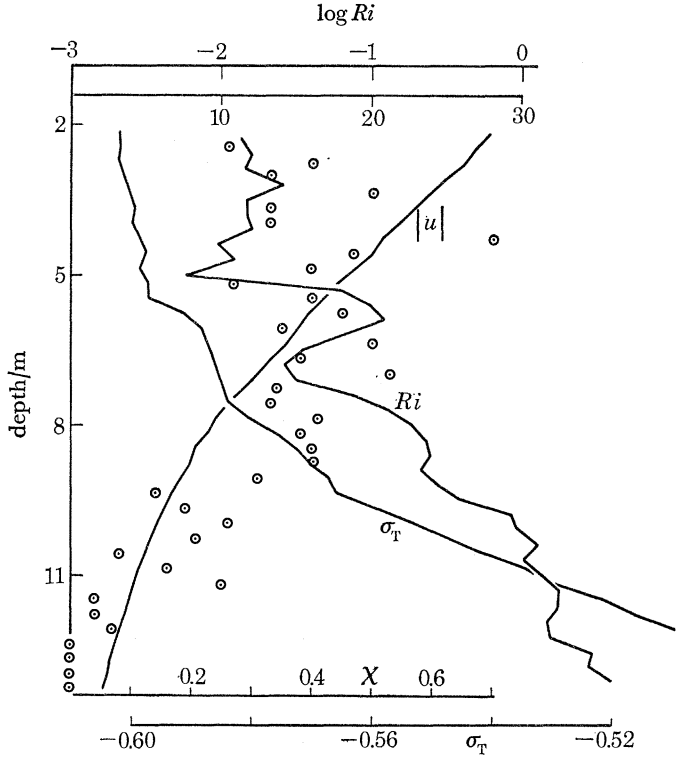

FIGURE 20. The mean values of density (σ_T), Richardson number (Ri, plotted on a log scale and based on the mean density and current), current magnitude, u, and χ shown by the circles, in the upper layer for the set of runs 6–9 on 6 September.

profiles are approximately linear with a mean value of Richardson number of about 0.015. There is a dramatic fall in χ from 0.4 to zero in about 4 m where the density gradient becomes large and *Ri* exceeds 0.25.

3.2.3. 24 *September; wind rising after early calm*

This particular day was interesting mainly because it illustrates the motions in the Loch in calm weather and the effects associated with the start of wind. Except for a short period on 22 September when the wind reached 3–4 m s^{-1}, the weather of the preceding four days was exceptionally calm, with daytime temperatures reaching 12 °C (a little less than the Loch surface temperature) and night-time minima of about 7 °C, conditions in which some convective cooling might be expected.

In the early morning of 24 September the Loch was shrouded in mist, but this cleared at about 11h00 G.M.T. and was followed by warm sunshine. The wind was southwesterly, and

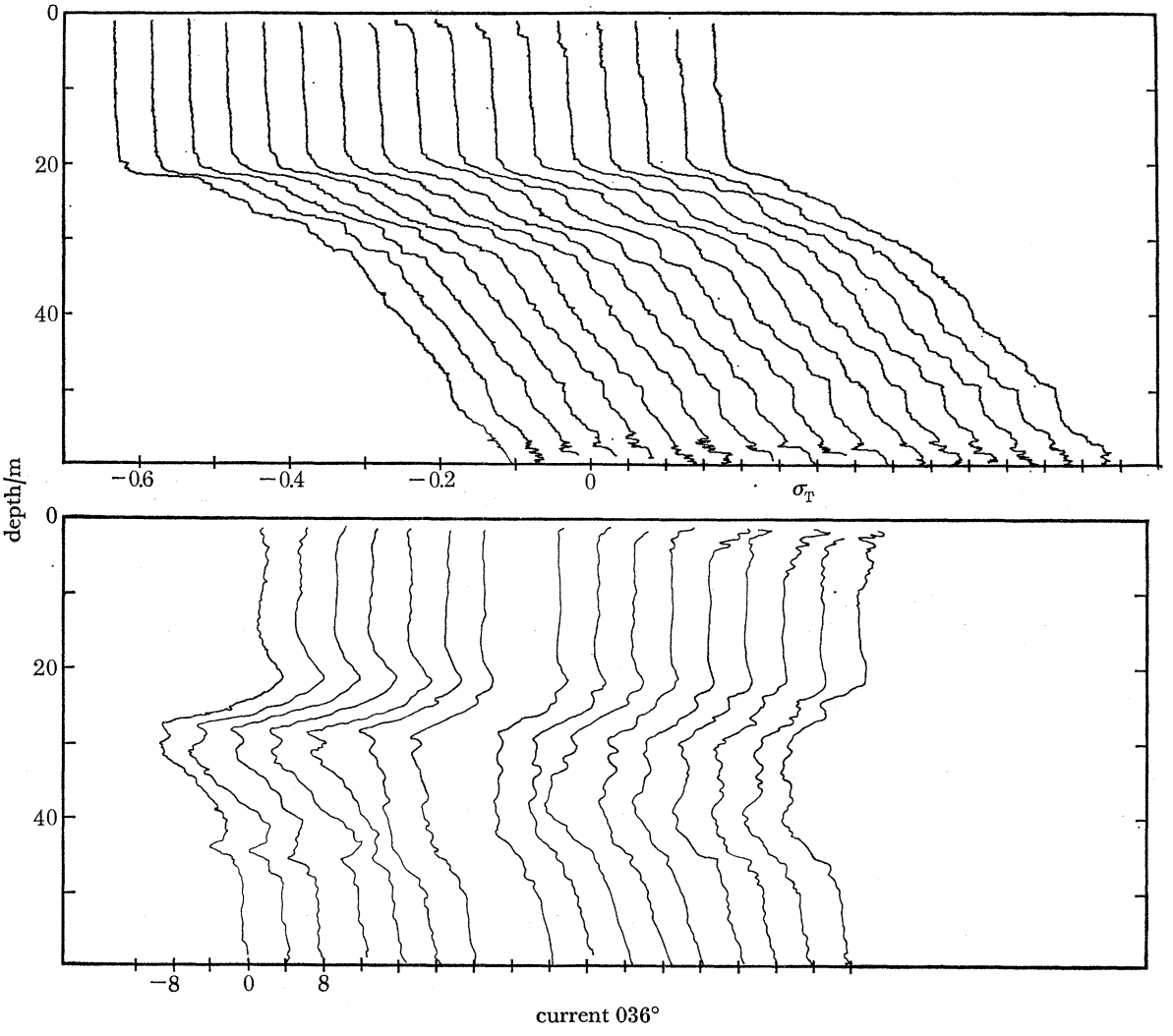

FIGURE 21. Profiles of density (σ_T) and current along the Loch in direction 036° on 24 September. The profiles were made at intervals of approximately 15.3 min. There was a fault in the eighth velocity profile and it is omitted.

less than 1 m s^{-1} until it rose at 11h45 G.M.T. to about 3.5 m s^{-1}. In the early morning the air temperature was 5 °C less than the surface water temperature, but with the clearing mist and rising wind it rose to within 0.2 °C of the water temperature.

The profiles (figure 21) reveal the presence of a submerged jet in the thermocline which lessens in intensity during the day. 'Thermocline jets' were found to dominate the internal flow in other periods of calm weather and were also found on 31 August (§ 3.2.1). The early density profiles are remarkable for the large gradients and occasional inversions (the first profile especially) at the foot of the very-well-mixed near-surface layer. Nocturnal convection is probably responsible for establishing this profile. In one day an abrupt step change in temperature would be smoothed to a gradual change of width 38 cm by molecular diffusion alone, and some dynamic process is needed to produce and maintain the observed gradients. The inversions near the bottom of the profiles result from the disturbance as the probe is being lowered and provide further evidence that the currents are very small.

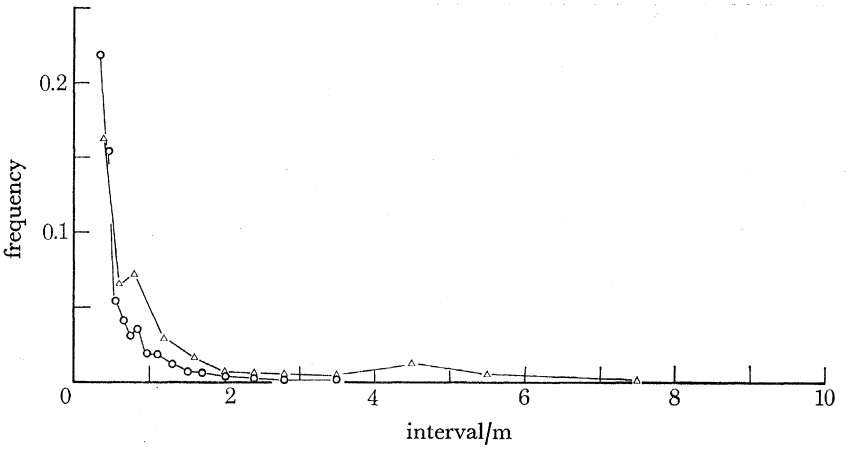

FIGURE 22. The 'structure histogram' (see figure 6) for profiles of density on 24 September. The triangles are for threshold values of gradient $6.0 \times 10^{-4}\sigma_T$ units cm^{-1} and the circles for $1.1 \times 10^{-4}\sigma_T$ units cm^{-1}.

The structure histogram, figure 22, reveals a layer thickness of about 4.5 m and, as on 31 August, shows that the regions of large gradient have embedded within them a structure consisting of several large and small gradients.

With the rising wind and surface heating, a minor thermocline and near-surface shear zone appears, and extends downwards at a fairly uniform rate, approximately 0.1 cm s^{-1}. The r.m.s. displacement in the region between 20 and 35 m is only 7.5 cm indicating a very low level of mixing. The mean (30 cm scale) Richardson number is 8.9 and $\chi = 0.045$.

3.2.4. 28 *September; strong southwest wind*

This was the first of three days in which a number of interesting and connected phenomena were observed. It was preceded by a period of generally light winds, but with the arrival of a depression on the evening of 27 September the southwest wind increased giving speeds exceeding 10 m s^{-1} at mid-day, falling to 7 m s^{-1} at 17h00 G.M.T. and producing frequent white caps on the Loch. The air temperature was some 1.5 °C less than the Loch surface for most of the day, but with clearing skies and warm sunshine between rain squalls, the direction of the net heat flux

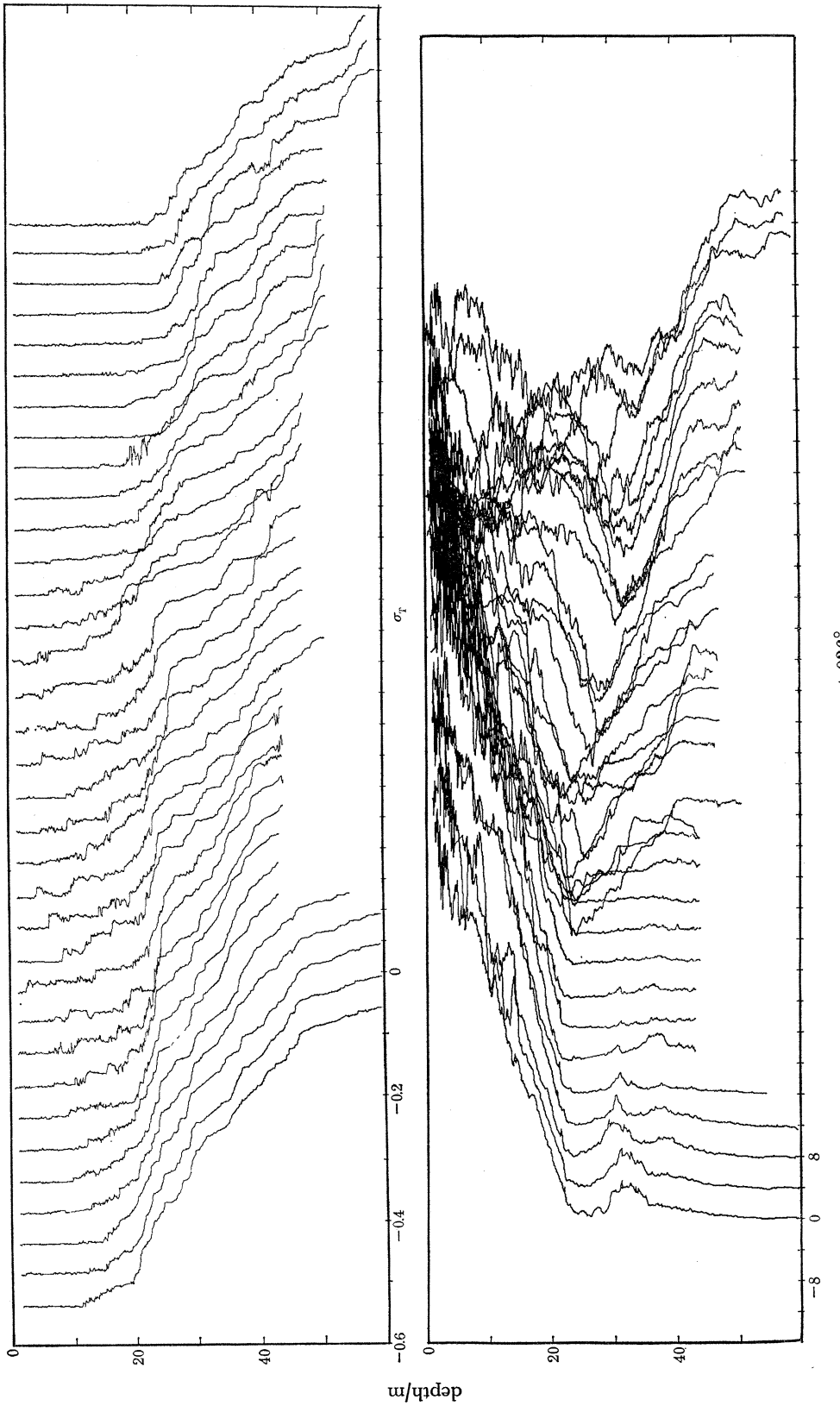

FIGURE 23. Profiles of density (σ_T) and current along the Loch in direction 036° on 24 September. Each successive density profile is displaced by $0.05\sigma_T$ units to the right, and each velocity profile by 4 cm s^{-1}. The times of the profiles are shown in figure 24.

PHILOSOPHICAL TRANSACTIONS OF THE ROYAL SOCIETY A MATHEMATICAL, PHYSICAL & ENGINEERING SCIENCES

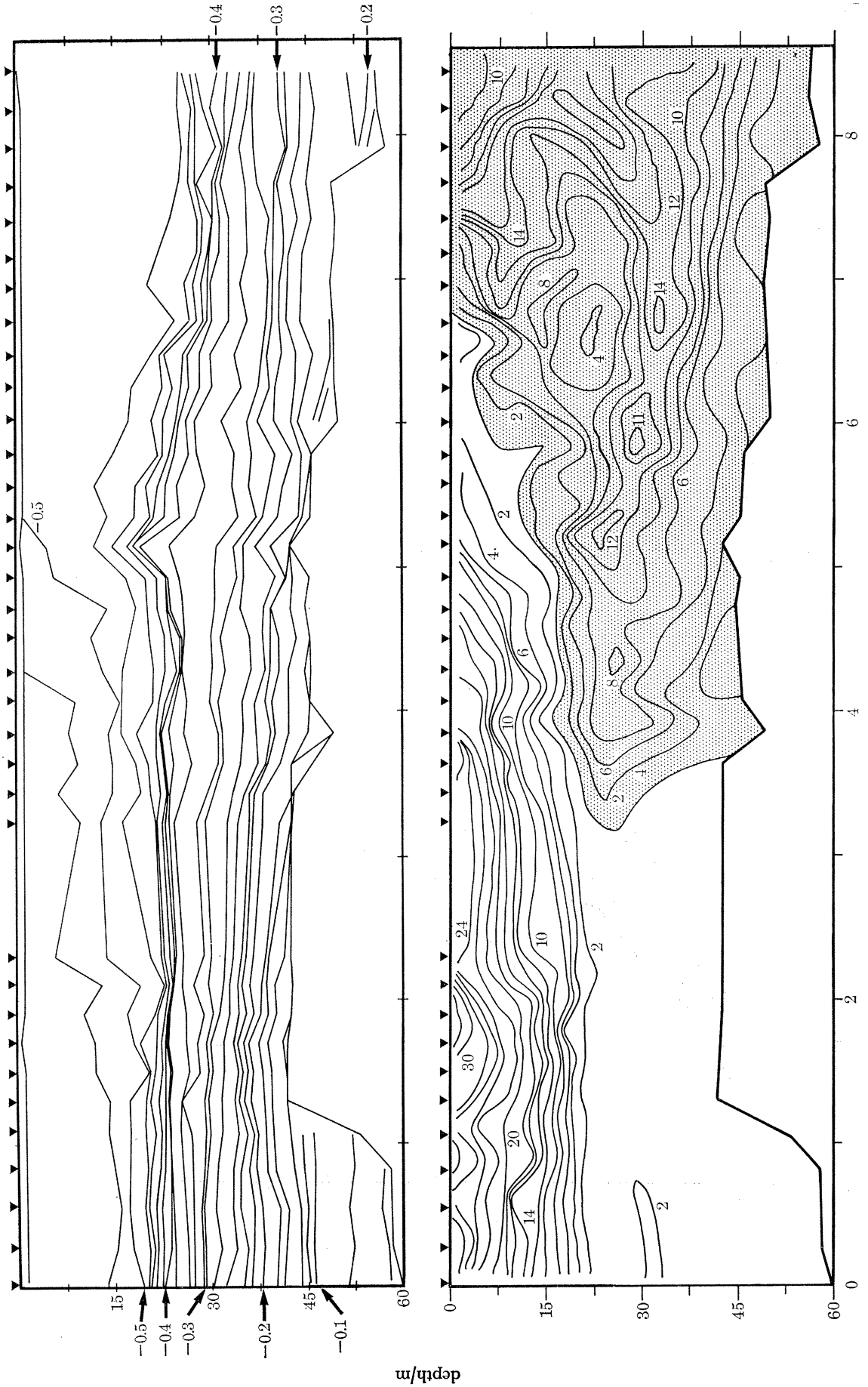

FIGURE 24. Contours of density (σ_T) (top), and current (bottom) along the Loch (in direction 036°T) on 28 September. The time is measured from 08h07 G.M.T. The region of southwesterly current (that where the current has a positive component in direction 216°T) is hatched. Other details are as given in the caption to figure 9.

to or from the Loch is uncertain. The surface of the Loch exhibited lines of foam and slicks suggesting the presence of Langmuir vortices.

The density and velocity profiles and contours are shown in figures 23 and 24. The density profiles show the development of a well-mixed near surface layer following a period in which the upper layers exhibit frequent inversions similar to the upper layers on 6 September. Below about 20 m the Loch is almost entirely stably stratified at the start of observations, except for probe produced inversions near the bottom of the profiles, similar to those of 24 September (§ 3.2.3). Later however frequent small-scale inversions appear. The velocity profiles in the early records show a considerable current shear extending from 25 m up to the surface with water moving in the direction of the wind with maximum, near-surface, speeds of about 3 % of the wind speed. The details of the near-surface profiles are almost obliterated by the effects of wave motion which extend down to about 5 m.

There is a general deepening of the isotherms during the day, with reduced surface temperatures. A considerable change occurs in the currents at about 11h00 G.M.T., 3 h after observations started, when the flow begins to reverse in direction, first at 30 m, and eventually results in a southwesterly flow at all depths, against the wind! The current reversal was dramatically demonstrated on the surface of the Loch by the motion of the spar buoy which, having dragged on its mooring strongly towards the northeast early in the day, turned into the wind and waves and was noted to be dragging southwest at 14h54.

The effect of the changing current regime on the internal stability is shown in the contours of χ, D and Ri (figure 25). The Richardson numbers are significantly reduced and there is a notable increase in small-scale mixing as reflected in D and χ. An example of the displacements produced is shown in figure 26. A temperature record obtained from a moored instrument carrying a thermistor at 44 m also showed the considerable increase in thermal activity (figure 27). The frequent inversions and rapid fluctuations in temperature during this period and on other occasions when a current counter to the wind has developed, represent the most intense and persistent local mixing in the thermocline which we have observed.

In view of the large change in flow pattern the observations have been divided into two sets for part of the analysis. Figure 28 shows mean profiles for the first fourteen runs (referred to as 28–9A below). The reduction in χ as Ri increases at 20 m is very marked. The r.m.s. displacements for the same set of profiles are also shown in figure 28. The near-surface displacements are generally larger than those observed on 6 September. Above 12 m 3 % of the displacements exceed 6 m while 20 % exceed 3 m. Below 22 m however no displacement exceeds 3 m. The excess of the displacement histogram is low between 9 and 15 m, but increases slightly towards the surface and considerably at greater depths.

In the period between 10h00 and 11h00 the P.C.M. was held at a constant depth at 6 levels between 5 and 22 m. While the instrument is not profiling it is not of course possible to obtain a record of current speed (although if the vane were completely free to point in any direction, the direction of the relative flow could be measured), but temperature may be recorded (figure 29). The time scale is the same for all these records and has been related to the length scales shown by assuming that the motion is advected past the P.C.M. at the speed of the mean relative current, determined from preceding and succeeding vertical profiles. (This is a Taylor hypothesis.) The variations are irregular, symptomatic of turbulence, but contain structures with scales of a few metres as suggested by the displacement data.

Mean profiles for the final 14 runs are shown in figure 30 (referred to as 28–9B below). Near the

PHILOSOPHICAL TRANSACTIONS OF THE ROYAL SOCIETY A MATHEMATICAL, PHYSICAL & ENGINEERING SCIENCES

PHILOSOPHICAL TRANSACTIONS OF THE ROYAL SOCIETY A MATHEMATICAL, PHYSICAL & ENGINEERING SCIENCES

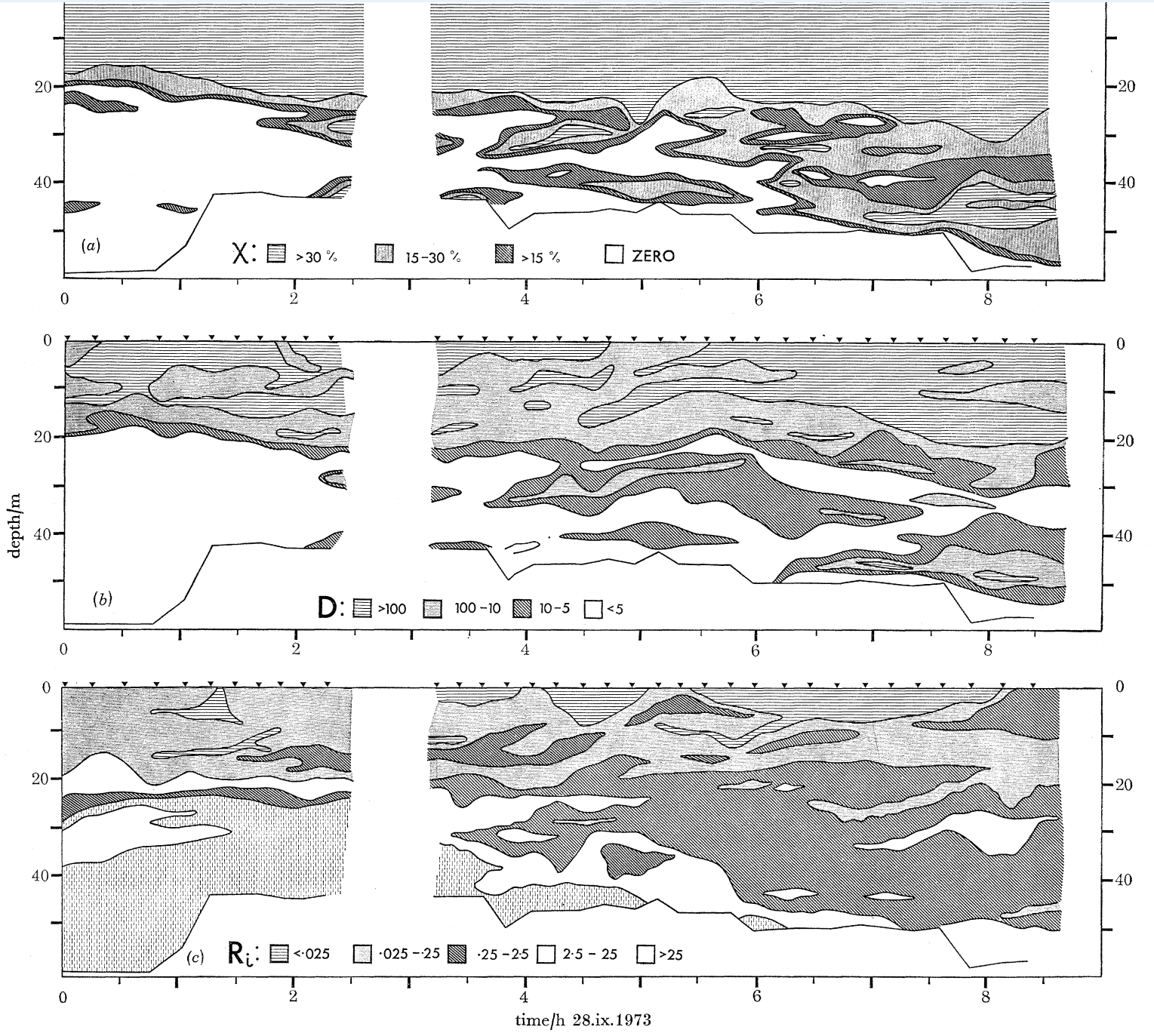

FIGURE 25. Contours of (*a*) frequency of density inversions, χ, (*b*) the parameter D (equation (3)) and (*c*) Richardson number, Ri, based on averages taken over 1.5 m on 28 September. The time is measured from 08h07 G.M.T.

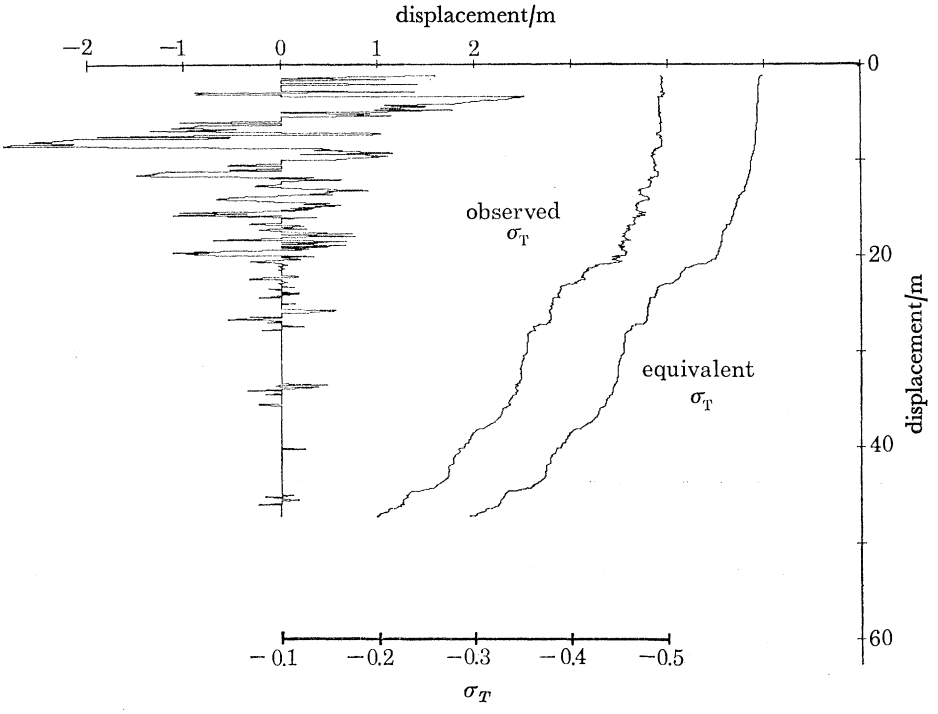

FIGURE 26. The 22nd profile of density (σ_T) on 28 September as observed, the 'equivalent' stable profile moved $0.1\sigma_T$ units to the right, and the displacements needed to produce the stable profile from that observed, as explained in §3.1.

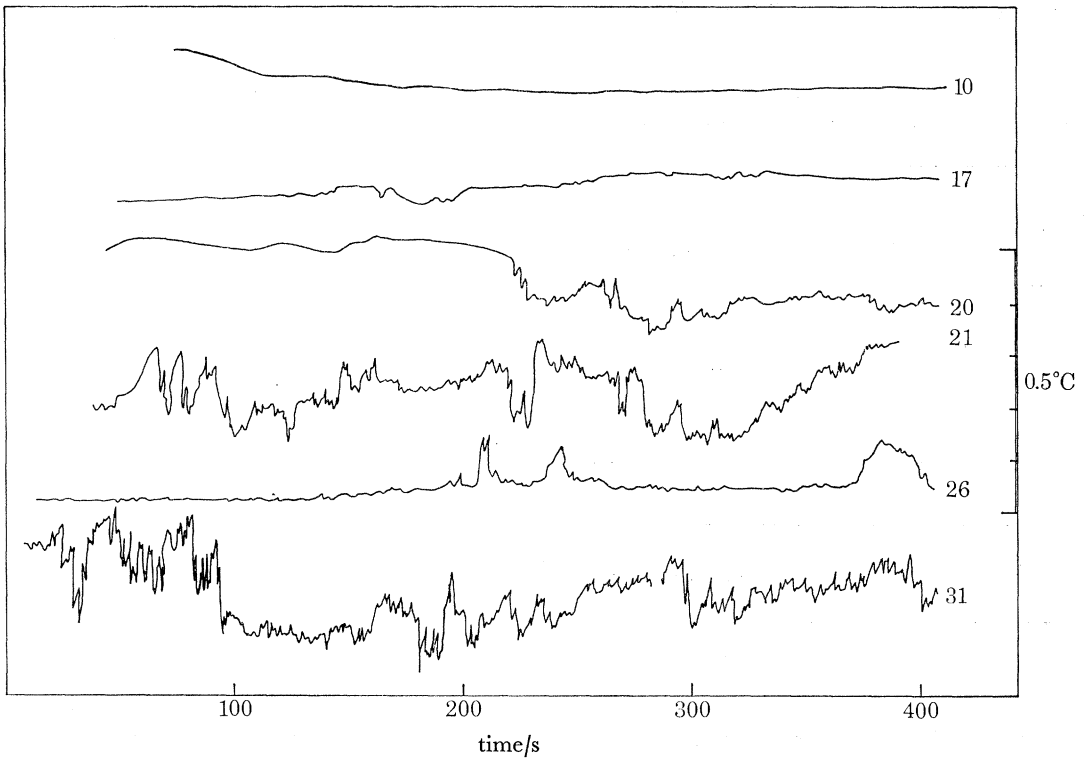

FIGURE 27. Temperatures measured by a thermistor at 44 m depth about 15 m SW of the P.C.M. mooring on 28 September. Each record is on the same sensitivity, according to the scale shown on the right. The numbers shown against each record refer to the number of the P.C.M. profile being made simultaneously (see figure 24 for the times of these profiles).

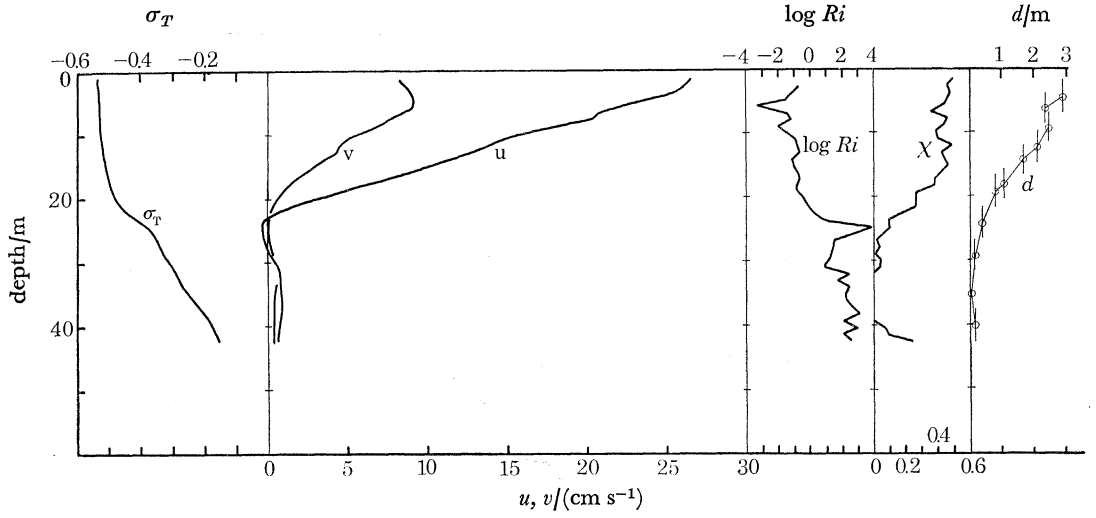

FIGURE 28. Mean values of density (σ_T), velocity components (u in direction 036°T along the Loch and v in direction 126°T across), log Ri (calculated from the mean currents and densities), χ and r.m.s. displacements. The averages (except those of d) are taken over successive 1.06 m depth intervals for profiles 28–9, set A. The vertical bars on the d-profile indicate the vertical distances over which the r.m.s. displacements are calculated. The rise in χ and d at 40 m appear to be due to the disturbance caused by the P.C.M. during its descent.

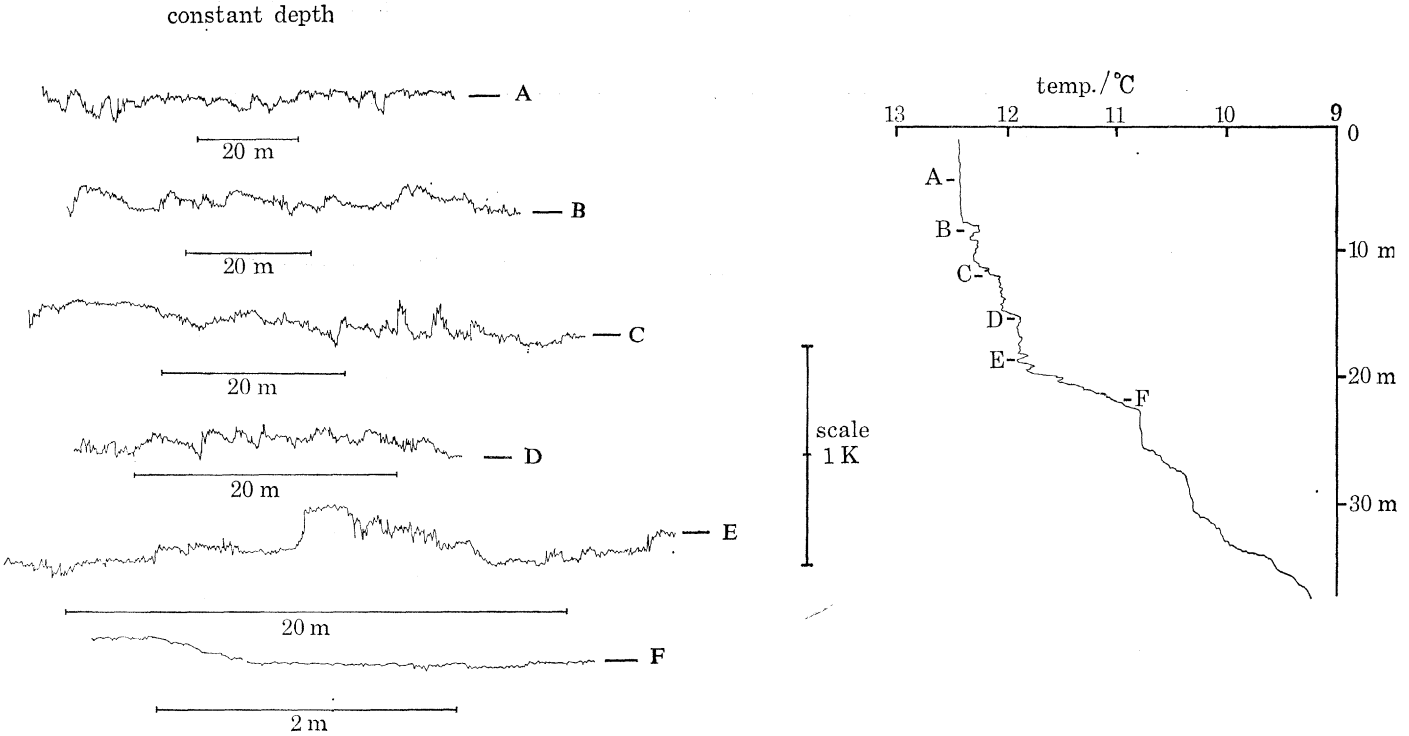

FIGURE 29. Records of temperature at fixed levels below the surface on 28 September between 11h00 and 12h00 G.M.T. A profile of temperature made immediately after the series of fixed depth measurements is shown, and on it are marked the depths of the six records A–F. Each record is made on the same sensitivity according to the scale shown. The length scales shown against each record are derived from the mean current at each level using a Taylor hypothesis.

surface the mean density gradient is positive and the Richardson number takes small negative values. Although a decrease occurs at about 23 m, χ has a value of about 0.17 in the region below 30 m where the Richardson number is of order one, and a demarcation between the layer directly mixed from the surface and that below is much less clearly defined than in the profiles 28–9A. The r.m.s. displacements however clearly demonstrate a difference in the character of the motion above 20 m, where the r.m.s. displacements exceed 4 m and that below 30 m where the displacements are less than 30 cm. Above 30 m, 4 % of the displacements exceed 8 m and 12 % exceed 4 m, while below 27 m only 2 % of the displacements exceed 1 m. The potential energy involved in this unstably stratified fluid is 0.168 ± 0.124 erg cm^{-3} averaged over the whole depth for the second set. This compares with changes of about 10 erg cm^{-3} in kinetic energy between successive runs.

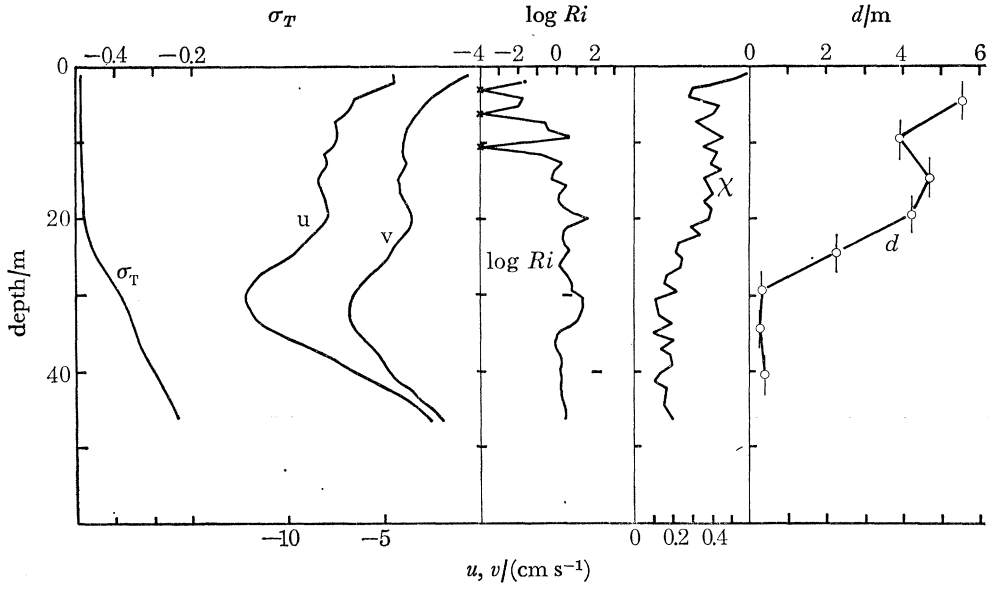

FIGURE 30. Mean values of density (σ_T), velocity components (u in direction 036°T along the Loch and v in direction 126°T across), log Ri (calculated from the mean currents and densities), χ and r.m.s. displacements. The averages (except those of d) are taken over successive 1.06 m depth intervals for profiles 28–9, set B. The vertical bars on the d-profile indicate the vertical distances over which the r.m.s. displacements are calculated. The mean Richardson number is negative at the points marked by crosses.

3.2.5. 29 *September; strong northeast wind, deep mixed layer*

The trough of low pressure which had brought the strong southwesterly winds on 28 September had by the 29th reached Southern Scandinavia, bringing a colder north to northeasterly wind to the area. The mean wind (averaged over the time taken for one profile) strengthened from 4 to 10.5 m s^{-1} during the first 4 h observation, and became very strong in squalls (speeds exceeding 20 m s^{-1}). The wind moderated to about 8 m s^{-1} during the last hour of observation. The air temperature rose gradually from 1.9 °C below the Loch surface temperature to 0.2 °C below when the wind reached its peak and then fell sharply to 2.0 °C below at the end of the observation period. The surface temperature of the Loch was fairly steady. The sky remained overcast throughout the day with showers of rain during the squalls. The Loch was rough with much whitecapping and waves of 3 s period and 50–60 cm height.

The mixed layer, seen to be developing on 28 September, was found to have become partly broken by a minor thermocline near 35 km (figure 31) below which the water was almost

stationary, and the main feature of the day was the gradual erosion of this transient thermocline and the re-establishment of a well-mixed layer some 43 m deep by the end of the observations, bounded by a very abrupt increase in density. There was a slow and steady rise of the main thermocline from about 50 to 45 m during the day (figure 32) and the currents in the upper layer were consistently directed towards the southwest in the same direction as the wind. With increasing wind speed the structure of the currents becomes more irregular as they had on the preceding day when the stability of the upper layer decreased, although coherent structures can be seen which last for periods of 30 min or more, and with vertical scales comparable to the layer depth.

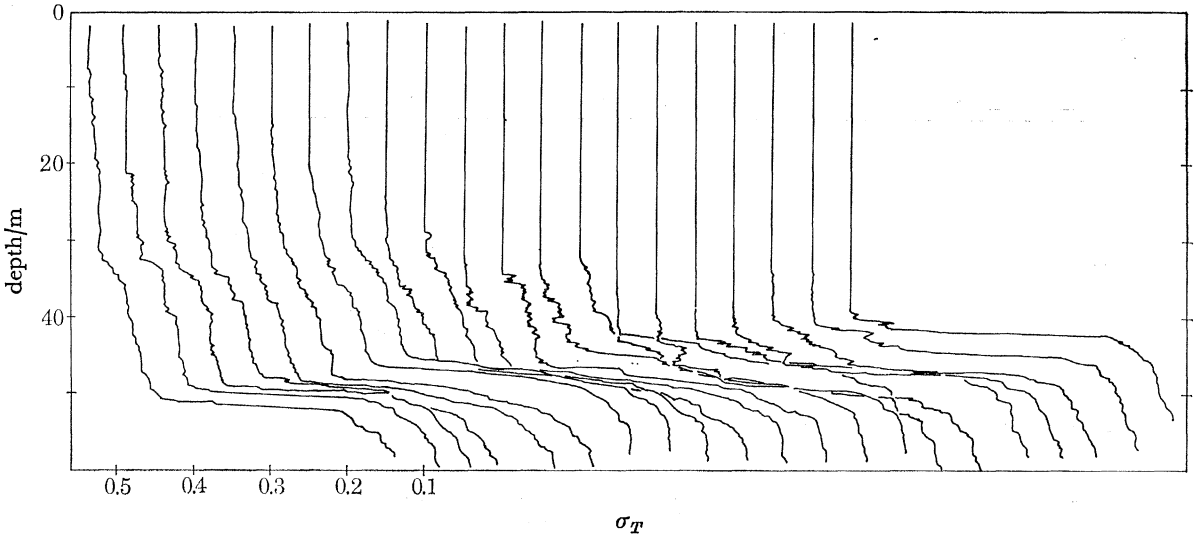

FIGURE 31. Profiles of density (σ_T) on 29 September. Each successive profile is displaced to the right by $0.05\sigma_T$ units. The times of the profiles are shown in figure 32.

The small gradients in σ_T in the upper layer make the accuracy of the estimates of Ri and D in the upper layer rather poor. During the destruction of the transient thermocline there are frequent density inversions both above and below it (figure 31), although on the 1.5 m scale the Richardson number below the transient is generally high and a Richardson number based on a smaller vertical scale seems appropriate. At the end of the observation period there was evidence in the profiles of convective activity with surface cooling.

The presence of eddies with large vertical scale above the interface at the foot of the mixed layer imposes a shear of variable character, but generally the density step is much more abrupt than is the velocity and the latter has an inflexion point somewhat above the density interface where the mean shear has maximum value.

3.2.6. 30 *September; the internal surge*

In comparison with the preceding days, the weather was calm with mean northeast winds of 3.5 m s^{-1} and air temperatures beginning 4.5 °C below the water surface temperature and rising no more than 2.0 °C during the day.

The period of the internal seiche of the first longitudinal mode and first internal mode is about 52 h (Thorpe 1974). The impulses to the upper layers of the Loch on the previous days, first imposed by the southwest winds on 28 September depressing the thermocline at the northeast

end and enhanced in effect by the northeasterly winds of the 29th which aided the return of near-surface water to the southwest, resulted in the generation of an internal surge. The northeastward travelling surge reached the observation site at about 07h00 G.M.T. on the 30th where it was recorded by the current meters (figure 33) and later by the P.C.M. (figure 34). The surge followed the pattern already recognized and referred to in §§ 1 and 2, with three distinct leading waves with periods of about 40 min followed by a less regular train of waves.

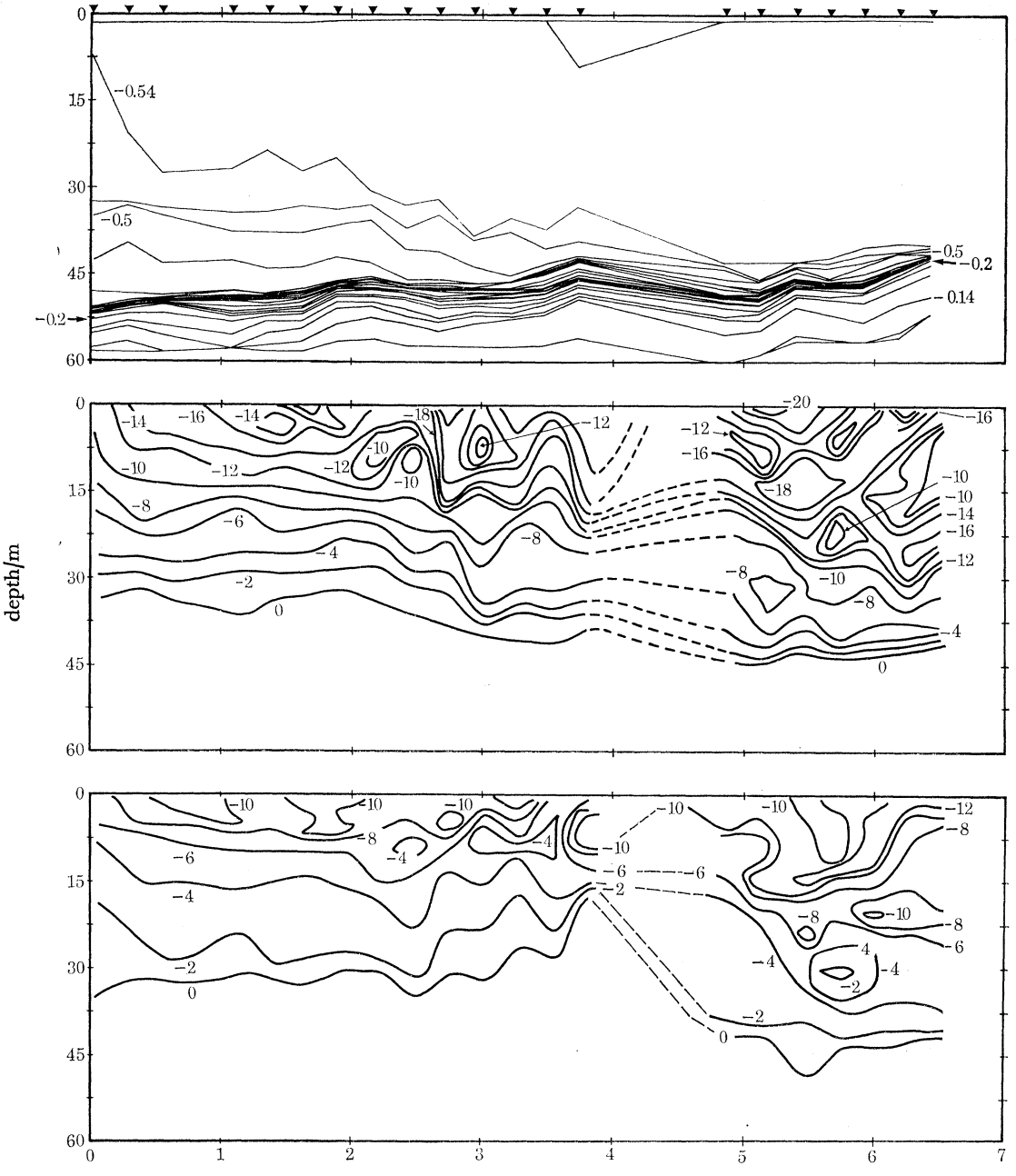

FIGURE 32. Contours of density (σ_T) (top), current along (longitudinal, in direction 036° T middle) and across (lateral, 126° T bottom) the Loch on 29 September. The time is measured from 08h28 G.M.T. Other details are as given in the caption to figure 9.

The wave amplitudes exceeded 5 m, and their speed, c, is estimated as about 35 cm s^{-1}. The motion of the spar buoy towing first one way and then the other on its mooring was the only obvious sign on the surface of their presence. Surface ripple bands and slicks as discussed by Gargett & Hughes (1972), Lafond (1962) and Apel, Byrne, Proni & Charnell (1975) were not apparent. The return surge travelling back towards the southwest was recorded by the current meter early in the morning of 1 October (figure 33).

The first two waves shown in figure 34 are actually the second and third behind the front of the surge. The currents are in phase with the wave troughs (or temperature maxima in the current

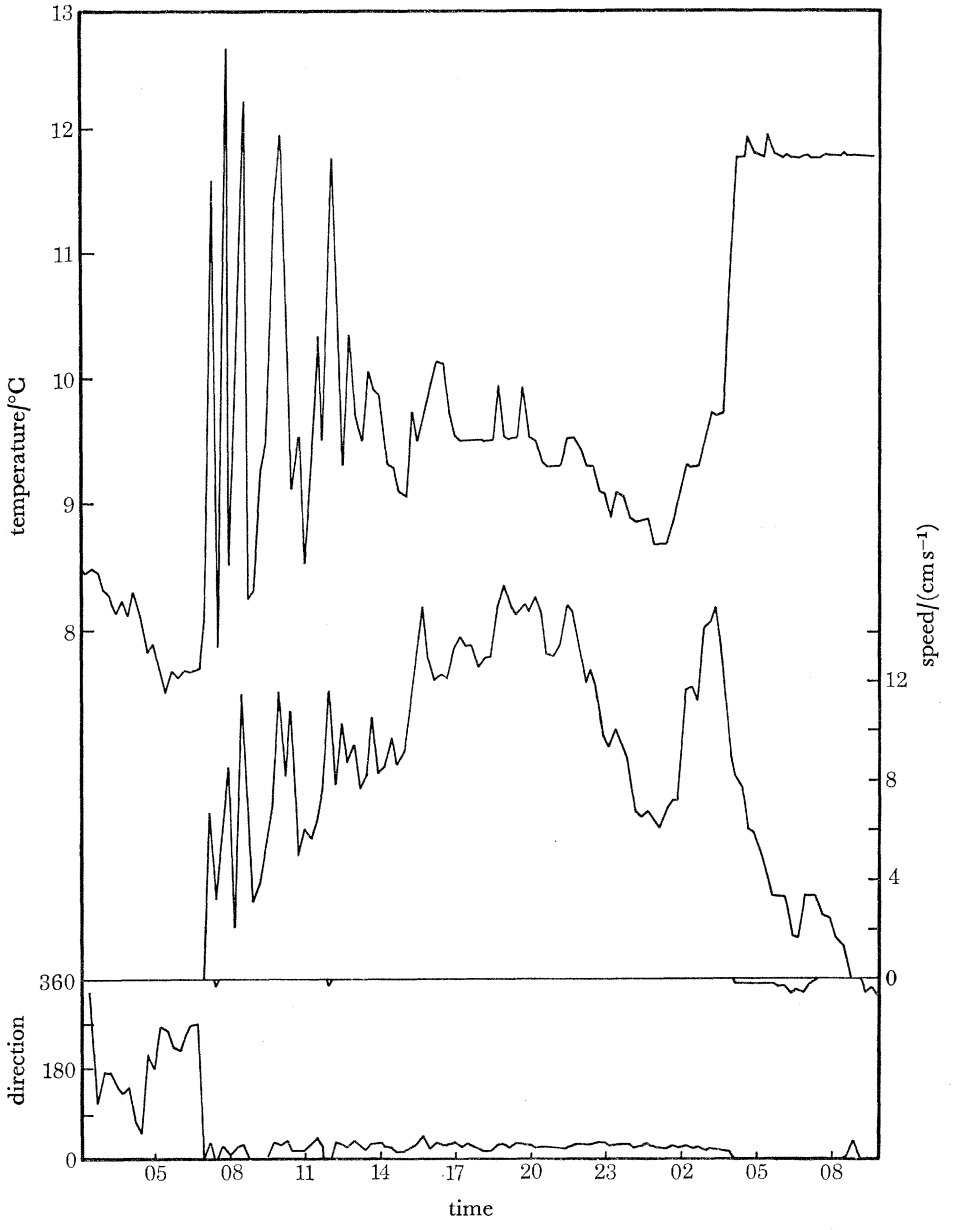

FIGURE 33. The temperature, speed, and direction of the current measured at 15 min intervals by a current meter moored at 35 m depth and about 50 m northeast of the p.c.m. mooring from 02h00 G.M.T. 30 September to 10h00 G.M.T. 1 October, showing the passage of the internal surge at about 07h00 G.M.T. 30 September, and its return at about 04h00 G.M.T. on 1 October.

meter record). The current in the upper layers is towards the northeast, although some reduction towards the surface is apparent in the last three profiles, perhaps due to the opposing wind stress. The mean northeasterly current is about 8 cm s^{-1}, approximately equal to $c\Delta h/h_1$ where Δh is the estimated surge height and h_1 is the depth of the thermocline behind the surge, as expected by continuity. The waves produce a modulation of about 2 cm s^{-1}, approximately equal to $a\sigma$ where a is the amplitude of the waves and σ their frequency.

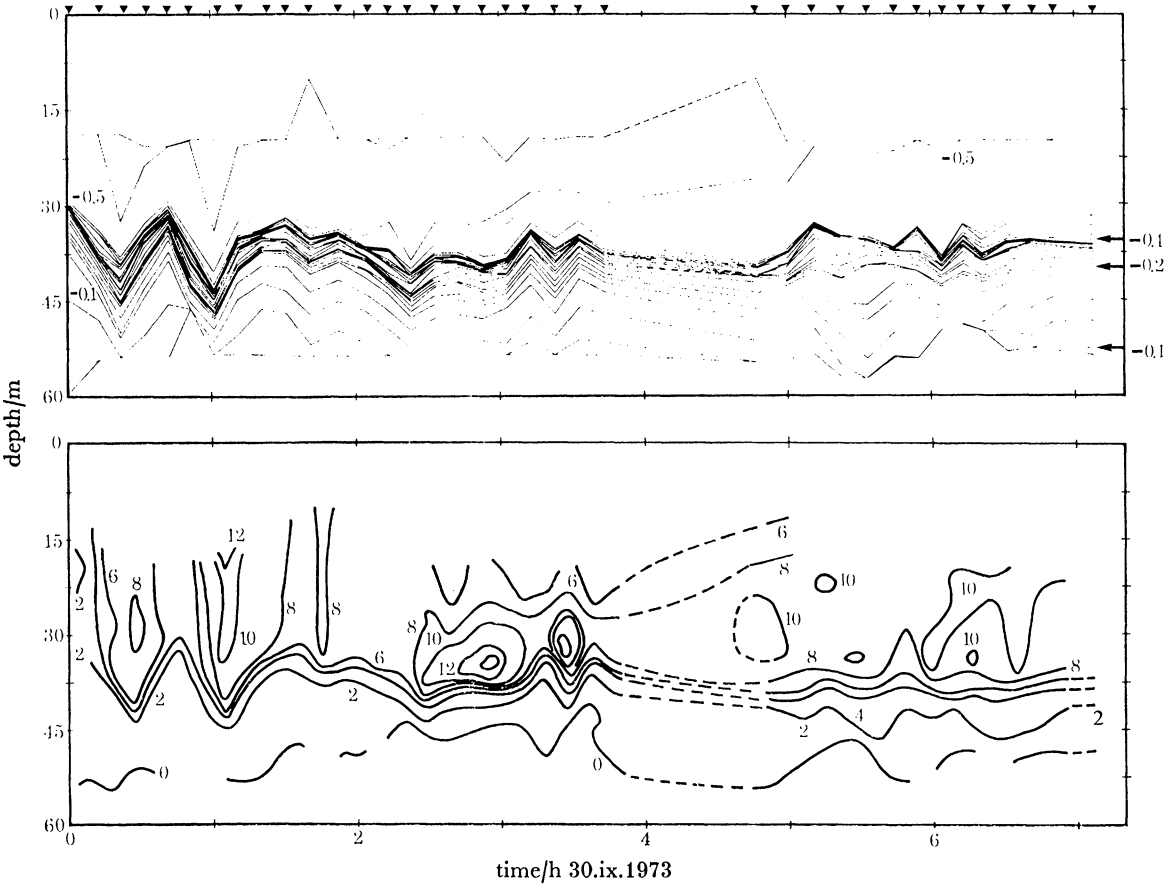

FIGURE 34. Contours of density (σ_T top) and current along (longitudinal, in direction 036° T bottom) the Loch on 30 September. Time is measured from 08h00 G.M.T. Other details are as given in the caption to figure 9.

Density, displacement, northeast component of current and Richardson number profiles through the waves are shown in figure 35. The first profile, immediately preceding the second wave, is entirely stable with no inversions which exceed the noise level of the P.C.M., but with small Richardson numbers developing in the thermocline at the trough of the second wave, instability is observed (profile 3) with inversions first occurring in the main gradient region of the thermocline and later at the edges, a pattern following that of Kelvin–Helmholtz instability in laboratory experiments (Thorpe 1973). It is not evident from the profiles that the whole thermocline has become involved in violent instability. What is likely, judging by the Richardson numbers involved, is that very weak billows of small amplitude are produced (see Thorpe 1973, figure 2*e*, *f*). Their wavelength may be inferred from the density or velocity structure to be approximately 10–20 m, much less than the length of the waves. The amplitude of the displace-

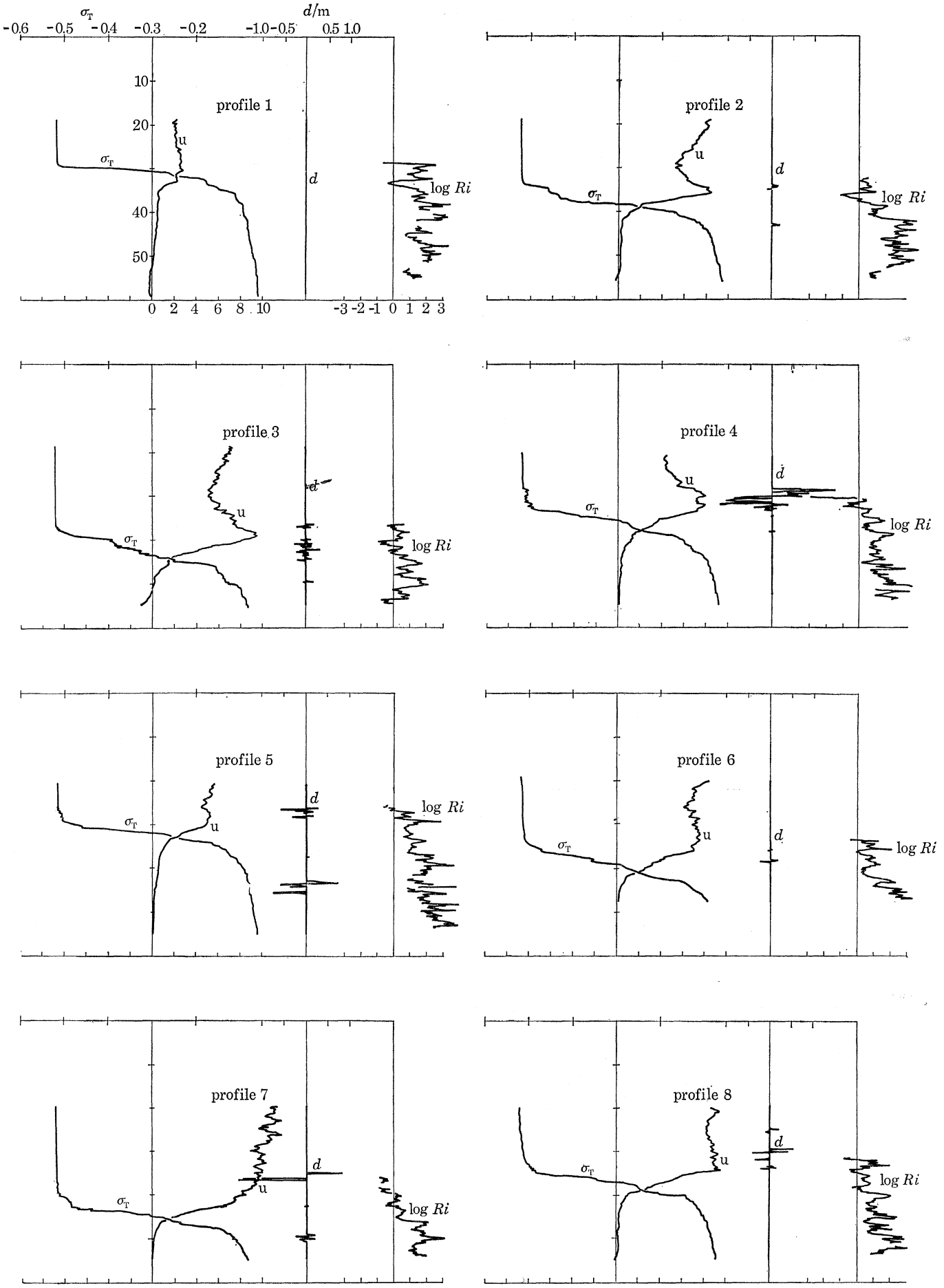

FIGURE 35. Density (σ_T), the current component in direction 036°T along the Loch (u), the displacements (d) and log Richardson number (log Ri) measured by taking differences in density and current over 1.06 m, for the first eight profiles on 30 September during the passage of the leading waves in the internal surge. The times at which the profiles were made are shown in figure 34.

PHILOSOPHICAL TRANSACTIONS OF THE ROYAL SOCIETY A MATHEMATICAL, PHYSICAL & ENGINEERING SCIENCES

ments is at first about 25 cm (profile 3) but assumes a larger scale at the edges of the main thermocline (profiles 4, 5). The profiles of Richardson number are very irregular as expected in internal wave trains (see § 3). Profiles 2–4 show an interesting jet-like feature near the regions of largest density gradient. In the third wave (profiles 6–8) the Richardson number at the main thermocline does not fall below 0.3 and the displacements which indicate the presence of gravitational instability are neither so numerous or as large as those which followed the passage of the second wave.

The mean (1.06 m) Richardson number in the subsequent, less regular, wave train is about 6. The turbulence generated by the waves is not sufficient to destroy the thermocline, but it appears to be effective in causing significant diffusion, as may be seen from the spread of the contours of constant density (figure 32) which was accompanied by occasional unstable regions resulting possibly from occasional breaking or shear induced instability of the internal waves. Assuming a constant diffusion coefficient in the neighbourhood of the thermocline, we estimate that a mean value of

$$K_B = 6.2\,\mathrm{cm^2\,s^{-1}}$$

is needed to account for the spread of the thermocline in the last 7 hours of observation. This assumes horizontal uniformity and that mixing at the sides of the Loch do not contribute to the observed diffusion.† The change in potential energy associated with this diffusion is about $5.4 \times 10^4\,\mathrm{erg\,cm^{-2}}$. This is probably only some 20 % or less of the total energy lost by the surge, and is comparable with the energy available in the leading waves, about $9.6 \times 10^4\,\mathrm{erg\,cm^{-2}}$. Since the speed of the surge is known, the rate of change in potential energy per unit width of the Loch may be calculated as $1.9 \times 10^6\,\mathrm{erg\,s^{-1}\,cm^{-1}}$. If the energy contained in the leading waves is entirely destroyed by breaking at each end of the Loch (it is unlikely that so much energy is lost), the mean rate of energy dissipated in this way in each seiche period is about $5.1 \times 10^5\,\mathrm{erg\,s^{-1}\,cm^{-1}}$, less than that dissipated by mixing processes behind the front of the surge. When the surge is being resonantly forced by the wind, the total energy dissipation in each period is equal to the energy supplied by the wind. This latter cannot, however, be estimated directly from this equality because the rate of dissipation of kinetic energy in the Loch is not known.

4. Discussion

It is not our purpose to discuss in detail the general circulation of the Loch, although many of the observations reported have a direct bearing on the understanding of the large-scale water motions. The circulation pattern observed is similar to that described by Mortimer (1955), with a general tendency for anticlockwise circulation in the same sense as the Earth's rotation to develop during periods of wind forcing.

The 'displacement' defined in § 3.1 has so far been used as a descriptive tool to quantify the vertical motions in the turbulence and to assess the potential energy involved in the mixing.

† The flow of waves of the observed amplitude up and down the sloping sides of the Loch (see figure 41) must result in considerable mixing. Evidence for this may be found in the absence of stratified organic deposits down to at least 50 m depth reported by Pennington, Hawroth, Bonny & Lishman (1972). What we are concerned with here is whether those mixed regions in the thermocline will spread to affect the water in the neighbourhood of the P.C.M. mooring. Various estimates of the spread of intrusions are given by Thorpe (1973) and when applied to this situation give spreads of the order of one hundred metres during the period of observation, just sufficient for the effects to reach the P.C.M. mooring. The estimates ignore however the constriction imposed by the rotation of the Earth which is expected to restrict the spread, and the effect of the sides is thus in some doubt.

PHILOSOPHICAL TRANSACTIONS OF THE ROYAL SOCIETY A MATHEMATICAL, PHYSICAL & ENGINEERING SCIENCES

The excess, calculated from the histograms of the displacements on the days of large winds and stable conditions, is very large within the generally stably stratified thermocline where χ is small, consistent with the very intermittent nature of the overturning events. In the mixing region at the top of the thermocline where χ is near 0.4, the excess is small, and so is the skewness, although the latter becomes negative towards the surface indicating the presence of water which has been mixed upwards from below. In the most active mixing region the displacements are almost normally distributed.

The r.m.s. displacement in a small depth interval averaged over several profiles is a measure of the outer vertical scale of the turbulence, the vertical scale over which, in the mean, turbulence acts at a particular level to produce overturning, and as such is a measure of the vertical length over which the turbulent eddies are isotropic. The r.m.s. displacement may thus be identified with the length scale

$$l_c = \alpha \epsilon^{\frac{1}{2}} N^{-\frac{3}{2}} \tag{4}$$

(Ozmidov 1965; α is a constant near unity as remarked above) for turbulence which is generated by a cascade of energy through turbulent eddies at a rate ϵ in a fluid of mean Brunt–Väisälä frequency N (for consistency averaged over a vertical scale corresponding to the r.m.s. displacement). It is an assumption of the theory that the large-scale turbulent eddies are characterized locally by ϵ and N only, and that no other dimensional scales or parameters are available to characterize their motion, so that, in particular, the distance from the surface of the Loch is not an important scale. Near the free surface where stratification is very weak the turbulence is, in rough conditions, probably controlled by breaking surface waves. (Dobroklonskiy & Kontoboytseva (1973) have made experiments which show that turbulence generated by surface waves decays rapidly with depth, and gave a relation

$$l = 0.75h + 0.0081\lambda \tag{5}$$

for the depth of penetration l of the turbulence below waves of height h and wavelength λ, which is less than 1 m for the waves on the Loch on the days of observation. Stewart & Grant (1962) also conclude that energy dissipation by surface waves takes place in a very shallow zone but direct evidence is as yet very meagre.) In the very stable conditions always found at greater depths, the vertical excursion of fluid particles is limited by buoyancy forces and mixing cannot extend to the surface. The distance from the surface is therefore no longer an important parameter and local parameters may determine the flow. It is probably sufficient for such independence that the distance from the surface exceeds the Monin–Obukhov length scale (Turner 1973, p. 131) determined from the surface fluxes.

Ozmidov's argument is central to the discussion of the scales on which a meaningful Richardson number should be measured. In a steady laminar flow it is the gradient Richardson number which determines the stability of the flow, and no difficulty is found in defining the vertical scales although their measurement may pose problems. The scales must be small enough to define the gradients accurately. However, in a turbulent flow definition is more difficult. If very small separations are taken between sampling points, the turbulence, having larger scales, is not characterized by the Richardson number (Tennekes 1973). Alternatively, if very large vertical distances are taken between the sampling points, detail of all the internal mean structure is lost and the Richardson number calculated from the differences may not characterize the internal motions (see Turner 1973, p. 320). Some intermediate scale is appropriate, and that which

characterizes the largest scale of the overturning eddies in the turbulence will, it is argued by Ozmidov, give a universal critical Richardson number of order unity.

In practice, because of the random nature of turbulence, such a conclusion can only be valid in statistical 'ensemble' sense. The outer scale of the turbulence cannot be defined instantaneously by observation, and at best a mean value can be defined. Using this scale the mean Richardson numbers should have a constant value, although of course individual values will have a wide scatter. Observations at different levels should be statistically similar. (Indeed if Ozmidov's assumptions are valid, the vertical variation of the outer scale of the turbulence might be inferred by adjusting the length used in determining the Richardson numbers at each depth until their statistical distributions are uniform.)

Having identified the displacement, d, with l_c, we can now estimate ϵ by inverting (4) to give

$$\epsilon = C_0 d^2 N^3 \tag{6}$$

where C_0 is a constant near unity. Here ϵ, d and N are averaged over many profiles which are supposed statistically similar, and averaged over some vertical scale exceeding d. We note that if a fraction δ of the fluid is turbulent, and in this fraction the r.m.s. displacement is d' and the dissipation is ϵ', whereas elsewhere they are zero,† then since $d = d'\sqrt{\delta}$ and $\epsilon = \delta\epsilon'$, the relation (6) for the mean values is consistent with an identical relation for the turbulent patches only.

The dissipation in the turbulent patches can be found if the intermittency δ (approximately 2χ) is known. We note that in making this deduction it is assumed that N does not vary systematically between the turbulent and non-turbulent patches, that is the turbulence is induced mainly by shear variation, consistent with the momentum transport by internal waves.

In locally isotropic turbulence the eddy diffusion coefficient K follows the four-thirds power law

$$K = C_1 \epsilon^{\frac{1}{3}} l^{\frac{4}{3}}, \tag{7}$$

where l is the length scale over which diffusion is measured and C_1 is a universal dimensionless constant. Following Ozmidov we find the maximum vertical eddy diffusion coefficient for buoyancy (or heat) by equating l to $l_c = d$:

$$K_B = C_1 \epsilon^{\frac{1}{3}} d^{\frac{4}{3}} \tag{8}$$

and using the estimate for ϵ we find

$$K_B = C_1 N d^2 \tag{9}$$

as an estimate for the vertical eddy diffusion coefficient. This is again a valid estimate in an intermittent flow provided that the total diffusion is dominated by diffusion in the turbulent patches.

It is implicit in the theory from which these equations (6) and (9) for ϵ and K_B are deduced, that the intermittency factor is not an important factor and that Reynolds number of the turbulence is high. A sufficient condition for the latter is

$$Re = d^2 U'/2\nu\chi \tag{10}$$

† This is valid if the energy dissipated in the non-turbulent fluid is far less than that in the turbulent regions, that is if

$$\epsilon \gg 2\nu u'^2,$$

where u' is the r.m.s. vertical velocity gradient, supposed to be much greater than the horizontal gradients when turbulence is very infrequent.

PHILOSOPHICAL TRANSACTIONS OF THE ROYAL SOCIETY A MATHEMATICAL, PHYSICAL & ENGINEERING SCIENCES

is much greater than unity, where U' is the modulus of the mean velocity gradient and ν is the kinematic viscosity. Since the r.m.s. shear may exceed the mean by an order of magnitude (see § 3.2.2), this estimate (and those in table 1) are probably an order of magnitude less than the Reynolds numbers which characterize the large eddies of the turbulence.

The coefficient C_1 has a value of about 0.1, and can be related to the flux Richardson number, J_f. In a statistically steady state in which the energy flux is non-divergent the energy balance equation is

$$\epsilon = -\overline{uw}\,U' + \overline{bw} \tag{11}$$

(Phillips 1966), where $\tau = -\rho\overline{uw}$ and $\overline{bw}$ are the Reynolds stress and rate of change of potential energy of the fluid per unit volume respectively, and ρ is the water density. The flux Richardson number

$$J_f = \overline{bw}/\overline{uw}\,U'$$

and so

$$\epsilon = -\overline{bw}(1 - J_f)\,J_f^{-1}.$$

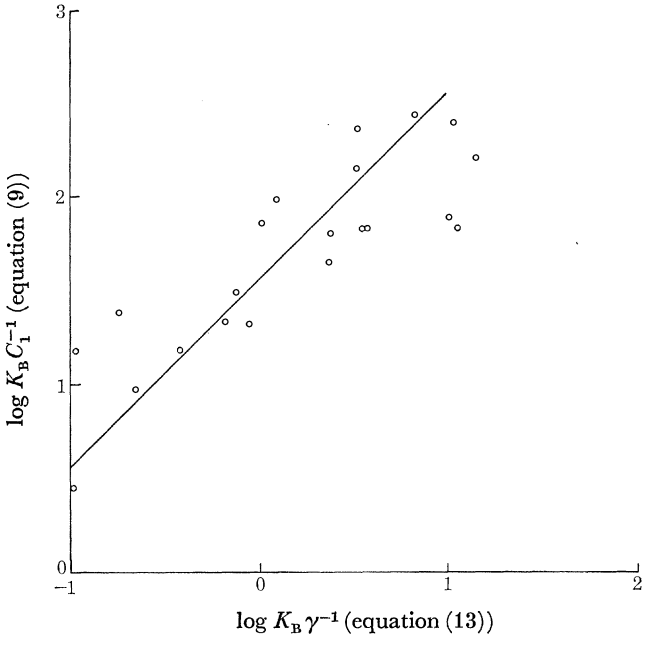

FIGURE 36. Comparison of the estimates of the coefficient of vertical diffusion of heat based on Kullenberg's empirical formula (equation (13)) and on equation (9).

But

$$\begin{aligned} -\overline{bw} &= K_B N^2 \\ &= C_1 N^3 d^2 \quad \text{(by (9))} \\ &= (C_1/C_0)\,\epsilon \quad \text{(by (6))}. \end{aligned}$$

Hence

$$C_1/C_0 = J_f/(1 - J_f). \tag{12}$$

Kullenberg (1971) has proposed a semi-empirical formula based on dye diffusion experiments for the diffusivity K_B in stratified oceans,

$$K_B = 10^{-8}\gamma u_{10}^2\,U'/N^2, \tag{13}$$

where U_{10} is the wind speed, U' the magnitude of the shear in the water, N is the Brunt–Väisälä frequency and γ is a dimensionless constant found to be about 8 from experiments in the

open ocean, but rather lower, near 2, in Lake Ontario (Kullenberg, Murthy & Westerberg 1973). The estimates of K_B (equation (9)) have been compared with estimates based on equation (13), and the result is shown in figure 36. The scatter is rather large, but the general trend shows an agreement in the two estimates. A best fit is obtained with a value of the ratio of the constants $\gamma/C_1 = 23$, which falls within the ranges of values found empirically.

As a further check of the consistency in the estimate of K_B we may compare the estimate made in § 3.2.6 with that by applying (9) in the thermocline region. The latter gives $K_B = 33C_1$ $\mathrm{cm^2\,s^{-1}}$ which, for the supposed value of C_1, is in as close agreement with the previous value, $6.2\,\mathrm{cm^2\,s^{-1}}$, as might be expected in view of the possible errors involved.

TABLE 1

date	depth range m	$\epsilon C_0^{-1} \times 10^3$ $\mathrm{cm^2\,s^{-3}}$ (equation (6))	K_B/C_1 $\mathrm{cm^2\,s^{-1}}$ (equation (9))	Re (equation (10))	$\frac{\tau}{\tau_a}(C_0+C_1)^{-1}$	R
31.viii	2–7	0.32	69.6	2.4×10^4		
	4–9	0.51	77.5	2.9×10^4	$0.077 \pm$	0.209
	8–13	1.60	68.1	1.6×10^4	0.037	
	10–15	1.34	45.1	8.2×10^3	(2–15 m)	(2–15 m)
	14–19	0.90	26.3	2.8×10^3		
	17–22	1.09	21.0	2.0×10^3		
6.ix	2–6	2.6	68.7	4.4×10^4		
	4–8	4.06	64.5	3.1×10^4	$0.201 \pm$	0.103
	6.5–10.5	4.21	31.1	6.8×10^3	0.016	
	8.5–12.5	2.79	15.2	3.1×10^3	(2.17 m)	(2–17 m)
	11–15	1.36	9.4	3.1×10^3		
28.ix	2–7	1.96	109	3.8×10^5		
set A	4–9	1.38	145	1.1×10^5		
	7–12	5.39	58.8	1.1×10^5		
	10–15	6.42	33.3	6.0×10^4	$0.270 \pm$	0.100
	12–17	4.50	33.3	4.0×10^4	0.139	
	16–21	8.00	12.5	2.1×10^4	(2–21 m)	(2–21 m)
	17–22	6.99	10.3	1.4×10^4		
	22–27	3.01	1.1	1.0×10^3		
	27–32	0.32	1.0	4.1×10^2		

It is possible to extend the argument using the observed values of the potential energy associated with the density inversions. A measure of the time scale of the turbulent motions is given by $l_c|\overline{uw}|^{-\frac{1}{2}}$. Using appropriate estimates of the constants, this is found to be much longer than the time taken for the P.C.M. to ascend a distance l_c. If ΔV is the local mean value of the difference between the potential energies of the observed and 'equivalent stable' profiles of σ_T, per unit volume (defined in § 3.1), the rate of change of potential energy associated with the turbulent motions may be estimated as

$$\rho\overline{bw} = -C_2\,\Delta V|\overline{uw}|^{\frac{1}{2}}l_c^{-1}, \tag{14}$$

where C_2 is a constant, about unity. If the motion in the Loch is statistically steady we may use (12), with (14) and (7), to deduce

$$R \equiv \frac{\Delta V}{\rho}U'^{-\frac{1}{2}}d^{-2}N^{-\frac{3}{2}} = \frac{C_1}{C_2(C_0+C_1)^{\frac{1}{2}}}, \tag{15}$$

and so R should be a constant, about 0.1. The Reynolds stress in the water is

$$\tau = \rho d^2 N^3 U'^{-1}(C_0+C_1), \tag{16}$$

using (6) and (11), and this may be compared with the wind stress calculated from the empirical formula

$$\tau_a = \rho_a C_D u_{10}^2, \tag{17}$$

where ρ_a is the density of air, C_D is a drag coefficient (approximately 1.3×10^{-3}) and U_{10} is the wind speed 10 m above the water surface.

In table 1 we present estimates of ϵC_0^{-1} (equation (6)), $K_B C_1^{-1}$ (equation (9)), Re (equation (10)), $(\tau/\tau_a)\ (C_0 + C_1)^{-1}$ (equations (16) and (17), with $C_D = 1.3 \times 10^{-3}$) and of R (equation (15)) for the near-surface observations presented in §§ 3.2.1, 3.2.2 and 3.2.4. At greater depths than are shown in the table the r.m.s. displacements are small and are not well resolved by the vertical sampling interval, and moreover the Reynolds number, Re, and the intermittency, χ, are becoming small so the conditions for isotropic turbulence, implicit in assumptions involved in (6) and (9), are no longer valid. The very near-surface values of ϵ appear to be small, but it is unlikely that at these depths l_c is independent of distance from the surface, and the local scale of the turbulent eddies is probably reduced by the presence of the boundary, so that the assumptions inherent in (6) are invalid. K_B and ϵ show a tendency to decrease as depth increases. R is found to be much less than unity, in accordance with the estimated values of the coefficients $C_0 \sim 1$, $C_1 \sim 0.1$ and $C_2 \sim 1$, and with these values the stress within the water is much less than the wind stress, consistent with a dominant momentum transfer from the wind to the surface wave field. The Monin–Obukhov length, L, is given by

$$L = \frac{(-\overline{uw})^{\frac{3}{2}}}{kK_B N^2} = \frac{C_0}{kC_1}\left(\frac{\tau}{\tau_a}\frac{\rho_a}{\rho_1}C_D\right)^{\frac{3}{2}}\frac{u_{10}^3}{\epsilon}$$

(where k is Von Kármán's constant, approximately 0.41) from (9), (6) and (17). Using the estimated values for the coefficients and values of ϵ for the upper layers given in table 1, we find that $L = 5.5$ m, 1.3 m, 2.0 m for 31–8, 6–9 and 28–9 set A respectively. The assumptions that the depth of observation exceeds L is thus consistent with the observations on 6–9 and 28–9 set A but doubtful on 31–8, and this may account for some of the variation of the estimates of R.

We next consider the Richardson number variation. Figure 37 shows the variation of χ against Richardson number (or log Ri), the latter calculated over a scale corresponding to the r.m.s. displacements defined in § 3.1. Both negative and positive values of Richardson number have been included. The incidence of negative gradients increases rapidly as Ri decreases from 2 to 0.05. Higher values show a slight decrease in χ while lower positive values are almost constant. A slight decrease is observed as Ri decreases negatively. If, as we postulate, χ can be used as a turbulence index, the observations show that turbulence is persistent when the Richardson number is less than 0.05, but becomes less common at higher values of Ri. The spread of the transition and the continuing presence of some negative gradients at high Richardson numbers are consistent with turbulence in a field of variable current shear caused by eddies or waves, where the time scale of the collapse of a turbulent structure is comparable with that of the variable field. It is also however the case that local temperature inhomogeneities or velocity fluctuations measured at a finite sensor separation occasionally give rise to anomalously high Richardson numbers which do not reflect the local state of the fluid even though we have avoided their selection by using the locally defined (in depth but averaged over time) displacements in calculating Ri.

PHILOSOPHICAL TRANSACTIONS OF THE ROYAL SOCIETY A MATHEMATICAL, PHYSICAL & ENGINEERING SCIENCES

On the other hand it is known that Kelvin–Helmholtz instability takes a finite time to develop unstable gradients and, in a uniform flow with a single interface as modelled in laboratory experiments, leads to a transition from a Richardson number less than one quarter to a Richardson number of about one third (Thorpe 1973) and so for even a single Kelvin–Helmholtz event a spread in the transition region in which χ falls in value is only to be expected. At high Richardson

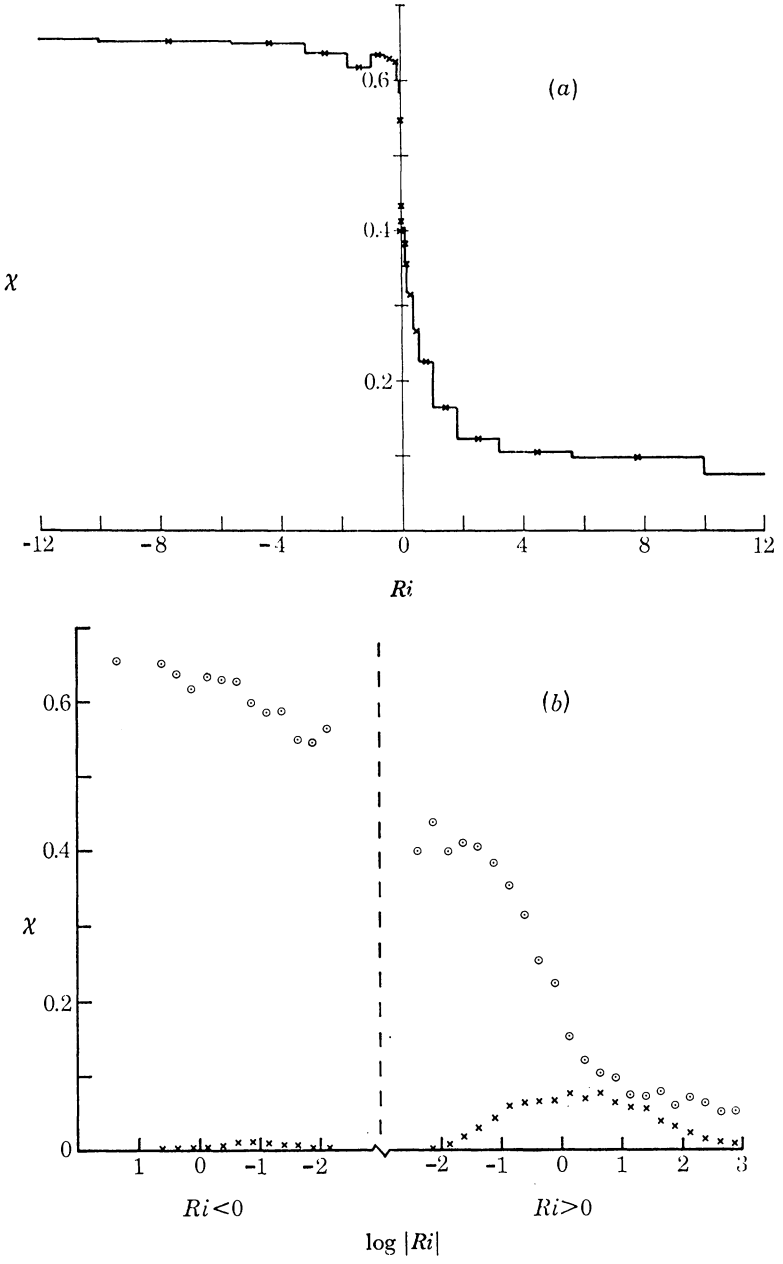

FIGURE 37. The variation of ensemble estimates of the fraction of fluid in which the density decreases with depth, χ, with (*a*) the Richardson number, Ri, and (*b*) log Ri (the circles), for the profiles described in §3. The estimate of Ri is based on differences in density and current measured over vertical distances equal to the r.m.s. displacement at each level in the several sets of profiles. The crosses in (*b*) show the proportion of values of log Ri which were found in each interval $n < 4 \log |Ri| < n+1$, where n is an integer, $-12 \leqslant u < 12$, and positive and negative values of Ri are considered separately.

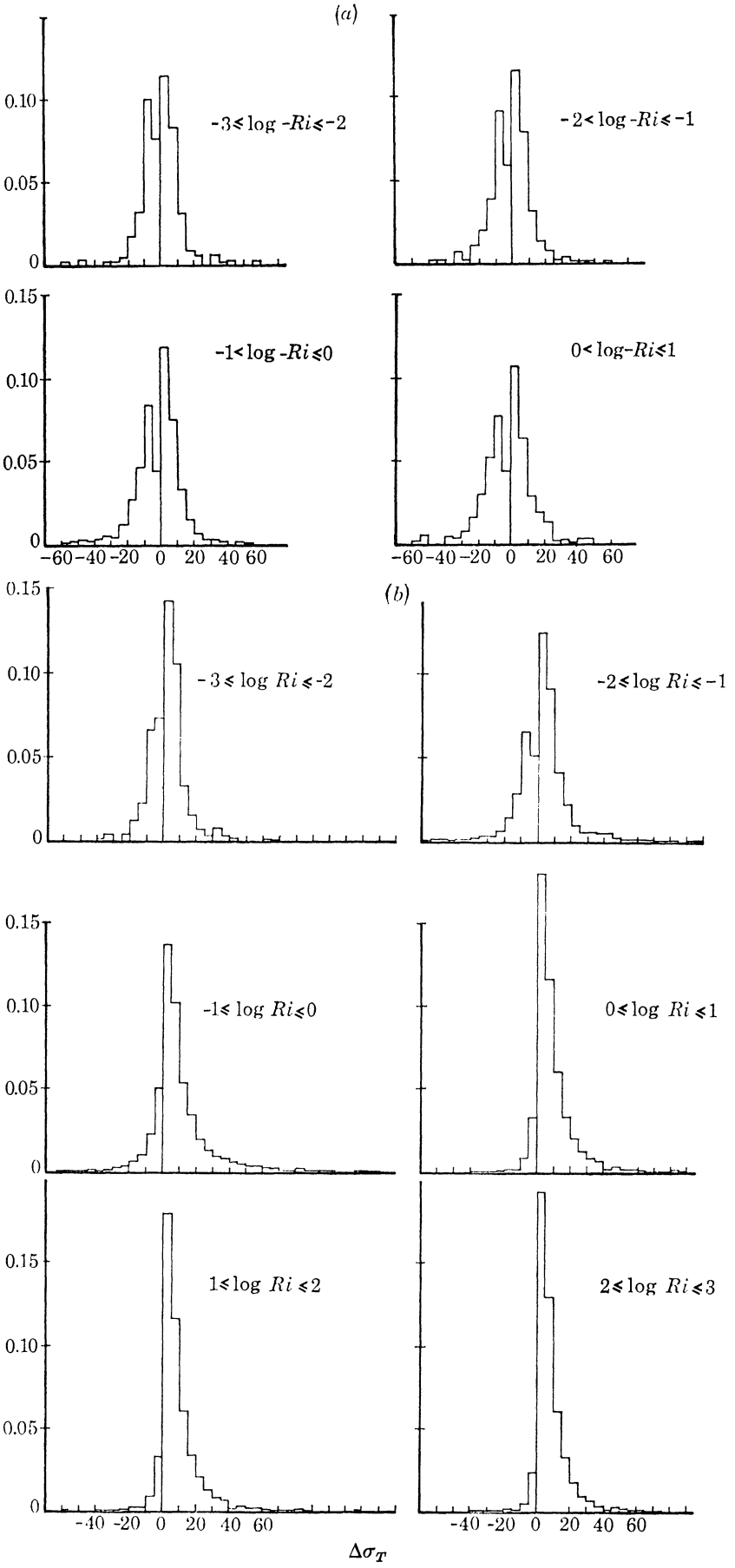

FIGURE 38. Histograms of the density difference ($\Delta\sigma_T = 10^4\sigma_T$, where $\Delta\sigma_T$ is the difference in σ_T measured over vertical intervals of approximately 6.7 cm) in regions of fluid in which the Richardson number (as defined in the caption of figure 37 and in the text) is in a range specified on the figure. (*a*) Negative Richardson numbers, *Ri*, (*b*) positive Richardson numbers.

numbers less than 5 % of the fluid has negative gradients. About 53 % of the negative gradients occur for Ri less than 0.18.

This analysis can be refined by examining the histograms of the density gradient within each Richardson number band. Figure 38 shows those calculated from the profiles obtained on 28 September (§ 3.2.4). The density gradients are calculated by taking differences over the vertical sampling interval, about 6.7 cm. A reduction in the symmetry of the histograms as Ri increases from 0.1 to 10 is well marked. The range in observed gradients is also greatest in this range,

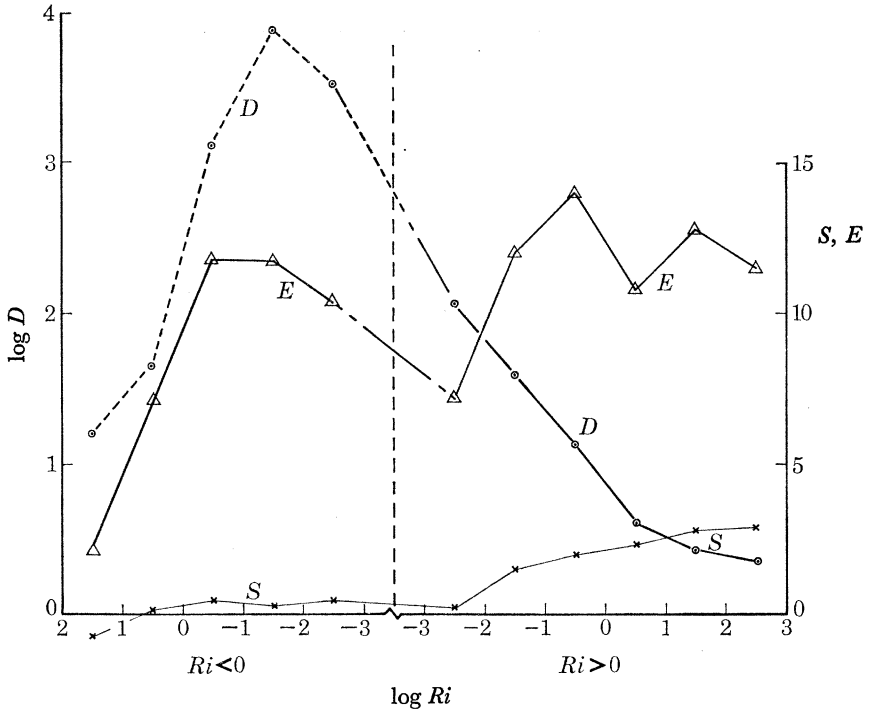

FIGURE 39. The variation of skewness, S, excess, E, and D (defined in equation (3)) of the density gradient distributions shown in figure 38, with log $|Ri|$.

suggesting that it is in the transition between stable and turbulent flow that the largest gradients are established. Some mean values of the distributions from all the days of observation are summarized in figure 39. The skewness of the distribution defined as $S = m_3/m_2$, where m_i is the ith moment of the distribution about the mean, falls as Ri decreases, being near zero when Ri is less than 0.01, consistent with the concept that turbulence is becoming more nearly isotropic at small or negative values of Ri. The excess, $E = m_4/m_2^2 - 3$, has a tendency to fall as Ri decreases, but like the other parameters characterizing the distribution, is probably affected by the exclusion of Richardson numbers which arise from small differences in σ_T lying below the noise level of the instrument. The Cox number, D, rises rapidly from a value of about 3 as Ri decreases from 1 to 0.01, having values exceeding 100 for Ri less than 0.01. The reduction in D for large negative values of Ri are due to the increasingly large negative mean values of the density gradient, the variance changing only by a factor of 4 throughout the range.

No universal form is found for distributions of Richardson numbers at different depths calculated from differences measured over a distance corresponding to the r.m.s. displacement. Although the most frequent values are in a range neighbouring unity, the median values of log

Ri vary by almost two orders of magnitude even when the data analysed are selected as having the best signal to noise level. In figure 40 is shown the distribution of log *Ri* in the upper layers where χ exceeds 0.3 and in the lower layers where χ is less than 0.1. In the lower layers the general form is not unlike that which might be found in a train of internal waves (see appendix 3). We conclude therefore that while scaling with Ozmidov's length, l_c, and the deductions which follow, may be valid when the Reynolds number is very high and turbulence is very persistent, so that χ is about 0.4, the data do not support the idea of a universal form for the Richardson number at all depths, at least when the length scale is chosen as the r.m.s. displacement.

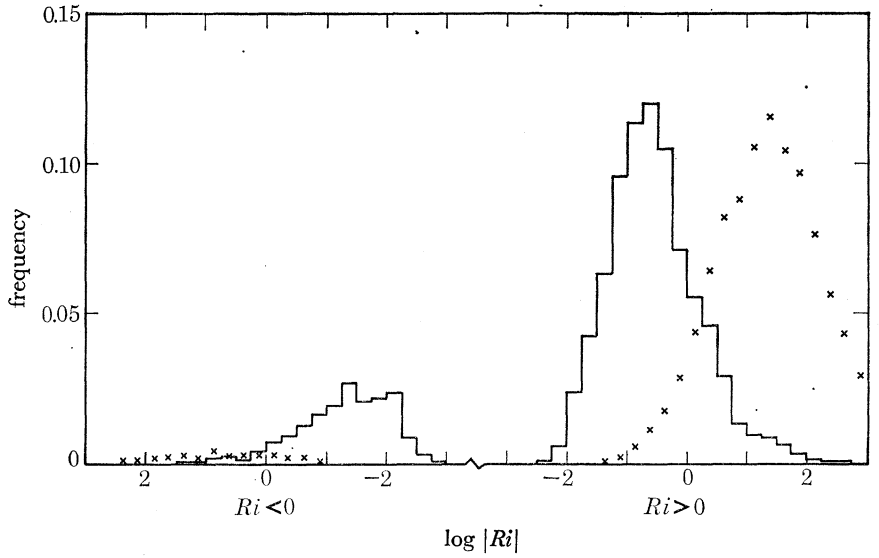

FIGURE 40. The frequency distributions of log Richardson number (*Ri*, defined in the text) for regions where χ exceeds 0.3 (full line) or where χ is less than 0.1 (crosses). Values of *Ri* exceeding 10^3 have not been included.

5. CONCLUSION

This paper reports a number of observations on the small-scale structure of density and velocity by using a novel measuring instrument in a large fresh water lake. In addition to documenting several interesting situations in the Loch in § 3, a method of analysis has been developed which may now be applied to a wider variety of phenomena, particularly mixing in the surface layers of the ocean. The study has provided estimates of the rate of dissipation of energy and the eddy diffusivity in the near-surface water, which appear to be consistent with other measurements and existing estimates of flux Richardson number and other coefficients which appear in the equations. We have here dealt mainly with mixing in non-convective situations.† Observations in convective situations are as yet insufficient for us to describe them in much detail. The greater variability which is then observed imposes a need for longer averaging times (more profiles), and reasonably steady conditions are relatively rare.

The Richardson number has been discussed and used as a parameter to categorize the state of the fluid, and it has been shown that *Ri* does provide a useful indicator of the proportion of fluid which is unstably stratified, and which, having high Rayleigh number, may be identified as being turbulent or at least in a stage transitional to turbulence. We would stress that results obtained in a fresh water lake should be applied only with some caution to the ocean. Not

† For more recent work see Thorpe, Hall, Taylor & Allen (1977), Thorpe & Hall (1977).

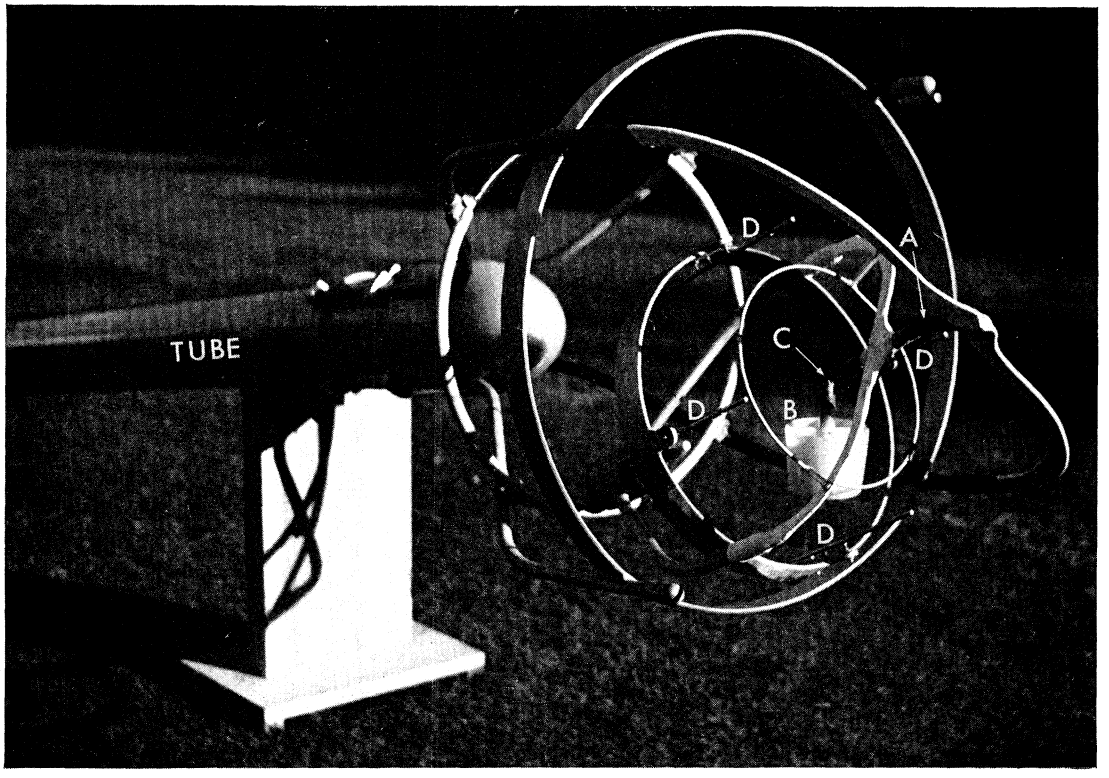

FIGURE 42. The P.C.M. current sensor. The letters are explained in the text.

(*Facing p.* 172)

PHILOSOPHICAL TRANSACTIONS OF THE ROYAL SOCIETY A MATHEMATICAL, PHYSICAL & ENGINEERING SCIENCES

only may salinity play an important role in determining the form of the microstructure, but the effect of surface waves may be much more profound, particularly when the dominant waves have a wavelength which exceeds the depth of the mixing layer. The generation of turbulence by surface waves and its effect on the stratification of the ocean deserves more investigation, perhaps on a laboratory scale. Nevertheless the study serves to illustrate the variety and complexity of motion in a turbulent stratified fluid.

The electronics for the P.C.M. and the winch control were designed and constructed by Mr Alan Hall. It is a pleasure to record my thanks to him and the many other members of staff and students at the I.O.S. who have helped in this work. I am also grateful to Dr J. Simpson of the Marine Science Laboratories at Menai Bridge, Anglesey, for his advice on the P.C.M. system.

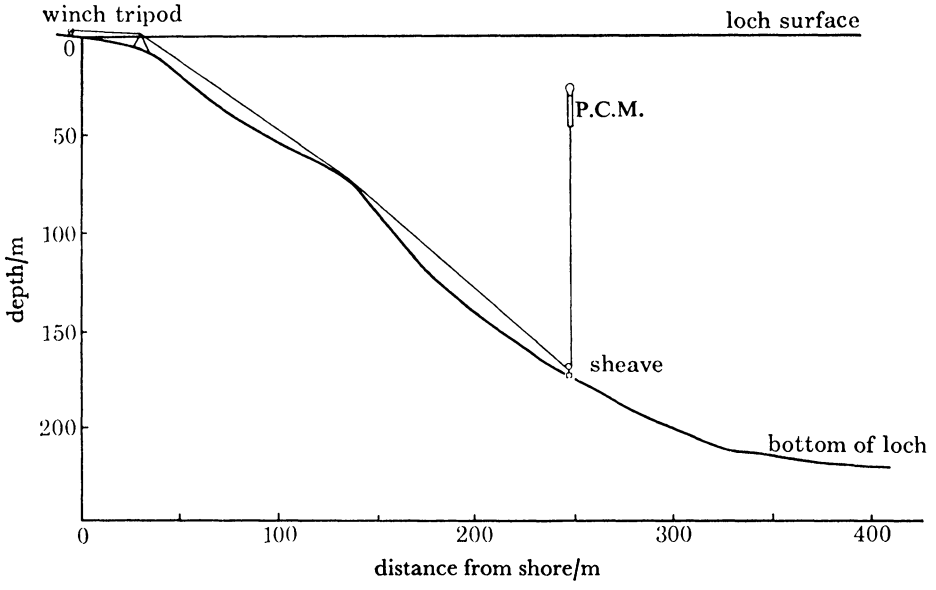

FIGURE 41. Section across the Loch, showing the arrangement of the P.C.M. mooring.

APPENDIX A. THE PROFILING CURRENT METER (P.C.M.) AND OTHER INSTRUMENTS

(*a*) *The principle of measurement*

The sensing elements of the P.C.M. are based on those of PROTAS (Simpson 1972) and the instrument is similar in form, although not free fall, but connected to shore as illustrated in figure 41. It consists of a 10 ft, 7 in outside diameter, aluminium tube which contains electronics and an electrically recording magnetic compass and gives a net 43 kgf buoyancy. At its upper end it carries a framework supporting a cage (shown in figure 42, plate 1) to which two pairs of electrodes (D) are attached. The cage hangs on a universal joint (A) supported by narrow bars of aerofoil section and is weighted so that, when hanging freely, the electrodes are vertical. In the centre of the cage is a neutrally buoyant vane (B) 15 cm long which is itself supported by a universal joint (C) below the first, and is free to orientate in any direction imposed by the relative water flow. The vane carries an electrode at its lower end. To the lower end of the tube is connected an 8-core cable which passes through a sheave anchored on the floor of the Loch 250 m

from shore in a depth of 174 m at the position marked A on figure 1. The cable then passes up the side of the Loch, through a pulley block on a tripod and onto a winch on shore. The winch is fitted with an automatic spooling device. The tube can be raised or lowered at a speed of about 13.4 cm s^{-1} by paying out or hauling in the cable on the winch. Signals from the sensors on the probe are transmitted through the cable and winch slip-rings to an 11-channel digital recorder housed in a shed near the winch. Measurements are recorded at $\frac{1}{2}$ s intervals while the probe is rising through the water. The depth of the probe is measured by a pressure transducer mounted on the top end plate of the tube. The speed of ascent, determined by differencing its depth calibrated output signal, or by examining the analogue output, is found to be quite steady over 30 s periods and fully controlled by the winch with no jerking. The vertical speed of the probe was subject to some 7 % variation as successive layers of wire (never more than three) were unwound from the winch. The position of the vane relative to the two pairs of electrodes is found in exactly the same way as is that on PROTAS†. The single electrode on the vane acts effectively as a potential wiper in two alternating fields provided by the two pairs of electrodes. The output of this pick-up electrode thus contains two signals at different frequencies which may be separated using tuned amplifiers and phase sensitive detectors to give two output voltages.

This output signal serves to define the position of the vane tip, relative to the electrodes, and thus both the orientation of the vane within the cage and its inclination to the vertical. Provided that the vane is properly aligned in the direction of the relative velocity, the vane orientation, when added to the orientation of the electrodes (which is given by the compass housed in the tube), supplies the horizontal direction of the flow past the vane. The vane inclination to the vertical is the inverse tangent of the horizontal relative current divided by the vertical speed of ascent of the tube through the water. A thermistor is attached to the framework supporting the cage. Five signals or data channels are transmitted to shore through the cable. They correspond to depth, temperature, electrode orientation, and the two output voltages which define the vane position and thence the two components of the relative horizontal current. Profiles could be made between 60 m depth and the surface at a rate of about 4/h. The instrument may be set to sample in a given depth range and left to make repeated profiles until the capacity of the recorder is exceeded or the power (supplied by a petrol generator) fails, a time of about 5 h.

(*b*) *Calibration and sensitivity*

Calibration of all five channels of the P.C.M. were made both in the laboratory and, where possible, in situ. The pressure and temperature signals were recorded regularly whilst the probe was at the surface of the Loch, and the water temperature recorded nearby and simultaneously by mercury in glass thermometer from a rubber boat. The pressure sensor was found to be stable to within 0.5 m over 45 days, and short term accuracy limited only by the digital resolution which was ± 3.1 cm. The vertical mean speeds were calculated by differencing over the time of the profile. The overall drift in thermistor calibration over 45 days was 0.2 °C and appeared to be gradual. As we are concerned mainly with short term changes of a few hours or less, these are not serious. The thermistor signal was transformed into a measure of density, σ_T, where

$$\sigma_T = \left(\frac{\rho - 1}{\rho_m}\right) \times 10^3,$$

† In practice much larger vane deflexions are measured with the P.C.M. than with PROTAS, but as the processing is by computer, the resulting nonlinearity poses no problems.

and ρ is the density of the water and ρ_m the maximum density (near 4 °C) at normal atmospheric pressure, using the empirical formula

$$\sigma_T = -0.07376 + 0.04728\,T - 0.00672\,T^2,$$

where T is the temperature, which is a good fit in the 6 °C to 15 °C range of temperature observed. Sigma T is negative in this range. The noise level of the electronics and logger limit the resolution of σ_T to 0.001 and thus, in particular, smaller variations in near-surface layers cannot be resolved.

The vertical sampling interval is equal to the time sampling interval (0.5 s) times the vertical speed of the probe, and is about 6.7 cm. The response time of the thermistors and electrical circuitry was about 0.075 s, much less than the sampling interval.

The estimates of current past the vane, the relative current, depend on estimates of the vertical speed of the vane through the water, the accuracy of the compass, the mechanical response of the vane, the electrical response of the vane circuitry, as well as the resolution, accuracy, and relative accuracy of the estimates of vane position in the electrode framework.

The compass consisted of a bar magnet which is periodically brought into contact with a ring potentiometer by a solenoid, and a voltage drop between the break-point in the potentiometer and the compass needle then gives a measure of the orientation of the potentiometer to magnetic north. The variation of output with orientation was measured in the laboratory, and also in the Loch, where the electrodes were aligned with prominent features around the Loch whose bearings were taken by prismatic compass. The interval between samples was 18 s and intermediate values inferred by linear interpolation. The tube rotated slowly and apparently steadily, usually about one revolution or less during a vertical profile from 60 m depth to the surface, or less than about 0.8 deg s^{-1}. The absolute accuracy of the compass is about $\pm 5°$, and this determines how well the electrode orientation is known.

The mechanical response of the vane was determined by tests in a towing tank in which the vane was disturbed from a direction aligned with the flow, and the time taken for a 90 % recovery of its original position was measured. The vane was critically damped with no overshoot and the distance for recovery independent of speed through the water (equivalent to the flow speed past the vane), about 34 cm, corresponding to about 2.5 s or less when on Loch Ness. (The greater the relative flow, the more rapid the response.) The electrical response time was about 2 s tested by suddenly changing the vane position when the probe was in the Loch, and measuring the recorded analogue outputs from the relevant channels.

The calibration for the position of the vane in the electrode framework was made by fixing the vane in a series of 84 known positions of inclination and direction with the aid of 'calibration boards' which fitted into the framework, while the probe was in the Loch on its mooring cable. This complete procedure was carried out from the rubber boat three times during the period of measurements. A set of probe positions were thus built up at which the values of the corresponding data logger channels were known. By smoothed graphical interpolation, the inclination and orientation of the vane were determined at a regular lattice of logger values, and from this lattice the actual angles during measurement runs were computed by linear interpolation, except for small angles of vane inclination, less than 8°, where a quadratic fit was used. Figure 43 shows the calibration curves of equal vane inclination and orientation. They are single valued at the maximum angle of vane inclination which was expected.

The sensitivity of the channels recording vane position is dependent on the actual values of the vane's inclination and orientation. At small inclinations the speed sensitivity is greatest, but

PHILOSOPHICAL TRANSACTIONS OF THE ROYAL SOCIETY A MATHEMATICAL, PHYSICAL & ENGINEERING SCIENCES

the direction is poorly resolved, while the converse holds at large inclinations. The resolution and relative accuracy of consecutive observations (which determine the shear measurement) is about 0.07 cm s^{-1} at 55° inclination, corresponding to a maximum observed relative velocity of about 19.1 cm s^{-1}, and was considerably better at the smaller angles commonly found, about 0.01 cm s^{-1} at 10° inclination. The accuracy of the speed estimate which derives from the vane

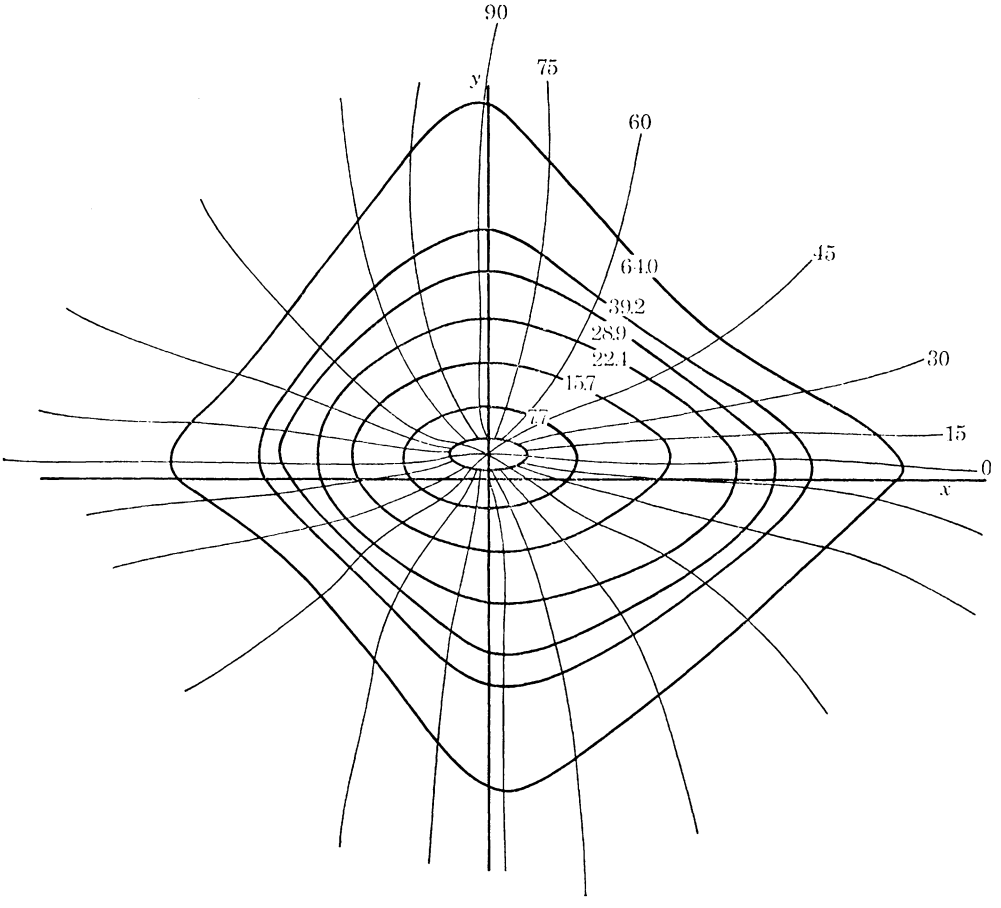

FIGURE 43. The calibration curves obtained for the P.C.M. x and y are proportional to the two output voltages obtained from the pick-up electrode on the vane. The broad lines are obtained when the inclination of the vane to the vertical is kept constant, whilst the narrow lines are obtained by moving the vane in a direction fixed relative to the pairs of electrodes. The numbers represent the inclination of the vane or the angle between the fixed direction and one pair of electrodes in degrees.

inclination was approximately ± 2.2 cm s^{-1} estimated from the mean variation of the three calibrations. The corresponding accuracy of the estimate of vane orientation in the electrode framework is about 10° over most of the range, but much worse at small angles of inclination (small relative horizontal flows), but the relative accuracy of consecutive observations was probably better than 1°. The vane was carefully made to be symmetrical, was of fairly high drag and carefully balanced in the Loch, and the framework heavily weighted and of low drag.

The actual horizontal currents were found from the relative currents by a correction in which the lateral speed of the tube was estimated. This is described in appendix B. The horizontal acceleration of the tube and the cable is determined by the drag of the relative current and the net buoyancy of the tube. The forward integration of an equation expressing this balance was

made numerically on a computer. The tube was kept at its lowest position before starting each upward profile for 38 s to allow it to equilibrate with the flow at that level so that the initial absolute motion was close to zero.

An example of the correction is shown in figure 44. The corrections do not account for vibrations of the tube and some records, notably those in strong currents, were marked by a regular periodic oscillation in the apparent current of amplitude 0.5 cm s^{-1}, or less, and of frequency about 8 s, which seems to arise from vortex shedding from the cylinder. The presence of this oscillation effectively increases the minimum resolving interval of the P.C.M. to about 1.06 m.

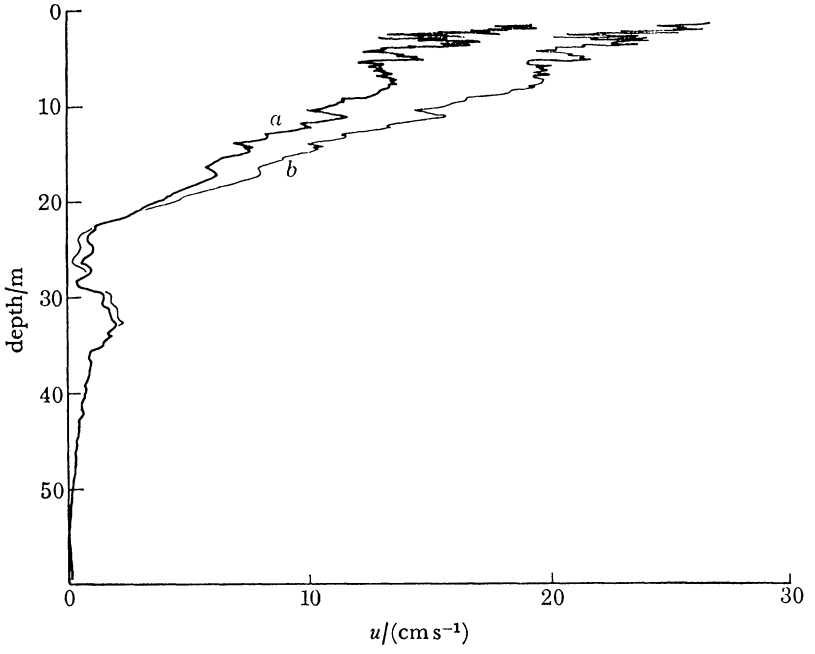

FIGURE 44. An example showing one component of current observed relative to the P.C.M. (*a*, broad line) and the profile of actual current obtained by accounting for the horizontal motion of the tube (*b*, narrow line); this is the first profile of 28 September (see §3.2.4).

The currents measured by the P.C.M. were compared with simultaneous measurements made by three Aanderaa current meters at 35, 45 and 65 m on a mooring 50 m northeast of the P.C.M. The agreement was in general within 15° for the direction estimate and about 20 % for speed, although it appears that the waiting time for equilibrium at the lowest position was not sufficiently long when large currents were present at this depth. The shear values, estimated by differencing the current meter velocities, agree to within 15 %. The estimates of Richardson number on the 1 m scale would appear to be accurate to within thirty per cent.

(*c*) *The spar buoy*

Measurements of wind speed, air temperature and near-surface water temperature were made from a spar buoy moored 125 m off shore. The wind was measured by a cup anemometer 2.1 m above the water surface. The values reported below are corrected to 10 m assuming a logarithmic boundary layer structure, constant drag coefficient (C_D) taken as 1.3×10^{-3}, and a

Von Karman's constant (k) of 0.41; wind at 10 m (u_{10}) was then 1.164 times† the wind at 2.1 m. The air temperature was measured by a thermistor at 1.8 m above the water, protected from rain and direct radiation, and the water temperature was measured by a second thermistor at 2.6 m below the surface. The electrical outputs of these sensors were transmitted to shore through the mooring cable and recorded at half second intervals during the P.C.M. profiles. Regular calibration checks were made, and the meteorological observations supplemented by a barograph, a thermograph, a hair hygrometer, wet and dry bulb thermometers, a rain gauge and a water level gauge, which were read twice daily.

Appendix B. Correction of the observed relative currents to absolute currents

As the P.C.M. rises through the water it is subjected to a horizontal acceleration due to the drag of the water moving past and the horizontal component of the tension and drag of the cable. We suppose that the cable leads in a straight line from the sheave at the bottom of the Loch to the tube, so that the velocity of the cable at any position is proportional to the tube velocity, and that the tension in the cable is constant. The cable mass is small and is neglected and the tension is taken equal to the buoyancy of the tube.

The rate of change of horizontal momentum of the tube is given by the product of its virtual mass, M_v, equal to its mass plus displacement, and horizontal acceleration, $\dot{v}$. This is equated to the horizontal component of the cable tension on the sheave and the net drag of the water past the tube and cable, with signs being taken appropriately:

$$M_v \dot{v} = (\text{tube drag}) + (\text{wire drag}) - (\text{force on the sheave}).$$

The drag forces per unit length are equal to $C_d \rho u^2$ in the direction of the relative flow where C_d is a drag coefficient, taken to be a constant equal to 1.15 appropriate to cylinders (Goldstein 1938), and u is the relative flow past the probe of the water of density ρ. For the most part the Reynolds number of the flow past the instrument is in the range for which C_d is almost constant and variations have therefore not been included. The speed u is equal to the difference between the probe speed and the absolute water speed, which is to be found. It is assumed that the water at each level continues at the speed which it had when the sensors passed through it, and that before beginning its upward motion the probe is at rest, so that the drag balances the force on the sheave and the relative velocity, first measured by the P.C.M. at the level of the tube, is equal to the absolute velocity. Currents at greater depth than the tube in this position are supposed to be equal to a linear interpolation between this current and zero flow at the bottom of the Loch. The inclination of the wire to the vertical α as the tube begins its upward motion can be calculated from the initial force balance.

† This derives from the familiar formulae for the stress, τ,

$$\tau = \rho_a u_*^2 = \rho_a C_D u_{10}^2,$$

and for the wind u at height z,

$$u = \frac{u_*}{k} \log (z/z_0),$$

where u_* is defined by the first equation, z_0 is a length scale and ρ_a the density of air.

The absolute current is calculated by a forward numerical integration of the force balance equation and an expression for,

$$\dot{\alpha} = v/D - (\alpha/D)\,\dot{D},$$

(where D is the height of the probe above the bottom of the Loch), using the measured relative current and depth of the tube.

Appendix C. The Richardson number in a simple internal wave train

Consider the motions induced by a small amplitude internal wave of frequency σ and horizontal wave number k propagating in the x-direction in a fluid of Brunt–Väisälä frequency $N(z)$. The horizontal velocity is given by

$$u = \Psi'(z)\sin(kx - \sigma t),$$

where $\Psi(z)$ is given by

$$\Psi'' - k^2(1 - N^2/\sigma^2)\,\Psi = 0,$$

and Ψ tends to zero at the horizontal boundaries, say $z = 0, H$ (Thorpe 1968).

The Richardson number is

$$Ri = \frac{N^2}{\Psi''^2 \sin^2(kx - \sigma t)} = \frac{Ri_0(z)}{\sin^2(kx - \sigma t)},$$

where $Ri_0 = (N^2\sigma^4)/\Psi^2 k^4 (N^2 - \sigma^2)^2$ is the smallest Ri in the wave field at level z. For long waves ($\sigma \ll N$), Ri_0 tends to $\sigma^4/k^4\Psi^2N^2$. Quantity Ψ is proportional to the vertical velocity and is therefore continuous and varies only slowly in the vertical, so that N^2 variations in Ri_0 dominate the depth variability of Ri_0, as remarked by Phillips (1966).

Consider measurements made at a fixed location, which without loss of generality, may be taken as $x = 0$. The probability $p(J, z)$ of finding the Richardson number between $J - \frac{1}{2}\mathrm{d}J$ and $J + \frac{1}{2}\mathrm{d}J$ at any depth z is proportional to the time for which the Richardson number lies within this range in one quarter period (see Longuet-Higgins 1952. Over larger time periods the cycle is repeated). Hence

$$p(J, z) = c\,\mathrm{d}t = c\frac{\mathrm{d}J}{(\partial Ri/\partial t)|_{Ri=J}}$$

$$= -\frac{c}{2\sigma}\frac{\mathrm{d}J}{J\sqrt{(J/Ri_0 - 1)}}.$$

The total probability of finding Ri in $J - \frac{1}{2}\mathrm{d}J$, $J + \frac{1}{2}\mathrm{d}J$ is then found by integration over the depth of the fluid for which Ri^* is less than J

$$p(J) = \text{constant}.\int_{z:\,J > Ri^*_i} \frac{Ri_0^{\frac{1}{2}}}{J\sqrt{(J - Ri_0)}}.$$

For example, if N is constant, then

$$Ri_0(z) = R\sin^{-2}(n\pi z/H),$$

where R is constant and n is the number of the internal mode, and

$$p(J) = \text{constant}\int_z \frac{R^{\frac{1}{2}}\,\mathrm{d}z}{J\sqrt{(J\sin^2(n\pi z/H) - R)}}.$$

where the integration is over the range $z > (H/n\pi)\arcsin(R/J)^{\frac{1}{2}}$. This may be transformed into an elliptic integral and evaluated by using the formulae given in Abramowitz & Stegun (1965, equation 17.4.43). The form of the probability distribution for $R = 0.25$ and $n = 1$ is shown in figure 45.

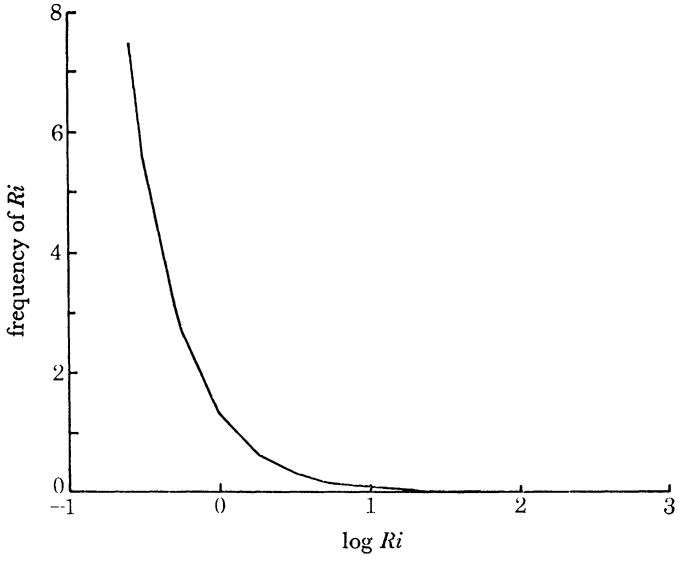

FIGURE 45. The non-normalized probability $p(J)$ of Richardson number J (the frequency of J) in a first mode train of internal waves in a fluid of constant Brunt–Väisälä frequency. The lowest value of the Richardson number in the waves is taken to be 0.25, which gives the cut-off in the distribution.

REFERENCES

Abramowitz, M. & Stegun, I. A. 1965 *Handbook of mathematical functions*. New York: Dover.

Apel, J. R., Byrne, M., Proni, J. R. & Charnell, R. L. 1975 Observations of oceanic internal waves from the Earth Resources Technology Satellite. *J. geophys. Res.* **80**, 865–871.

Batchelor, G. K. 1953 The conditions for dynamical similarity of motions of a frictionless perfect-gas atmosphere. *Qu. Jl R. met. Soc.* **79**, 224–35.

Chandrasekhar, S. 1961 *Hydrodynamic and hydromagnetic stability*. Oxford University Press.

Crofts, I. 1975 Microstructure of density and velocity in the thermocline (observations in Loch Ness). Ph.D. dissertation. Univ. College of N. Wales, Bangor.

Crystal, G. 1910 *Bathymetrical survey of the Scottish fresh water lakes* (eds Murray & Puller), vol. 1, pp. 29–90. Edinburgh: Challenger Office.

Dobroklonskiy, S. V. & Kontoboytseva, N. V. 1973 Empirical relationships between steady-state waves and wind speeds for a wide range of fetches. *Oceanology* **13** (5), 640–645.

Gardener, R. 1745 Letter XXI to Dr John Stevenson published in connection with the great Lisbon earthquake. *Phil. Trans. R. Soc. Lond.* 387–389.

Gargett, A. E. & Hughes, B. A. 1972 On the interaction of surface and internal waves. *J. Fluid Mech.* **52**, 179–191.

Goldstein, S. 1938 *Modern developments in fluid dynamics*, vol. 1. Clarendon Press, Oxford.

Grant, H. L., Moilliet, A. & Vogel, W. M. 1968 Some observations of the occurrence of turbulence in and above the thermocline. *J. Fluid Mech.* **34**, 443–448.

Gregg, M. C. 1975 Microstructure and intrusions in the California current. *J. Phys. Oceanogr.* **5**, 253–278.

Gregg, M. C., Cox, C. S. & Hacker, P. W. 1973 Vertical microstructure measurements in the central North Pacific. *J. Phys. Oceanogr.* **3**, 458–469.

Hedley, T. B. & Keffer, J. F. 1974 Turbulent/non-turbulent decisions in an intermittent flow. *J. Fluid Mech.* **64**, 625–644.

Johnston, T. N. 1904 The bathymetrical survey of Loch Ness. *Geog. J.* **24**, 429–430.

Kullenberg, G. 1971 Vertical diffusion in shallow water. *Tellus* **23**, 129–135.

Kullenberg, G., Murthy, C. R. & Westerberg, H. 1973 An experimental study of diffusion characteristics in the thermocline and hypolimnion regions of Lake Ontario. *Proc. 16th Conf. Great Lakes Res.* 774–790.

Lafond, E. C. 1962 Internal Waves, Part 1. In *The sea* (ed. M. N. Hill), vol. 1, p. 731. New York: Interscience.

PHILOSOPHICAL TRANSACTIONS OF THE ROYAL SOCIETY A MATHEMATICAL, PHYSICAL & ENGINEERING SCIENCES

Longuet-Higgins, M. S. 1952 On the statistical distribution of the heights of sea waves. *J. mar. Res.* **11**, 245–266.
Monin, A. S. 1962 On the turbulence spectrum in a thermally stratified atmosphere. *Bull. (Izvestiya), Acad. Sci. U.S.S.R., Geophys.* Ser. (3), 266–271.
Mortimer, C. H. 1955 Some effects of the Earth's rotation on water movements in stratified lakes. *Proc. Intern. Assoc. Limnol.* **12**, 66–77.
Obukhov, A. M. 1959 The influence of hydrostatic forces on the structure of the temperature field in turbulent flow. *Proc. (Doklady) Acad. Sci. U.S.S.R.* **125**, 1246–8.
Orlanski, I. & Bryan, K. 1969 Formation of the thermocline step structure by large-amplitude internal gravity waves. *J. geophys. Res.* **74**, 6975–6983.
Osborne, T. R. 1974 Vertical profiling of velocity microstructure. *J. Phys. Oceanogr.* **4**, 109–115.
Osborne, T. R. & Cox, C. 1972 Oceanic fine structure. *Geophys. Fluid Dyn.* **3**, 321–345.
Ozmidov, R. V. 1965 On the turbulent exchange in a stably stratified ocean. *Izvestiya, Acad. Sci. U.S.S.R., Atmos. & Ocean Phys.* **1**, 861–871.
Pennington, W., Haworth, E. Y., Bonny, A. P. & Lishman, J. P. 1972 Lake sediments in northern Scotland. *Phil. Trans. R. Soc. Lond.* B **264**, 191–294.
Phillips, O. M. 1966 *The dynamics of the upper ocean*. Cambridge University Press.
Simpson, J. H. 1972 A free fall probe for the measurement of velocity microstructure. *Deep-Sea Res.* **19**, 331–336.
Simpson, J. H. & Woods, J. D. 1970 Temperature microstructure in a fresh water thermocline. *Nature, Lond.* **226**, 832.
Stewart, R. W. & Grant, H. L. 1962 Determination of the rate of dissipation of turbulent energy near the sea surface in the presence of waves. *J. geophys. Res.* **67**, 3177–3180.
Tennekes, H. 1973 Intermittency of the small-scale structure of atmospheric turbulence (Part II). *Boundary-Layer Met.* **4**, 241–250.
Thorpe, S. A. 1968 On the shape of progressive internal waves. *Phil. Trans. R. Soc. Lond.* A **263**, 563–614.
Thorpe, S. A. 1968 A method of producing a shear flow in a stratified fluid. *J. Fluid Mech.* **32**, 693–704.
Thorpe, S. A. 1971 Asymmetry of the internal seiche in Loch Ness. *Nature, Lond.* **231**, 306–308.
Thorpe, S. A. 1973 Turbulence in stably stratified fluids: a review of laboratory experiments. *Boundary-Layer Met.* **5**, 95–119.
Thorpe, S. A. 1973 Experiments on instability and turbulence in a stratified shear flow. *J. Fluid Mech.* **61**, 731–751.
Thorpe, S. A. 1974 Near resonant forcing in a shallow two-layer fluid: a model for the internal surge in Loch Ness? *J. Fluid Mech.* **63**, 509–527.
Thorpe, S. A. & Hall, A. J. 1974 Evidence of Kelvin–Helmholtz billows in Loch Ness. *Limnology & Oceanography* **19**, 973–976.
Thorpe, S. A. & Hall, A. J. 1977 Mixing in upper layer of a lake during heating cycle. *Nature, Lond.* **265**, 719–722.
Thorpe, S. A., Hall, A. J. & Crofts, I. 1972 The internal surge in Loch Ness. *Nature, Lond.* **237**, 96–98.
Thorpe, S. A., Hall, A. J., Taylor, C. & Allen, T. 1977 Billows in Loch Ness. *Deep-Sea Res.* **24**, 371–379.
Townsend, A. A. 1956 *The structure of turbulent shear flow*. Cambridge University Press.
Turner, J. S. 1973 *Buoyancy effects in fluids*. Cambridge University Press.
Watson, E. R. 1904 Movements of the waters of Loch Ness as indicated by temperature observations. *Geog. J.* **24**, 430–437.
Wedderburn, E. M. 1907 The temperature of the fresh water lochs of Scotland, with special reference to Loch Ness. *Trans. R. Soc. Edinb.* **45**, 407–489.
Wedderburn, E. M. & Watson, W. 1909 Observations with a current meter in Loch Ness. *Proc. R. Soc. Edinb.* **19**, 619–647.
Woods, J. D. 1969 On Richardson's number as a criterion for laminar–turbulent–laminar transition in the ocean and atmosphere. *Radio Sci* **4**, 1289–1298.

PHILOSOPHICAL TRANSACTIONS OF THE ROYAL SOCIETY A MATHEMATICAL, PHYSICAL & ENGINEERING SCIENCES

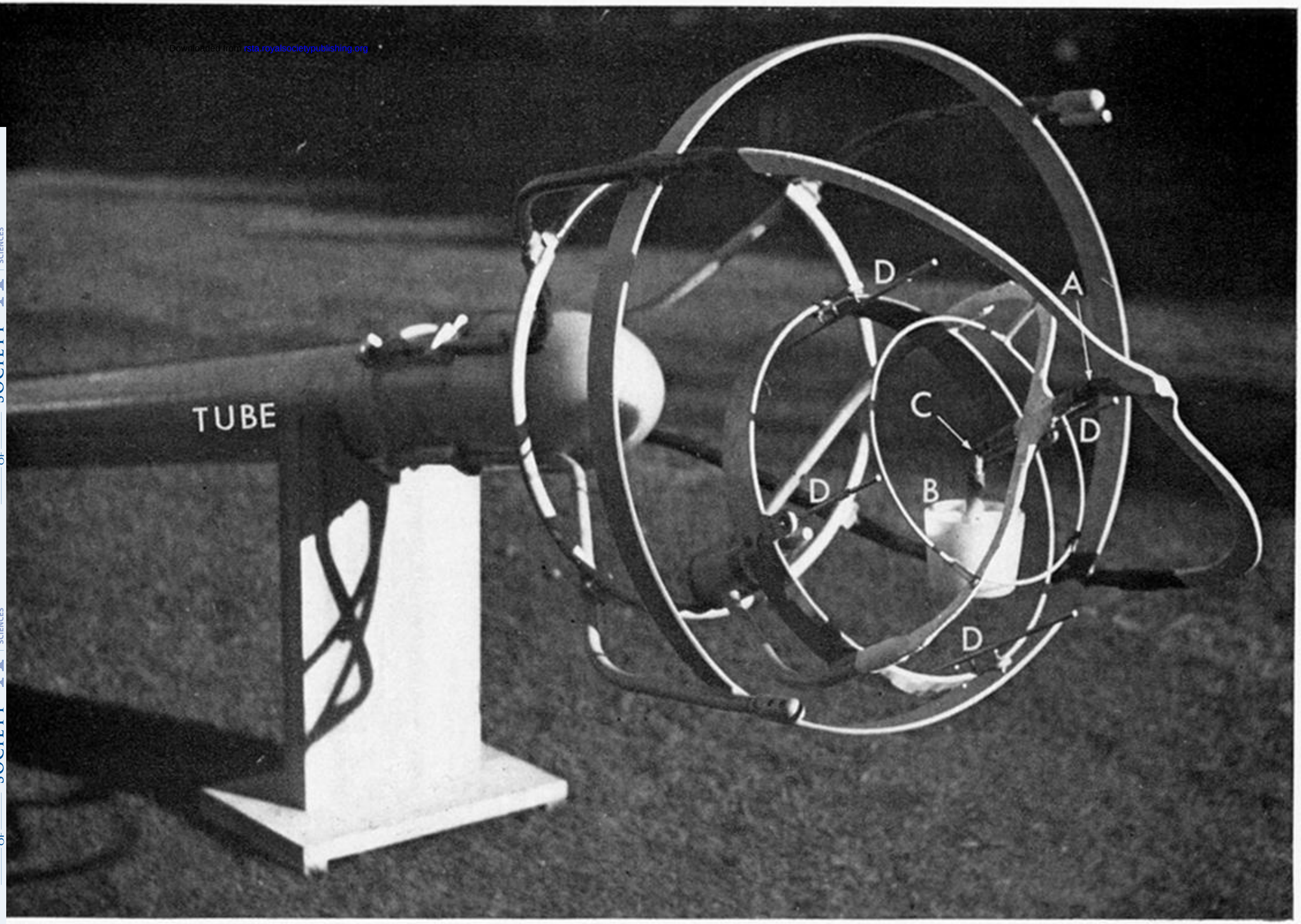

FIGURE 42. The P.C.M. current sensor. The letters are explained in the text.

PHILOSOPHICAL TRANSACTIONS OF THE ROYAL SOCIETY A MATHEMATICAL, PHYSICAL & ENGINEERING SCIENCES